Analysis of protein SUMOylation and its role in Alzheimer's disease using mouse models

Dissertation

for the award of the degree
"Doctor rerum naturalium" (Dr. rer. nat.)
of the Georg-August-Universität Göttingen

within the doctoral program Biology
of the Georg-August University School of Science (GAUSS)

submitted by
Trayana Hristova Stankova

from Harmanli, Bulgaria

Göttingen, 2016

Thesis Committee

Prof. Dr. Nils Brose
Department of Molecular Neurobiology, Max Planck Institute for Experimental Medicine

Dr. Judith Stegmüller
Department of Neurology, University Clinical Centre Aachen

Prof. Dr. Thomas Bayer
Division of Molecular Psychiatry, University Medical Center Göttingen

Members of the Examination Board

Reviewer: Prof. Dr. Nils Brose
Department of Molecular Neurobiology, Max Planck Institute for Experimental Medicine

Second Reviewer: Dr. Judith Stegmüller
Department of Neurology, University Clinical Centre Aachen

Further members of the Examination Board:

Prof. Dr. Thomas Bayer
Division of Molecular Psychiatry, University Medical Center Göttingen

Prof. Dr. Christian Griesinger
Department of NMR-based Structural Biology, Max Planck Institute for Biophysical Chemistry

Prof. Dr. Dr. Hannelore Ehrenreich
Department of Clinical Neuroscience, Max Planck Institute for Experimental Medicine

Prof. Dr. Ralf Heinrich
Department of Cellular Neurobiology, Schwann-Schleiden Research Centre

Date of the oral examination: February 2nd, 2017

Declaration

I hereby declare that this thesis was written independently with the help of no other sources than those cited.

Trayana Stankova

Table of contents

List of abbreviations

AD	Alzheimer's disease
ALS	amyotrophic lateral sclerosis
AMPA	α-amino-3-hydroxy-5-methyl-4-isoxazolepropionic acid
A. nidulans	*Aspergillus nidulans*
ANOVA	analysis of variance
APH-1	anterior pharynx-defective 1
APLP	amyloid precursor-like protein
APOE	apolipoprotein E
APP	amyloid precursor protein
AR	androgen receptor
Atg	autophagy-related
ATP	adenosine triphosphate
BAC	bacterial artificial chromosome
BACE1	β-site APP-cleaving enzyme 1
BCA assay	bicinchoninic acid assay
BMAL1	brain and muscle Arnt-like protein 1
BSA	bovine serum albumin
CALHM1	calcium homeostasis modulator 1
CASK	calcium/calmodulin-dependent serine protein kinase
CA	*Cornu ammonis*
CREB	cAMP response element binding protein
CtBP1	C-terminal-binding protein 1
Ctip2	chicken ovalbumin upstream promoter transcription factor-interacting protein 2
ddH_2O	double-distilled water
DEAE	diethylaminoethyl
DeSI	deSUMOylating isopeptidase
DMEM	Dulbecco's modified eagle medium
DMSO	dimethyl sulfoxide
DUBs	deubiquitinating enzymes
DNA	deoxyribonucleic acid
dNTPs	deoxynucleotide triphosphates
DRP1	dynamin-related protein 1
E15	embryonic day 15
EAAT2	excitatory amino acid transporter 2
ECL	enhanced chemiluminiscence
E. coli	*Escherichia coli*
EDTA	ethylendiaminetetraacetic acid
El	eluate
ER	endoplasmic reticulum
ES cells	embryonic stem cells
FAD	familial Alzheimer's disease
FAT10	human leukocyte antigen F-associated transcript 10

FBS	fetal bovine serum
GFP	green fluorescent protein
GLUT	glucose transporter
HBmg cells	H4 cells stably expressing human Myc-BACE1
HDAC	histone deacetylase
HEK cells	human embryonic kidney cells
HEPES	4-(2-hydroxyethyl)-1-piperazineethanesulfonic acid
het	heterozygous
HRP	horseradish peroxidase
HSV-TK	herpes simplex virus thymidine kinase
Hub1	homologous to ubiquitin 1
IDE	insulin-degrading enzyme
INP	input
ISG15	interferon-stimulated gene 15
KI	knock-in
LB	Luria broth
LTD	long-term depression
LTP	long-term potentiation
MAP2	microtubule-associated protein 2
MCF-7	Michigan Cancer Foundation 7
MeCP2	methyl-CpG-binding protein 2
MEF2A	myocyte-specific enhancer factor 2A
MEFs	mouse embryonic fibroblasts
min	minutes
mRNA	messenger ribonucleic acid
Nedd8	neural precursor cell expressed, developmentally down-regulated 8
NEM	N-ethylmaleimide
NGFR	nerve growth factor receptor
NGS	normal goat serum
NIID	neuronal intranuclear inclusion disorder
NMDA	N-methyl-D-aspartic acid
OD	optical density
Pax	paired box
PBS	phosphate buffered saline
PBST	phosphate buffered saline with Tween 20
PCNA	proliferating cell nuclear antigen
PCR	polymerase chain reaction
PE	phosphatidylethanolamine
PEN-2	presenilin enhancer 2
Pen/Strep	penicillin/streptomycin
PFA	paraformaldehyde
PIAS	protein inhibitor of activated STAT
PML	promyelocytic leukemia
PMSF	phenylmethylsulfonyl fluoride

PS	presenilin
PTEN	phosphatase and tensin homologue
RAGE	receptor for advanced glycation endproducts
RanBP2	Ran-binding protein 2
RIM1α	Rab3-interacting molecule 1α
RING	really interesting new gene
RIPA buffer	Radioimmunoprecipitation assay buffer
RNF4	RING finger protein 4
RT	room temperature
RT-PCR	reverse transcription polymerase chain reaction
RanGAP1	Ran GTPase-activating protein 1
Rhes	Ras homologue enriched in striatum
rpm	revolutions per minute
SAE1	SUMO-activating enzyme 1
SAE2	SUMO-activating enzyme 2
sAPP	secreted APP
SBMA	spinal and bulbar muscular atrophy
SDS-PAGE	sodium dodecyl sulfate polyacrylamide gel electrophoresis
sec	seconds
SEM	standard error of the mean
SENP	sentrin-specific protease
SERCA	sarco/endoplasmic reticulum Ca^{2+}-ATPase
SIM	SUMO-interacting motif
Smchd1	structural maintenance of chromosome flexible hinge domain containing 1
SOC	super optimal broth with catabolite repression
SOD1	superoxide dismutase 1
SORL1	sortilin-related receptor, L (DLR class) A repeats containing
S. pombe	*Schizosaccharomyces pombe*
STET buffer	sucrose/Triton/EDTA/Tris buffer
SUMO	small ubiquitin-like modifier
TBE buffer	Tris/borate/EDTA buffer
TDG	thymine DNA glycosylase
TE buffer	Tris-EDTA buffer
TGN	trans-Golgi network
TIF1	transcription intermediary factor 1
TOPORS	TOP1 binding arginine/serine rich protein
tRNA	transfer ribonucleic acid
UBL5	ubiquitin-like protein 5
UBQLN1	ubiquilin 1
Ufm1	ubiquitin-fold modifier 1
Ulp1	ubiquitin-like-specific protease 1
Urm1	ubiquitin-related modifier 1
WT	wild type
Zbtb20	zinc finger and BTB domain containing 20

List of figures

Abstract

Post-translational modifications serve as a cellular mechanism for the regulation of the activity, stability and localization of proteins. SUMOylation is a dynamic and reversible post-translational modification, which entails the attachment of a SUMO protein to a lysine residue of the target protein. SUMOylation is involved in the regulation of numerous cellular processes including transcription, nucleocytoplasmic trafficking, and DNA repair. Three or four SUMO paralogs are present in mammals – SUMO1, SUMO2, SUMO3 and SUMO4. SUMO2 and SUMO3 exhibit extremely high sequence homology and therefore cannot be distinguished by antibodies. Interestingly, SUMO2/3 conjugation has been shown to change dramatically in response to aberrant cellular conditions. The identification of endogenous SUMO substrates has long been hindered by the transient nature of SUMOylation, the lack of reliable antibodies for affinity purification, and the modification of only a small percentage of a given SUMO substrate at a given time.

Thus, in a first project, analogous to a His_6-HA-SUMO1 knock-in mouse model generated in our lab, we generated a Strep-Myc-SUMO3 knock-in mouse model expressing Strep-Myc-tagged SUMO3 instead of wild type SUMO3 from the endogenous *SUMO3* locus. Importantly, a main advantage of this model is the possibility to distinguish specifically SUMO3 from SUMO2. Strep-Myc-SUMO3 knock-in and wild type mice brain homogenates were used to perform anti-Myc affinity purification, which resulted in the enrichment of free SUMO3 and SUMO3 conjugates in the eluate from the knock-in mice. Thus, we proved that the newly generated mouse model can be used as a tool for the identification of SUMO3 substrates. However, despite the utilization of several anti-Myc and one anti-Strep antibody, we were not able to clearly localize Strep-Myc-SUMO3 in brain sections of SUMO3 knock-in mice as the antibodies showed different staining patterns. This mouse model will be further used to study SUMO3 conjugation profiles under physiological and non-physiological conditions.

A constantly increasing number of studies have suggested a link between SUMOylation and Alzheimer's disease. Thus, in a second project, we crossbred His_6-HA-SUMO1 knock-in mice with 5xFAD, a mouse model of Alzheimer's disease, in order to assess SUMO1 conjugation profile in the context of Alzheimer's disease pathology. Using mice at different stages of disease progression, we intended to identify specific changes in the localization of SUMO1 and in the global SUMO1 conjugation levels. Anti-HA immunostaining of brain sections showed that in subiculum and cortical layer V SUMO1 exhibited nuclear presence in both His_6-HA-SUMO1 and His_6-HA-SUMO1;5xFAD mice at any of the ages examined. Furthermore, two

different anti-HA antibodies produced two different types of non-nuclear anti-HA signal in His_6-HA-SUMO1;5xFAD mice. While one of the antibodies produced anti-HA signal localizing to amyloid plaques, the other resulted in line-shaped signals or signals with the shape of amorphous mass, with some of the line-shaped signal surrounding amyloid plaques. Importantly, both anti-HA antibodies produced similar signals in the 5xFAD non-knock-in mice which strongly speaks against specificity of the signal. The predominantly nuclear localization of His_6-HA-SUMO1 in both 5xFAD and non-5xFAD mice was confirmed by subcellular fractionation followed by Western blot. Regarding SUMO1 conjugation levels upon Alzheimer's disease pathology, anti-HA Western blot did not reveal any significant differences between His_6-HA-SUMO1 and His_6-HA-SUMO1;5xFAD mice in both cortex and hippocampus at any of the examined ages. Furthermore, a quantitative comparison of the anti-HA signal in the neuronal nuclei of His_6-HA-SUMO1 and His_6-HA-SUMO1;5xFAD in both subiculum and cortical layer V did not reveal substantial differences between the two genotypes. A minor increase of 25.8% was observed in the pyramidal neurons of cortical layer V of 8-week-old His_6-HA-SUMO1;5xFAD mice when compared to age-matched His_6-HA-SUMO1 mice. In summary, we did not discover substantial changes in SUMO1 localization and SUMO1 conjugation levels in the context of increased amyloid burden. However, we cannot conclude that the SUMO1 profile is undisturbed upon Alzheimer's disease pathology as changes in the SUMOylation pattern of individual proteins may not be detected by the techniques utilized in this study. Thus, the next step will be the investigation of differentially SUMOylated substrates by anti-HA affinity purification of brain homogenates from His_6-HA-SUMO1, His_6-HA-SUMO1;5xFAD, 5xFAD and wild type mice followed by mass spectrometry analysis.

1. Introduction

Bacterial and eukaryotic cells face constantly changing external environments and internal conditions. In order to preserve their homeostasis, cells require mechanisms to carefully regulate the activity, stability, function and localization of proteins. One of the mechanisms used by cells in this context is the employment of post-translational protein modifications (van der Veen & Ploegh, 2012; Beltrao *et al.*, 2013). Typically, post-translational modifications are covalent modifications of amino acid residues of proteins (Prabakaran *et al.*, 2012). There is an enormous variety of post-translational modifications which contributes substantially to the large number of ways by which proteins are regulated. While some modifications, such as phosphorylation, acetylation and methylation, include the addition of a small moiety, others, such as ubiquitination and ubiquitin-like modifications, entail the attachment of a whole polypeptide to the target protein (Beltrao *et al.*, 2013). The focus of this thesis will be SUMOylation, a key ubiquitin-like protein modification.

1.1. Ubiquitination and ubiquitin-like protein modifications

1.1.1. Ubiquitin

In 1978, a group of scientists studying *in vitro* proteolysis by using lysates from rabbit reticulocytes described an ATP-dependent proteolysis process that requires a substance with an approximate molecular weight of 9 kDa, which is unusually heat-stable and is degraded by proteolytic enzymes (Ciechanover *et al.*, 2012; Callis, 2014). Two years later, the same authors reported that when the newly discovered protein is incubated with the reticulocytes fraction retained by DEAE cellulose in the presence of ATP, it ‘enters into high molecular weight conjugates’ (Ciechanover *et al.*, 1980; Callis, 2014). This work brought the team the 2004 Nobel Prize in Chemistry ‘for the discovery of ubiquitin-mediated protein degradation’ (Callis, 2014).

Ubiquitin is a eukaryotic 76-amino-acid polypeptide that adopts a β-grasp fold (Komander, 2009; Komander & Rape, 2012; Callis, 2014). Interestingly, the protein shows an extremely high degree of conservation (Komander & Rape, 2012; Callis, 2014). Ubiquitin is usually attached to its substrates by formation of a linkage between the C-terminal glycine residue of ubiquitin and the ε-amino group of a lysine (Komander, 2009; Callis, 2014).

The attachment of ubiquitin requires a specific enzymatic cascade including E1 activating enzymes, E2 conjugating enzymes and E3 ligases. Special deubiquitinating enzymes, referred as DUBs, release the ubiquitin from the substrates (Callis, 2014).

Substrates can be modified by only one ubiquitin molecule (monoubiquitination) and by multiple single ubiquitin molecules at multiple different sites (multi-monoubiquitination). Further, ubiquitin can be conjugated to substrates in the form of polyubiquitin chains. Depending on the residues used for the chain formation, polyubiquitin chains of types Met1, Lys6, Lys11, Lys27, Lys29, Lys33, Lys48, Lys63 can be generated. Additionally, the so-called 'linear' chains are generated by head-to-tail linkage of ubiquitin molecules through the α-amino group of their N-terminus. Furthermore, ubiquitin can form mixed chains including different types of ubiquitin-ubiquitin linkages and branched chains (Komander, 2009; Komander & Rape, 2012).

While ubiquitin was first described as a protein involved in ATP-dependent proteolysis, its involvement in a variety of non-proteolytic processes has become obvious. The proteolytic function of ubiquitin is mostly mediated by Lys48-linked ubiquitin chains. The proteins that need to be degraded are conjugated to Lys48 ubiquitin chains, which are recognized by the proteasome. Interestingly, another common type of ubiquitin chain formation - Lys63 - is not involved in proteasomal degradation but, for example, in DNA-damage response and signalling processes. Monoubiquitination and multi-monoubiquitination, likewise, are utilized for outcomes different from proteasomal degradation (Komander, 2009). Thus, the complexity of the biological outcomes of ubiquitination goes far beyond mere tagging for degradation.

1.1.2. Ubiquitin-like proteins

Ubiquitin-like proteins are eukaryotic proteins that resemble ubiquitin in sequence and three-dimensional structure. Most of the ubiquitin-like proteins also require an enzymatic cascade for their conjugation to proteins that is similar to the enzymatic cascade for the conjugation of ubiquitin (van der Veen & Ploegh, 2012). Furthermore, most of them possess a C-terminal diglycine motif which is uncovered after proteolysis of the proteins (Flotho & Melchior, 2013).

In 1987, a 15 kDa interferon-stimulated protein was shown to share a significant sequence similarity with ubiquitin (Haas *et al.*, 1987). Later, this protein was shown to be conjugated to other proteins (Loeb & Haas, 1992; Hochstrasser, 2009). This protein, called ISG15 (interferon-stimulated gene 15), was the first discovered ubiquitin-like modifier. ISG15 has two ubiquitin-like domains that show sequence and structural homology to ubiquitin (Zhang & Zhang, 2011). ISG15 expression is induced by type I interferons, which are secreted by cells infected with viruses. ISG15 is conjugated to both viral and host proteins.

Interestingly, ISG15 can also be secreted from IFN-treated T cells, monocytes, B cells and epithelial cells and might then function as a cytokine (D'Cunha *et al.*, 1996; van der Veen & Ploegh, 2012).

Nedd8 is one of the set of genes discovered to be downregulated in murine neural precursor cells during brain development. In 1993, this gene was named neural precursor cell-expressed, developmentally downregulated 8 (Kumar *et al.*, 1993; Herrmann *et al.*, 2007). Nedd8 is the ubiquitin-like modifier with the highest sequence similarity to ubiquitin. Nedd8 can be conjugated to almost all members of the cullin family, which are scaffold subunits of ubiquitin E3 ligase complexes (Herrmann *et al.*, 2007; van der Veen & Ploegh, 2012). Many of the cullin substrates play a role in cell cycle regulation, so that Nedd8 also has a function in this context (van der Veen & Ploegh, 2012). Interestingly, Nedd8 conjugation to proteins can also result in their degradation by the proteasome (Herrmann *et al.*, 2007).

FAT10 (human leukocyte antigen F-associated transcript 10) is a ubiquitin-like protein that contains two ubiquitin-like domains, and for this reason was first called ‘diubiquitin’ (Schmidtke *et al.*, 2014). In mammals, FAT10 is expressed in mature dendritic cells and B cells, while in other cell types its expression is induced by IFNγ and TNFα (van der Veen & Ploegh, 2012). FAT10 targets conjugated substrates for degradation by the 26S proteasome (Schmidtke *et al.*, 2014).

Ufm1 (ubiquitin-fold modifier 1) is a ubiquitin-like protein present in almost all eukaryotes with the exception of fungi. Even though not much is known about the biological function of Ufm1 conjugation, one of the processes that Ufm1 is mostly related to, is the endoplasmic reticulum stress response (Herrmann *et al.*, 2007; Daniel & Liebau, 2014). Furthermore, the Ufm1 cascade has been related to differentiation of erythroid progenitors and cell cycle control (Daniel & Liebau, 2014).

Atg8 and Atg12 are ubiquitin-like proteins related to the process of macroautophagy, which involves the sequestering of cytoplasm, macromolecules or whole organelles in the double-membrane autophagosome, subsequent autophagosome-lysosome fusion, and the degradation of cargo (van der Veen & Ploegh, 2012). Autophagy, in general, is a mechanism for elimination of non-functional cellular components and recycling of cellular constituents (Yang & Bassham, 2015). Atg8 and Atg12 are needed for the expansion and growth of the autophagosomal membrane. Atg12 is conjugated to a lysine residue of Atg5 which interacts with Atg16L1 and an Atg12-Atg5-Atg16L1 oligomer is formed by homo-oligomerization of Atg16L1. On the other hand, Atg8 does not get conjugated to proteins but to the phospholipid

phosphatidyletanolamine (PE), the Atg12-Atg5-Atg16L1 oligomer being involved in the conjugation (van der Veen & Ploegh, 2012).

Yet another ubiquitin-like protein that has been known is Hub1 (homologous to ubiquitin 1), also called beacon or UBL5 in mammals. A unique feature of Hub1 is the presence of dityrosine instead of diglycine at its C-terminus (van der Veen & Ploegh, 2012). In fission yeast, a role of Hub1 in pre-mRNA splicing has been described which is independent of conjugation (Wilkinson *et al.*, 2004; Herrmann *et al.*, 2007).

Urm1 (ubiquitin-related modifier 1) is regarded as a link between prokaryotic sulfur carriers and eukaryotic protein modifiers and is involved in two types of modifications (van der Veen & Ploegh, 2012). Firstly, resembling prokaryotic sulfur carriers, Urm1 transfers sulfur to the wobble uridine in several tRNA molecules. On the other hand, similar to protein modifiers, it can become conjugated to proteins (Vierstra, 2012).

1.2. SUMOylation

SUMOylation is a highly dynamic and reversible post-translational modification that involves the covalent attachment of a SUMO (small ubiquitin-like modifier) protein to a lysine residue of the target protein.

1.2.1. The SUMO proteins

The discovery of the first *SUMO* gene dates back to 1995 when Meluh and Koshland discovered it in a genetic screen for Mif2 suppressors (Meluh & Koshland, 1995). One year later, Matunis and collaborators demonstrated that RanGAP1 can be modified by SUMO (Matunis *et al.*, 1996; Geiss-Friedlander & Melchior, 2007).

The SUMO proteins have an approximate size of 10 kDa and are present in all eukaryotic organisms. While their three-dimensional structure closely resembles the one of ubiquitin, the SUMO proteins exhibit less than 20% sequence identity with ubiquitin and their surface-charge distribution is different from that of ubiquitin. A difference in the three-dimensional structures of the SUMO proteins and ubiquitin is the presence of an N-terminal unstructured domain in SUMO proteins, which is not present in ubiquitin. The formation of SUMO chains is attributed to this domain (Geiss-Friedlander & Melchior, 2007) .

While some eukaryotes, such as *Saccharomyces cerevisiae* and *Drosophila melanogaster*, have only one *SUMO* gene in their genome, in humans there are four SUMO proteins – SUMO1, SUMO2, SUMO3 and SUMO4. SUMO1, SUMO2 and SUMO3 are expressed ubiquitously while SUMO4 expression seems to be localized mainly to lymph

nodes, kidney and spleen. The sequence identity of the human mature forms of SUMO2 and SUMO3 is 97%. Thus, SUMO2 and SUMO3 are referred to as SUMO2/3. Conversely, mature human SUMO2 shares only approximately 50% identity with mature human SUMO1 (Johnson, 2004; Geiss-Friedlander & Melchior, 2007; Flotho & Melchior, 2013).

One of the main differences between SUMO1 and SUMO2/3 is the ratio between the free pool and the conjugated form. Almost all of the SUMO1 protein present in cells is conjugated to substrates. Oppositely, there is a large pool of free unconjugated SUMO2/3 (Saitoh & Hinchey, 2000; Johnson, 2004; Hay, 2005). However, upon certain aberrant cellular conditions, the conjugation of SUMO2/3 increases dramatically. Indeed, several studies have demonstrated a dramatic increase of SUMO2/3 conjugates upon heat shock in cell cultures (Saitoh & Hinchey, 2000; Golebiowski *et al.*, 2009; Castoralova *et al.*, 2012). Furthermore, oxygen and glucose deprivation in dissociated primary rat cortical neurons also results in an increase of SUMO2/3 conjugation (Geiss-Friedlander & Melchior, 2007; Guo *et al.*, 2013; Guo & Henley, 2014). Dramatic increase in SUMO2/3-ylation has also been shown *in vivo* upon conditions such as hibernation torpor, hypothermic cardiopulmonary bypass, etc. (Lee *et al.*, 2007; Cimarosti *et al.*, 2008; Yang *et al.*, 2008a; b; Yang *et al.*, 2009; Wang *et al.*, 2012; Yang *et al.*, 2014).

Another important difference between SUMO1 and SUMO2/3 is the presence of a consensus ψKxE sequence (Lys11) in SUMO2/3 but not in SUMO1, which is used as a conjugation site for SUMO chain formation (Johnson, 2004). Tatham and collaborators first demonstrated the formation of polySUMO chains by SUMO2 and SUMO3 *in vitro* involving the aforementioned Lys11 residue. The study also demonstrated formation of poly-SUMO2 chains in cell culture (Tatham *et al.*, 2001; Vertegaal, 2010; Flotho & Melchior, 2013). However, there is evidence that the formation of SUMO chains may not only depend on the presence of consensus SUMOylation sites. Even though Matic and collaborators implied that conjugation of SUMO1 terminates the formation of SUMO2/3 due to the lack of a consensus site (Matic *et al.*, 2008), other groups demonstrated the formation of SUMO1 chains *in vitro* (Pichler *et al.*, 2002; Pedrioli *et al.*, 2006; Yang *et al.*, 2006). Furthermore, mass spectrometric analyses have provided evidence in cell culture for the formation of SUMO chains that involve several non-consensus SUMOylation sites in SUMO1, SUMO2 and SUMO3 (Hsiao *et al.*, 2009; Blomster *et al.*, 2010; Matic *et al.*, 2010; Bruderer *et al.*, 2011; Flotho & Melchior, 2013). The knowledge about the functional significance of SUMO chain formation is restricted (Flotho & Melchior, 2013). Notably, one of the interesting functions of SUMO chain formation is linked to the ubiquitin-proteasome system. The ubiquitin ligase in

mammals RNF4 is a SUMO chain binder that conjugates ubiquitin to polySUMOylated proteins and thus mediates their degradation via the proteasome (Tatham *et al.*, 2008). Furthermore, SUMO chains have been shown, for example, to exhibit a profound accumulation upon heat shock (Golebiowski *et al.*, 2009). SUMO chains have also been implicated in mitosis and meiosis (Vertegaal, 2010).

An important point that needs to be mentioned is that the usage of the mammalian SUMO2 and SUMO3 nomenclature has been confusing. Several groups follow the nomenclature that was initially introduced by Saitoh and Hinchey in 2000, which defines SUMO2 as the protein whose mature form is 92 amino acids long, while the mature form of SUMO3 is 93 amino acids (Saitoh & Hinchey, 2000; Flotho & Melchior, 2013). However, in the online databases, the nomenclature has been switched and this type of nomenclature is used by other research groups. This can be misleading since not everybody is aware of these discrepancies and publications rarely give a clear definition of the nomenclature that they use. In this doctoral thesis, I have used the nomenclature that has been adopted by the online databases.

The fourth SUMO paralog, SUMO4, shows high sequence similarity to SUMO2. However, despite this high similarity, several reasons argue against an ability of SUMO4 to be conjugated to substrates. First, the gene encoding SUMO4 lacks introns, which hints towards SUMO4 being a pseudogene. Second, even though SUMO4 mRNA is expressed in lymph, kidney and spleen (Bohren *et al.*, 2004; Guo *et al.*, 2004), information about the presence of endogenous SUMO4 protein is lacking. Last, Owerbach and collaborators have demonstrated that the presence of proline at a critical position in SUMO4 inhibits the maturation needed for conjugation to substrates (Owerbach *et al.*, 2005). However, exogenously expressed SUMO4 can be processed to a mature form and be conjugated to substrates upon stressful conditions (Geiss-Friedlander & Melchior, 2007; Wei *et al.*, 2008; Wilkinson & Henley, 2010; Flotho & Melchior, 2013).

1.2.2. SUMO conjugation

The enzymatic cascade for the conjugation of SUMO to substrates closely resembles the ubiquitination cascade. SUMO proteins are first activated by the action of an E1 activating enzyme. This enzyme is a heterodimer of two subunits, SUMO-activating enzyme 1 (SAE1; also called Aos1) and SUMO-activating enzyme 2 (SAE2, also called Uba1). Initially, the activation reaction involves the formation of a SUMO adenylate intermediate, a step that requires ATP hydrolysis (Flotho & Melchior, 2013). Then, a thioester bond is formed

between the C-terminal glycine of SUMO and the cysteine at the active site of SAE2. Afterwards, the SUMO moiety is transferred from the active-site cysteine of the E1 enzyme to the active-site cysteine of the E2 conjugating enzyme Ubc9 (Wilkinson & Henley, 2010). Ubc9 plays the role of a donor of activated SUMO for the final reaction of conjugation of SUMO to the ε-NH_2 group of a lysine residue (Johnson, 2004). Notably, and in contrast to the numerous E2 enzymes that conjugate ubiquitin to specific substrates, only one conjugating enzyme has been found to conjugate SUMO (Komander, 2009). Besides its role as a donor of activated SUMO, Ubc9 can also participate in the selection of substrates by directly binding to consensus SUMOylation sites (Flotho & Melchior, 2013). The sequence of the consensus site is ψKxD/E, where ψ is a large hydrophobic residue and x is any amino acid (Wilkinson *et al.*, 2010). The consensus SUMOylation sequence can be recognized if it is a part of an extended loop or of an unstructured area (Geiss-Friedlander & Melchior, 2007). However, it should be noted that SUMOylation can take place not only at a consensus SUMOylation site and not all consensus sites can be SUMOylated (Wilkinson & Henley, 2010).

Even though high concentrations of Ubc9 can be sufficient for SUMO conjugation *in vitro*, the process is normally assisted by the action of E3 ligases (Geiss-Friedlander & Melchior, 2007; Flotho & Melchior, 2013). The largest group of SUMO E3 ligases described till now possesses a characteristic SP-RING motif, which resembles the RING domain found in many ubiquitin E3 ligases (Geiss-Friedlander & Melchior, 2007). The SP-RING ligases bind non-covalently to Ubc9, the substrate, and SUMO (via a SIM (SUMO-interacting motif)). Thus, these E3 ligases act as a platform that brings together SUMO-loaded Ubc9 and the substrates and thus favours SUMO conjugation (Geiss-Friedlander & Melchior, 2007; Wilkinson & Henley, 2010). In yeast, the SP-RING ligase family includes Siz1, Siz2, Mms21 and potentially Zip3. In humans, the members of the family are the PIAS (protein inhibitor of activated STAT) proteins, namely PIAS1, PIAS3, PIASy, PIASxα, PIASxβ and Nse2/Mms21 (Flotho & Melchior, 2013).

A second type of SUMO E3 ligases is represented by the vertebrate-specific protein RanBP2 (Geiss-Friedlander & Melchior, 2007). In 2012, Werner and collaborators demonstrated that *in vivo* RanBP2 actually acts as an E3 ligase in a complex with Ubc9 and SUMO1-conjugated RanGAP1 (Werner *et al.*, 2012).

SUMO E3 ligase function has also been attributed to other proteins. One of them is Pc2, which is a part of the multimeric polycomb repressive complex (PRC1) that facilitates CtBP1 SUMOylation. Other proteins with E3 ligase activity are HDAC4, p14 Arf, and TOPORS (Geiss-Friedlander & Melchior, 2007; Flotho & Melchior, 2013).

The highly dynamic and reversible nature of SUMOylation is secured by the action of SUMO proteases, which can rapidly cleave the SUMO moiety from substrates. Besides deSUMOylation, the proteases are involved in the process of maturation of SUMO proteins. Since all SUMO proteins are translated in the form of inactive precursors, they undergo cleavage at their C-terminus, which exposes the diglycine motif needed for conjugation to substrates. The first identified family of proteases is the Ulp/SENP family. The Ulp/SENP family comprises two members in yeast, Ulp1 and Ulp2, and six in mammals, SENP1, SENP2, SENP3, SENP5, SENP6 and SENP7. The mammalian proteins show differences with regard to their SUMO paralog specificity, subcellular localization and preference for performing SUMO maturation and/or deSUMOylation of substrates. Additional SUMO proteases that were identified are DeSI-1 (deSUMOylating isopeptidase-1), DeSI-2, and USPL1 (Wilkinson *et al.*, 2010; Flotho & Melchior, 2013).

1.2.3. Essentiality of SUMOylation

The process of SUMOylation is essential for almost all eukaryotic organisms. Exceptions are the fission yeast *Schizosaccharomyces pombe* and the fungus *Aspergillus nidulans.* Even though not causing lethality, the disruption of the *SUMO* gene in both *S. pombe and A. nidulans* results in pronounced growth defects (Tanaka *et al.*, 1999; Wong *et al.*, 2008; Flotho & Melchior, 2013). Disruption of two of the eight SUMO genes in *Arabidopsis thaliana* (*AtSUMO1* and *AtSUMO2*) causes lethality (Saracco *et al.*, 2007; Flotho & Melchior, 2013). Disruption of Ubc9 in the chicken DT40 lymphocyte cell line, on the other hand, causes chromosome segregation defects and eventually death by apoptosis (Hayashi *et al.*, 2002; Wilkinson & Henley, 2010). Finally, Ubc9-deficient mice die as embryos (Nacerddine *et al.*, 2005).

An interesting question that still remains to be fully answered concerns the requirement of specific SUMO paralogs for the survival of an organism and the compensation for the loss of one SUMO paralog by other paralogs. Alkuraya and collaborators reported the case of a 5-year-old female with cleft lip and palate who has SUMO1 haploinsufficiency due to an insertion in the *SUMO1* gene. The authors went further and generated mice that bear a β-galactosidase insertion in the *SUMO1* gene and observed that 4 out of 46 heterozygous pups showed cleft lip and palate. Furthermore, some pups homo- and heterozygous for the insertion died as embryos or immediately after birth (Alkuraya *et al.*, 2006). However, in 2008, two studies reported the lack of lethality and any overt phenotypic changes in mice lacking SUMO1, indicating that SUMO2/3 can compensate for lacking SUMO1 (Evdokimov *et al.*,

2008; Zhang *et al.*, 2008; Wilkinson & Henley, 2010). Furthermore, a recent study by Wang and collaborators reported that while SUMO3-null mice are viable, SUMO2-null mice die as embryos. In view of the extremely high sequence similarity between SUMO2 and SUMO3, this finding was unexpected. However, using a quantitative RT-PCR to determine levels of SUMO1, SUMO2 and SUMO3 in E7.5 and E8.5 embryos, the authors identified SUMO2 as the most predominant form, being up to forty times more abundant than SUMO3 (Wang *et al.*, 2014).

1.2.4. Consequences of SUMOylation

SUMOylation can affect different protein characteristics, including localization, stability, and activity. The molecular consequences of SUMOylation fall into three main categories. First, SUMOylation can mask a binding site of a protein. For example, SUMOylation of the ubiquitin-conjugating enzyme E2-25K blocks its interaction with the ubiquitin E1 enzyme (Pichler *et al.*, 2005; Geiss-Friedlander & Melchior, 2007; Wilkinson & Henley, 2010). Second, conjugated SUMO can participate in the formation of a new interaction surface for proteins that interact directly with SUMO or with a domain that is created both by the substrate and conjugated SUMO. For example, transcriptional repression by p300 is achieved by SUMO conjugation since HDAC6 is recruited by SUMO (Girdwood *et al.*, 2003; Geiss-Friedlander & Melchior, 2007; Wilkinson & Henley, 2010). Three, SUMOylation can result in a change in the conformation of the substrate. Indeed, SUMOylation of thymine DNA glycosylase (TDG) results in a conformational change in TDG that leads to release from DNA (Geiss-Friedlander & Melchior, 2007; Wilkinson & Henley, 2010).

The majority of SUMO substrates described till now are nuclear. Thus, SUMOylation research has mainly focused on processes related to the nucleus, such as transcription, DNA repair, chromatin remodelling, or formation of nuclear bodies (Flotho & Melchior, 2013). Up to now, a large number of transcriptional activators, repressors, coactivators and corepressors have been shown to be SUMOylated. Even though there are cases where SUMOylation leads to transcriptional activation, SUMOylation appears to be mainly involved in transcriptional repression (Johnson, 2004). For example, SUMOylation of the transcription factor Elk-1 is required for its repressive activity (Yang *et al.*, 2003). The involvement of SUMOylation in DNA repair is exemplified by a variety of cases. One of them is the aforementioned SUMOylation of TDG, an enzyme acting in the base excision repair pathway (Gill, 2004; Bergink & Jentsch, 2009). Interestingly, histone proteins are also SUMO substrates (Gill,

2004). SUMOylation is further involved in the regulation of a variety of processes by its association with the formation of PML nuclear bodies (Sahin *et al.*, 2014). Not only is SUMOylation of PML of critical importance for the formation of nuclear bodies, but many of the other components of PML bodies can be SUMOylated (Gill, 2004).

In spite of the enrichment of SUMO targets in the nucleus, SUMOylation is unquestionably not restricted to this cellular compartment. A variety of SUMO modifications have been reported for substrates residing outside of the nucleus. In 2004, Harder and collaborators reported significant levels of SUMO1 conjugates in the mitochondrial fraction of COS7 cells. Furthermore, they identified dynamin-related protein 1 (DRP1) as a SUMO1 substrate. DRP1 is involved in mitochondrial dynamics by mediating mitochondrial fragmentation or fission. Upon transient transfection of SUMO1, mitochondrial fission was found to be increased, likely, due to the fact that SUMO1 overexpression stabilizes DRP1 (Harder *et al.*, 2004). Another example of a regulation of an extranuclear process by SUMOylation is plasma membrane association. In 2012, Huang and collaborators revealed that SUMOylation assists binding of PTEN (tumour suppressor phosphatase and tensin homologue) to the plasma membrane (Huang *et al.*, 2012; Flotho & Melchior, 2013).

Importantly, quantitative SUMOylation is attributed only to a few targets, such as RanGAP1, while for the rest of the SUMO substrates only a small fraction of the available protein is SUMOylated at any given time. The lack of quantitative SUMOylation complicates the identification of SUMO targets and poses the question as to how a small amount of modified protein can cause such a significant effect (Geiss-Friedlander & Melchior, 2007).

1.2.5. SUMOylation and human disease pathogenesis

The essential role of SUMOylation in regulating protein function decidedly determines its crucial role in human disease pathogenesis. A variety of studies have focused on the link between SUMOylation and tumorigenesis. For example, the levels of the E2 SUMO conjugating enzyme Ubc9 have been shown to be increased in several human cancers, such as lung adenocarcinoma, ovarian tumors, and melanoma-positive lymph nodes (McDoniels-Silvers *et al.*, 2002; Mo *et al.*, 2005; Moschos & Mo, 2006; Moschos *et al.*, 2007). Furthermore, overexpression of Ubc9 in MCF-7 human breast cancer tumor cells significantly increased their growth (Mo *et al.*, 2005; Sarge & Park-Sarge, 2009). Increased levels of the E3 ligase PIAS3 have also been associated with various types of human cancers such as lung, breast, and prostate cancer (Wang & Banerjee, 2004; Sarge & Park-Sarge, 2009). Interestingly, lower survival of patients with hepatocellular carcinoma correlates with

increased levels of the SUMO E1 activating enzyme, while, on the contrary, longer metastasis-free survival of patients with breast cancer with high Myc levels correlates with low levels of SUMO E1 activating enzyme (Lee & Thorgeirsson, 2004; Sarge & Park-Sarge, 2009; Kessler *et al.*, 2012; Flotho & Melchior, 2013).

A significant number of reports have also indicated a link between SUMO conjugation and heart disease. Two missense mutations of lamin A glutamic acid 203, E203G and E203K, have been associated with familial dilated cardiomyopathy and conduction system disease (Fatkin *et al.*, 1999; Jakobs *et al.*, 2001). Interestingly, in 2008, Zhang and Sarge demonstrated that lamin A is SUMOylated at lysine 201, which is located within the SUMOylation consensus motif ψKxE. Thus, it turned out that the two disease-associated mutations take place within the consensus motif and reduce SUMOylation of lamin A (Zhang & Sarge, 2008b; Sarge & Park-Sarge, 2009). Furthermore, Kho and collaborators associated decreased SUMO1 levels with failing human hearts, as well as with heart failure in mice. Notably, overexpression of SUMO1 in those mice ameliorated the cardiac function. In this report, the authors suggest that the reduction of SUMOylation of SERCA2a could contribute to heart failure (Kho *et al.*, 2011; Flotho & Melchior, 2013).

A very pronounced involvement of SUMOylation in the pathology of neurodegenerative disorders has been indicated by several studies. This issue will be discussed below.

1.3. SUMOylation in neurons

SUMOylation in neurons has received pronounced attention over the past decade. A large number of proteins that are essential for neuronal function have been proposed as SUMOylation substrates.

1.3.1. Subcellular localization of the SUMOylation machinery in neurons

Besides the nuclear SUMO substrates, evidence of a large variety of extranuclear SUMO substrates in neurons has just started to emerge. The affirmation of those proteins as SUMO targets, however, requires that an important question is answered: Where can the SUMOylation machinery be found in neurons? Notably, addressing this question has produced some quite controversial results, especially when the issue was investigated by immunostaining. For example, with regard to SUMO1, most studies in non-neuronal cell cultures show predominantly nuclear localization of endogenous and overexpressed protein. Furthermore, several studies using anti-SUMO1 antibodies for staining rat primary neurons

reported significant presence of SUMO1 labelling in axons, dendrites, and synapses besides the predominant nuclear localization (Martin *et al.*, 2007a; Chao *et al.*, 2008; Konopacki *et al.*, 2011; Loriol *et al.*, 2012; Girach *et al.*, 2013; Jaafari *et al.*, 2013; Loriol *et al.*, 2013; Henley *et al.*, 2014). In contrast, in 2012, Tirard and collaborators reported the generation of a SUMO1 knock-in mouse model expressing double affinity tagged His_6-HA-SUMO1 instead of wild type SUMO1 from the endogenous genetic locus. This proved to be an excellent mammalian model for the identification and localization of SUMO1 substrates *in vivo*. Staining primary hippocampal neuronal cultures from this model with a reliable anti-HA antibody, Tirard and collaborators observed His_6-HA-SUMO1 predominantly in the nucleus but it did not colocalize with synaptic markers. These results were confirmed *in vivo* by immunostaining of brain sections (Tirard *et al.*, 2012). Thus, the latter finding represents a reason to reconsider some of the previously published results obtained with the use of not very reliable antibodies. Apart from immunostaining, the subcellular localization of SUMO1 in neurons was studied by subcellular fractionation experiments. In 2007, Martin and collaborators presented data indicating high levels of SUMO1-conjugated proteins in the synaptosomal and the postsynaptic density fractions of rat brains (Martin *et al.*, 2007a). Tirard and collaborators also used subcellular fractionation of brains from the His_6-HA-SUMO1 KI mice to study the subcellular localization of SUMO1. The experiment revealed the expected high abundance of SUMO1-conjugated proteins in the nucleus. Furthermore, SUMO1 conjugates were found in cytosol, synaptic cytosol, and synaptic vesicle fractions, but SUMO1 conjugates were not present in the synaptic membrane fractions (Tirard *et al.*, 2012).

Regarding the localization of SUMO2/3, most immunostaining studies in non-neuronal cell cultures show that endogenous SUMO2/3 reside predominantly in the nucleus. Furthermore, overexpression of SUMO2 or SUMO3 in non-neuronal cell cultures results mainly in nuclear signal. Again, similar to SUMO1, in rat primary neurons SUMO2/3 were shown to be significantly present in axons, dendrites and synapses (Loriol *et al.*, 2012; Jaafari *et al.*, 2013; Loriol *et al.*, 2013; Henley *et al.*, 2014). Notably, some *in vivo* studies in rats show the presence of SUMO2/3 in the cytoplasm of different brain regions (Yang *et al.*, 2008a; Yang *et al.*, 2009; Wang *et al.*, 2012). Regarding the other components of the SUMOylation machinery, in rat primary neurons E1 complex, Ubc9, SENPs and PIAS proteins were also found in axons, dendrites and synapses (Martin *et al.*, 2007a; Loriol *et al.*, 2012; Jaafari *et al.*, 2013; Loriol *et al.*, 2013; Henley *et al.*, 2014). Furthermore, Ubc9, Aos1, SENP1 and SENP6 were found in the synaptosomal fraction of rat brains (Feligioni *et al.*, 2009; Loriol *et al.*, 2012; Henley *et al.*, 2014). However, given the controversial results for

SUMO1 and the fact that key controls were often missing in the relevant studies, further research is required to investigate these issues.

Recent research has also addressed the link between synaptic SUMOylation and neuronal activity. For example, Loriol and collaborators reported that upon KCl stimulation of rat primary neurons, the immunoreactivity of SUMO1 in the pre-synapse increases while the immunoreactivity of SUMO2/3 decreases in the postsynapse (Loriol *et al.*, 2013; Henley *et al.*, 2014).

1.3.2. Spatiotemporal distribution of the SUMOylation machinery in the developing mammalian brain

Another question that has received attention with regard to elucidating the role of SUMOylation in neuronal function is the spatiotemporal distribution of SUMOylation during mammalian brain development. In 2008, Watanabe and collaborators examined the levels of Ubc9 mRNA throughout the development of the rat brain. They noted that the expression of Ubc9 increases from E13 to E18 and after that decreases throughout development. Moreover, the protein levels of Ubc9 were also high during the embryonic stage and then decreased. Similarly, SUMO1 conjugates showed high levels during the embryonic stage and then decreased. Regarding the spatial distribution of Ubc9 mRNA during development, *in situ* hybridization showed that during the embryonic stage Ubc9 is present in many different brain regions, but it is predominantly present in areas with proliferating neural stem cells. In the adult brain, Ubc9 mRNA was mainly found in dentate granular neurons, pyramidal neurons in the hippocampus, and in large pyramidal neurons in the cortex. Considering these results, the authors suggested that SUMOylation participates in neuronal proliferation and differentiation in the developing brain and in neuronal plasticity in the adult brain (Watanabe *et al.*, 2008; Henley *et al.*, 2014). Additionally, another study investigated the levels of the SUMOylation machinery throughout the development of the rat brain. Similar to the study mentioned previously, SUMO1 conjugation levels were highest at E12 and then decreased slowly. Interestingly, the authors also investigated SUMO2/3 conjugation levels, which peaked at E12 and at birth. Ubc9 levels were also developmentally regulated, with highest levels of Ubc9 between E15 and E18, and decreasing after birth. The study also examined the levels of SENP1 and SENP6, which exhibited high expression early in development and decreased after that. Finally, the levels of Aos1 were almost stable throughout development (Loriol *et al.*, 2012; Henley *et al.*, 2014). The decrease of SUMO1 conjugates during mammalian development was also demonstrated by Tirard and collaborators who compared the SUMO1

conjugation levels in the brains of mice varying from postnatal day 0 to postnatal day 56 (Tirard *et al.*, 2012). Finally, a very detailed investigation of the spatiotemporal distribution of SUMO proteins and Ubc9 during mouse brain development was published by Hasegawa and collaborators in 2014. Ubc9 protein levels were shown to be highest at E10.5 and at E12.5 and decreased with development. Furthermore, total SUMO1 and SUMO2/3 conjugation levels were once again seen to decrease with development. Regarding the localization of the SUMO proteins, during the embryonic stage SUMO1 and SUMO2/3 immunoreactivity were localized to the nucleoplasm of nestin-positive neural stem cells. Interestingly, while many neurons in the adult brain had SUMO1, SUMO2/3 were mainly localized in neurogenic regions, such as the subventricular zone and the hippocampal subgranular zone (Hasegawa *et al.*, 2014).

1.3.3. SUMOylation in the neuronal nucleus

In agreement with the essential role of SUMOylation for regulating nuclear processes, a number of nuclear proteins have been shown to be SUMOylation targets in neurons. Some of them are transcription factors. The Pax family of transcription factors, for example, is involved in cell specification in the central nervous system, starting early in development. Several members of this family have been identified as SUMOylation substrates. Pax6, for instance, is involved in brain and eye development (Gwizdek *et al.*, 2013). Yan and collaborators showed that SUMOylation facilitates the binding of Pax6 to DNA and thus stimulates gene expression (Yan *et al.*, 2010; Gwizdek *et al.*, 2013; Henley *et al.*, 2014). Pax7, on the other hand, is a transcription factor with a role in neural crest and muscle development (Gwizdek *et al.*, 2013). SUMOylation of Pax7 was shown to play an essential role in the development of the neural crest (Luan *et al.*, 2013; Henley *et al.*, 2014). Another SUMOylated transcription factor, MEF2A, plays an important role in the formation of dendritic claws, specialized structures formed by the dendrites of cerebellar granule neurons to contact the terminals of mossy fibers to form synapses (Wilkinson *et al.*, 2010; Henley *et al.*, 2014). In 2006, Shalizi and collaborators demonstrated that SUMOylation of MEF2A represses its transcriptional activity and thus promotes dendritic claw formation. Neuronal activation, on the other hand, promoted a molecular switch from SUMOylation to acetylation which led to activation of MEF2A and inhibited dendritic claw formation (Shalizi *et al.*, 2006; Gwizdek *et al.*, 2013). SUMOylation of two transcription factors has also been shown to be involved in rod photoreceptor development. Nrl and Nr2e3 are transcription factors that activate the expression of rod-specific genes while suppressing the expression of cone-specific genes. SUMOylation of Nr2e3 was shown to be important for the repression of cone-

specific genes (Onishi *et al.*, 2009), while SUMOylation of Nrl promotes the expression of the rod-specific genes rhodopsin and Nr2e3 (Roger *et al.*, 2010; Gwizdek *et al.*, 2013; Henley *et al.*, 2014). Other SUMOylated transcription factors that are important for the proper function of neurons are MeCP2, the SUMOylation of which is involved in synapse development, BMAL1, which is SUMOylated in the context of circadian rhythms (Wilkinson *et al.*, 2010; Henley *et al.*, 2014).

Apart from SUMO targets, another protein related to SUMOylation is the *Drosophila* SUMO protease Verloren. Verloren has been shown to function in olfactory projection neurons target selection, i.e. in the targeting of their dendrites to antennal lobe glomeruli and of their axons to higher brain centers (Berdnik *et al.*, 2012; Henley *et al.*, 2014).

1.3.4. Extranuclear SUMOylation in neurons

As mentioned above, despite the fact that the majority of SUMO substrates reside in the nucleus, extranuclear roles of SUMOylation have received ever increasing attention. The interest in the identification of new extranuclear substrates is, naturally, also relevant for neurons.

An example of an extranuclear protein important for neuronal functioning and a SUMOylation target is the mRNA-binding protein La. La supports axonal protein synthesis by binding mRNAs and promoting their axonal trafficking (Wilkinson *et al.*, 2010). In 2007, van Niekerk and collaborators demonstrated La SUMOylation in cultured mouse dorsal root ganglion neurons and isolated mouse sciatic nerve and showed that SUMOylation of La determines its interaction with dynein, thus stimulating retrograde transport to the cell body. In mouse dorsal root ganglion neurons, La, which cannot be SUMOylated, moves only in anterograde direction (van Niekerk *et al.*, 2007; Wilkinson *et al.*, 2010).

Some proteins residing in the plasma membrane have also been shown to be substrates of SUMO modification. One report, for example, demonstrated the SUMOylation of the potassium leak channel K2P1, which helps the preservation of the resting membrane potential below the threshold in excitable cells (Rajan *et al.*, 2005). The channel mRNA is known to be strongly expressed in heart, brain and kidney (Orias *et al.*, 1997). The authors stated that SUMOylation is responsible for keeping the channel in an inactive state (Rajan *et al.*, 2005). However, later Feliciangeli and collaborators failed to observe SUMO modification of this channel, which left the question about the SUMOylation of K2P1 open (Feliciangeli *et al.*, 2007; Feliciangeli *et al.*, 2010). Finally, in 2010 Plant and collaborators revalidated the SUMOylation of K2P1 (Plant *et al.*, 2010; Wilkinson *et al.*, 2010; Henley *et al.*, 2014).

Another potassium channel which is expressed in the brain and is also considered to be SUMOylated is the voltage-gated Kv1.5 (Benson *et al.*, 2007; Wilkinson *et al.*, 2010). Furthermore, the glucose transporters GLUT1 and GLUT4 were the first membrane proteins described as SUMOylation targets. They have been shown to be highly expressed in the brain. Overexpression of Ubc9 resulted in a 65% decrease in the levels of GLUT1 and an eight-fold increase in the GLUT4 levels (Giorgino *et al.*, 2000; Martin *et al.*, 2007b; Wilkinson *et al.*, 2010).

A large number of studies reported important roles of SUMOylation in synapse formation and function by demonstrating SUMO modification of synaptic proteins. One of the synaptic proteins that has been shown to be SUMOylated is the calcium/calmodulin-dependent serine protein kinase (CASK). CASK is a scaffold protein that is necessary for dendritic spine formation. Chao and collaborators demonstrated that CASK SUMOylation reduces the interaction between CASK and protein 4.1. Furthermore, overexpression of SUMO1-CASK led to defective synapse formation (Chao *et al.*, 2008; Wilkinson *et al.*, 2010). Another proposed synaptic target of SUMOylation is the kainate receptor subunit GluK2. Kainate receptors are glutamate-gated ion channels which are strongly represented at synapses throughout the brain and can act both pre- and postsynaptically. In 2007, Martin and collaborators showed in rat hippocampal neurons that SUMOylation is triggered by agonist stimulation and that this leads to endocytosis of kainate receptors containing the GluK2 subunit (Martin *et al.*, 2007a; Wilkinson *et al.*, 2010; Henley *et al.*, 2014). Another study proposed as a synaptic SUMOylation substrate the active zone protein Rab3 interacting molecule 1 alpha (RIM1α). SUMOylation of RIM1α was shown to be required for the Ca^{2+} channel clustering function of the protein (Girach *et al.*, 2013; Henley *et al.*, 2014). Interestingly, in 2015 Tang and collaborators demonstrated that SUMOylation of synapsin Ia is needed for its proper functioning. Synapsins cluster presynaptic vesicles, bind them to the actin cytoskeleton and release the vesicles upon depolarization (Tang *et al.*, 2015). Very recently, one of the synaptic SNARE proteins, syntaxin1A, was identified to be SUMOylated and this SUMOylation was shown to be activity-dependent. The authors proposed that the SUMOylation of syntaxin1A regulates vesicle endocytosis (Craig *et al.*, 2015).

At present, it is unclear whether the currently available data on extranuclear and synaptic SUMOylation in neurons can be taken at face value. Essentially none of the relevant studies involving immunostaining in cells or tissues employed truly stringent controls, such as SUMO knock-outs, and knock-in mice expressing His_6-HA-SUMO1 instead of wild-type SUMO1 yielded no evidence for extranuclear or synaptic SUMO1 conjugation, apart from

annulate lamellae. Consequently, current and quite prominently published claims regarding extranuclear and synaptic SUMO conjugation in neurons have to be regarded with caution.

1.3.5. SUMOylation and neurodegenerative diseases

The essential role of SUMOylation in neuronal development and function explains the increasing number of studies attempting to elucidate the link between SUMOylation and the pathogenesis of a variety of neurological diseases. Special attention has focused on the involvement of SUMOylation in neurodegenerative disorders. Notably, major players in the pathogenesis of different neurodegenerative diseases, such as α-synuclein, ataxin-1, huntingtin, SOD1, are thought to be modified by SUMOylation.

Importantly, SUMO proteins are extremely soluble, which has led to utilization of SUMO as a tag for the expression and purification of proteins. Given the fact that the majority of neurodegenerative diseases are characterized by decreased solubility of specific proteins and their pathological aggregation, it has been suggested that SUMOylation can regulate protein solubility and aggregation in neurodegeneration (Krumova & Weishaupt, 2013).

Parkinson's disease is the second most common neurodegenerative disorder, characterized by degeneration of dopaminergic neurons in the *substantia nigra* in the midbrain and the presence of neuronal inclusions called Lewy bodies, with the major component α-synuclein. In 2006, Dorval and Fraser were the first to demonstrate the mono-SUMOylation of α-synuclein by overexpressing α-synuclein and SUMO in HEK293 cells (Dorval & Fraser, 2006). Later, Krumova and collaborators investigated the importance of SUMOylation for the aggregation of α-synuclein in both, *in vitro* fibril formation assay and in a cell-line based assay. It was reported that non-SUMOylated α-synuclein forms fibrils while SUMO modification of the protein abolishes the formation of fibrils. Additionally, the cell-based assay demonstrated that the overexpression of a SUMOylation-deficient form of α-synuclein correlates with higher cellular toxicity when compared to the wild type form. Finally, this study also confirmed the SUMOylation of α-synuclein *in vivo* utilizing a His_6-SUMO3 expressing transgenic mouse model (Krumova *et al.*, 2011; Krumova & Weishaupt, 2013). Yet another study explored the consequences of α-synuclein SUMOylation, demonstrating that SUMOylation enhances the release of α-synuclein via extracellular vesicles (Kunadt *et al.*, 2015). Furthermore, Shinbo and collaborators reported the SUMOylation of another protein that has been implicated in the pathogenesis of Parkinson's disease, DJ-1. The authors demonstrated that SUMOylation is required for all activities of this multifunctional protein (Shinbo *et al.*, 2006).

SUMOylation has also been linked to polyglutamine disorders, a group of diseases that results from toxic expansion of trinucleotide repeats, CAG. Huntington's disease is characterized by an extended polyglutamine repeat in the Huntingtin protein. In 2004, Steffan and collaborators showed that SUMO can modify a pathogenic fragment of Huntingtin. The authors reported that in cultured cells SUMOylation of this mutant fragment increases its stability and reduces its aggregation. Furthermore, they showed that in a *Drosophila melanogaster* model of Huntington's disease, animals heterozygous for a SUMO mutation exhibit decreased degeneration when compared to animals having normal levels of SUMO (Steffan *et al.*, 2004; Krumova & Weishaupt, 2013). Notably, in 2008 Subramaniam and collaborators reported that the striatal-specific protein Rhes stimulates SUMOylation of mutant Huntingtin (Subramaniam *et al.*, 2009).

Another polyglutamine disorder, spinocerebellar ataxia type I, is characterized by polyglutamine expansions in ataxin-1. In 2005, Riley and collaborators demonstrated that SUMOylation of ataxin is decreased in the polyglutamine-expanded form of the protein. Furthermore, the authors revealed that SUMOylation depends on the ataxin-1 being able to enter the nucleus (Riley *et al.*, 2005; Sarge & Park-Sarge, 2009).

Yet another polyglutamine disease that has been linked to SUMOylation is spinal and bulbar muscular atrophy (SBMA), which is caused by polyglutamine expansion of the androgen receptor (AR). AR has been shown to be SUMOylated, the modification resulting in repression of its transcriptional activity (Poukka *et al.*, 2000; Nishida & Yasuda, 2002; Wilkinson *et al.*, 2010; Henley *et al.*, 2014). Moreover, in a *Drosophila* model of SBMA, the overexpression of a catalytically inactive form of the SUMO1 activating enzyme results in enhanced neurodegeneration (Chan *et al.*, 2002; Krumova & Weishaupt, 2013). Furthermore, a recent study also revealed a link between SUMOylation and SBMA by coexpressing SUMO3 in HELA cells expressing the polyglutamine-extended form of AR. The coexpression of SUMO3 was found to decrease the aggregation of AR (Mukherjee *et al.*, 2009; Wilkinson *et al.*, 2010).

Notably, a link between SUMOylation and amyotrophic lateral sclerosis (ALS) has also been established. ALS is a motor neuron disease characterized by degeneration of both upper and lower motor neurons. A substantial number of familial ALS cases are caused by mutations in the gene for superoxide dismutase (SOD1) (Sarge & Park-Sarge, 2009). SUMOylation of human SOD1 was demonstrated by Fei and collaborators in 2006. The authors showed that SUMOylation of SOD1 increases protein stability and aggregation (Fei *et al.*, 2006). Another protein that has also been related to ALS pathogenesis is the astroglial

glutamate transporter EAAT2, which generates a CTE fragment upon cleavage by caspase-3. In a mouse model of ALS, Foran and collaborators showed that the CTE fragment is SUMO1-modified which triggers its accumulation in the nuclei of spinal cord astrocytes (Foran *et al.*, 2011; Krumova & Weishaupt, 2013).

Neuronal intranuclear inclusion disorder (NIID) is a rare slowly progressing neurodegenerative disease, characterized by the presence of neuronal intranuclear inclusions. Interestingly, it was demonstrated that these inclusions show strong SUMO immunoreactivity in familial, juvenile and sporadic cases of NIID (Pountney *et al.*, 2003; McFadden *et al.*, 2005; Takahashi-Fujigasaki *et al.*, 2006; Wilkinson *et al.*, 2010).

Finally, an increasing number of studies indicate a link between SUMOylation and Alzheimer's disease (AD) pathogenesis. This will be discussed in detail below.

1.4. Alzheimer's disease

In 1906, at the Meeting of the South-West German Psychiatrists held in Tübingen, the Bavarian psychiatrist and neuroanatomist Alois Alzheimer described the case of a 50-year-old woman who had been hospitalized for progressive memory disturbances, sleep problems, paranoia, confusion and aggression. Alzheimer reported the presence of plaques, neurofibrillary tangles and arteroscleriotic changes. This was the first description of AD which subsequently appeared in 1910 in the third edition of Psychiatrie (Alzheimer, 1907; Maurer *et al.*, 1997; Hippius & Neundorfer, 2003).

AD is the most common neurodegenerative disorder and it is the leading cause for dementia worldwide. Affecting millions of people throughout the world, AD places great financial and emotional burden on the patients, their families and the society in general (Huang & Mucke, 2012). AD occurrence is age-dependent, its prevalence becoming double every 5 years after the age of 65. Thus, with the increase of life expectancy, the disorder is expected to place an enormous challenge on healthcare systems worldwide (Minati *et al.*, 2009).

1.4.1. Symptoms of Alzheimer's disease

A major symptom occurring during AD is the progressive loss of memory. The slow impairment of episodic memory (encoding and recollecting daily experiences) starts from the preclinical phase (Dickerson & Eichenbaum, 2010). The initial manifestation of episodic memory impairment is the deficit in verbal and nonverbal anterograde memory. In mild AD, a progressive deficiency in semantic memory (the ability to learn and remember facts about the

world) can be observed (Manns *et al.*, 2003). Contrary to declarative memory (memory of facts and events which can be consciously recollected) (Squire, 1992), during the course of AD, implicit memory (knowledge which cannot be accessed consciously) is relatively spared (Ettlinger *et al.*, 2011). AD is also characterized by language problems, which are firstly manifested as semantic memory deficits. However, with disease progression, the problems become more and more serious reaching a complete inability of the affected individual to communicate at the phase of severe AD (Minati *et al.*, 2009). Besides deficits in memory and language, AD patients exhibit also deterioration of executive functions, which appear early during disease progression. These executive functions are related to the ability to mentally manipulate information, to form concepts, to solve problems, or to cue-directed behaviour (Weintraub *et al.*, 2012). AD patients can also exhibit visuospatial disabilities, which are evident as deficits in drawing, construction, or orientation (Minati *et al.*, 2009). Furthermore, people suffering from AD develop apraxic symptoms (inability to perform learned, skilled movements) (Gross & Grossman, 2008), the percentage of affected patients reaching 100% during severe AD (Minati *et al.*, 2009). An enormous burden for the patients and their caretakers are the behavioural abnormalities accompanying the course of AD which are exhibited by 90% of the patients. Common behavioural symptoms are agitation, apathy, and psychosis (Beier, 2007; Minati *et al.*, 2009).

1.4.2. Pathological changes in Alzheimer's disease

The two major histopathological hallmarks of AD are the extracellular senile amyloid plaques and the intracellular neurofibrillary tangles.

Amyloid plaques are mainly composed of Abeta (Aβ), a 4 kDa peptide produced by the amyloidogenic processing of amyloid precursor protein (APP). Their diameter ranges from 10 to 160 µm (Minati *et al.*, 2009). Often, plaques are surrounded by abnormal neuronal processes, which are referred to as dystrophic neurites (Dickson & Vickers, 2001). Furthermore, amyloid plaques are often surrounded by activated microglia and reactive astrocytes (Minati *et al.*, 2009). Different attempts have been made to define different subsets of amyloid plaques. Dickson and Vickers, for example, define the plaques as diffuse, dense-core or fibrillary. Diffuse plaques do not have a specific structure 'resembling a ball of homogenous labelling'. Fibrillar plaques, on the other hand, have a mass of β-amyloid in the center with emerging 'spoke-like extensions'. Finally, dense-core plaques consist of a compact centre, which is surrounded by a sphere of β-amyloid (Dickson & Vickers, 2001). According to Braak and Braak, the amyloid deposition can be separated in three stages.

During the first stage, the amyloid deposits are mainly detected in the basal frontal, temporal and occipital lobes. The second stage is characterized by deposition of amyloid in all isocortical association areas, with relative sparing of the hippocampus and lack of deposition in the primary sensory, motor and visual cortices. Finally, during the third stage amyloid deposits become manifested in those primary areas and sometimes in the molecular layer of the cerebellum and in subcortical nuclei – thalamus, striatum, hypothalamus, subthalamic nucleus, and red nucleus (Braak & Braak, 1991; Serrano-Pozo *et al.*, 2011).

Neurofibrillary tangles consist mainly of hyperphosphorylated variants of the microtubule-binding protein tau. The spreading of neurofibrillary tangles throughout the brain in AD patients has been used by Braak and Braak as a basis to define the stages I-VI of disease progression. During stage I, neurofibrillary tangles are present in the transentorhinal region and the entorhinal cortex proper. Stage II involves spreading of the pathological hallmark to the CA1 region of the hippocampus. During stage III, neurofibrillary tangles appear in the subiculum, while stage IV is characterized with their spreading to amygdala, thalamus and claustrum. Finally, during stages V and VI, the pathology spreads to the neocortex. The appearance of neurofibrillary tangles in the associative areas is earlier and more severe (stage V) than in the primary motor, sensory and visual areas (stage VI) (Braak & Braak, 1991; Serrano-Pozo *et al.*, 2011). Importantly, it should be noted that the appearance of neurofibrillary tangles within the brain is more closely related to the temporal progression of AD symptoms as compared to plaques (Minati *et al.*, 2009).

Besides the deposition of Aβ in the brain parenchyma as amyloid plaques, the peptide also accumulates in the walls of blood vessels, a phenomenon called congophilic angiopathy. Aβ is mainly deposited in the cortical capillaries, small arterioles, middle-size arteries, and leptomeningal arteries, while veins, venules and white-matter arteries are mostly spared (Perl, 2010; Serrano-Pozo *et al.*, 2011). Even though these depositions are known to not disturb the function of blood vessels, they could result in rupturing of the blood vessels and thus, in hemorrhages (Perl, 2010).

Another AD-related pathological hallmark, which is almost exclusive for the perikaryal cytoplasm of hippocampal pyramidal neurons, is granulovacuolar degeneration. Granulovacuolar degeneration is a lesion consisting of intraneuronal accumulation of small vacuoles, each of them containing a basophilic granule. Those granules are positive for tau, ubiquitin, tubulin, and neurofilaments (Perl, 2010; Serrano-Pozo *et al.*, 2011).

Yet another pathological change in AD is the presence of Hirano bodies, eosinophilic rodlike inclusions in the cytoplasm. The Hirano bodies are present in the CA1 region of the hippocampus (Perl, 2010; Serrano-Pozo *et al.*, 2011).

Another pathological hallmark of AD is the progressive loss of brain weight and volume, which results from enormous neuronal and synapse loss. Some brain regions are specifically affected by neuronal loss, such as pyramidal cells in lamina II of the entorhinal cortex and in the CA1 hippocampal region (Huang & Mucke, 2012). Importantly, the profound degeneration of the cholinergic neurons in the basal nucleus of Meynert and in the medial septal nucleus results in the loss of up to 95% of the cholinergic cortical innervation (Minati *et al.*, 2009). Synapse loss, the other contributor to brain atrophy, has been demonstrated by immunostaining of synaptic proteins and by electron microscopy (Serrano-Pozo *et al.*, 2011). It has been shown that synapse loss is more closely related to cognitive decline in AD than neuronal loss (Serrano-Pozo *et al.*, 2011; Huang & Mucke, 2012).

Besides morphological changes, the brains of AD patients exhibit changes in neural network activities. One of these is represented by alterations in the default mode network, most active when people are not thinking about anything specifically. Another alteration in the network activities is hippocampal hyperactivation during the performance of memory tasks (Huang & Mucke, 2012).

1.4.3. Etiology of Alzheimer's disease

The etiology of AD can be both familial and sporadic. Familial AD, which represents 5% of all AD cases, is caused by mutations in three genes, which encode amyloid precursor protein (APP), presenilin 1 (PS1) and presenilin 2 (PS2). These mutations are inherited in an autosomal dominant manner (Minati *et al.*, 2009).

A number of genes have been related to the development of sporadic AD. One of these encodes apolipoprotein E (APOE), which can exist in three alleles, *APOE* ε2, *APOE* ε3 and *APOE* ε4. AD patients show higher probability to be carriers of the *APOE* ε4 allele. Indeed, individuals carrying two *APOE* ε4 alleles have an approximately 60% chance to develop AD by the age of 85 while the chance for those carrying two *APOE* ε3 alleles is approximately 10% (Minati *et al.*, 2009; Huang & Mucke, 2012). Other genes which have been linked to sporadic AD encode insulin-degrading enzyme (IDE), ubiquilin 1 (UBQLN1), sortilin-related receptor, L (DLR class) A repeats containing (SORL1), calcium homeostasis modulator 1 (CALHM1), and several others (Minati *et al.*, 2009).

The main non-genetic risk factor that contributes to sporadic AD pathogenesis is old age. Besides this, many other non-genetic risk factors have been suggested, such as diabetes, obesity, smoking, low educational levels, diet, physical and mental inactivity, depression, head injury, and homocysteinemia (Huang & Mucke, 2012; Scheltens *et al.*, 2016).

1.4.4. Pathogenic mechanisms of Alzheimer's disease

In senile plaques, the main component, Aβ peptide, is present in the form of insoluble amyloid fibrils, a result of the conformational conversion of Aβ from α-helix to β-sheet structure (Serpell, 2000). Analogous to other amyloid fibrils, the Aβ fibrils have a cross-β structure, which means that the separate β-strands are located perpendicularly to the fibrillar axis. Importantly, the production of amyloid fibrils is the end result of a complex aggregation cascade that includes the formation of intermediary products, including soluble oligomers and protofibrils (Ahmed *et al.*, 2010).

Aβ peptide is produced by the amyloidogenic pathway of processing of APP. APP is a member of a protein family that in mammals includes APLP1 and APLP2. These proteins are transmembrane proteins and contain large extracellular domains. Alternative splicing gives rise to several APP isoforms, the most common of which are the 695-amino-acid isoform, mostly expressed in the central nervous system, and the 751- and 770-amino-acid isoforms, expressed more ubiquitously (O'Brien & Wong, 2011). Some of the proposed physiological functions of APP include a trophic role, a role in cell adhesion, and a function as a receptor (Thinakaran & Koo, 2008). The best-studied proteases that can cleave APP are α-secretase, β-secretase and γ-secretase. Depending on whether α- or β-secretase perform the first cleavage reaction, APP can be processed either by the nonamyloidogenic or by the amyloidogenic pathway. The nonamyloidogenic pathway commences with α-secretase cleaving APP to release the N-terminal soluble fragment sAPPα, while the 83-amino-acid C-terminal fragment (CTF) is retained within the membrane. Subsequently, γ-secretase cleaves the membrane-bound CTF releasing another fragment, p3. Notably, since α-secretase cleaves within the Aβ domain, the generation of Aβ is precluded. Conversely, the amyloidogenic pathway starts with β-secretase performing the first cleavage reaction, producing the soluble N-terminal fragment sAPPβ and the membrane-bound 99-amino-acid C-terminal fragment. Then, γ-secretase performs its function, generating Aβ peptides with a length of 38-43 amino acids. Very common forms are $A\beta_{40}$ and $A\beta_{42}$. $A\beta_{42}$ is more hydrophobic than $A\beta_{40}$ and is the main Aβ form residing in amyloid plaques (Thinakaran & Koo, 2008; O'Brien & Wong, 2011; Cavallucci *et al.*, 2012). α-secretase function is attributed to enzymes that belong to the

ADAM family of metalloproteinases. Importantly, α-secretase performs its function at the cell surface. On the other hand, the transmembrane aspartyl protease BACE1 (β-site APP-cleaving enzyme 1) is the major β-secretase in neurons and is mainly localized to the late-Golgi/trans-Golgi network (TGN) and endosomes. Finally, γ-secretase is a complex of 4 proteins – presenilin 1 or presenilin 2, nicastrin, APH-1 and PEN-2. γ-secretase has been shown to be present in different cellular compartments, including endoplasmic reticulum (ER), Golgi apparatus, TGN, endosomes, and plasma membrane (Thinakaran & Koo, 2008). Interestingly, N- or C-terminally truncated Aβ species exist. Apart from this, Aβ can be subject to different post-translational modifications, such as oxidation, phosphorylation, nitric oxide-caused modifications, glycosylation, pyroglutamylation, isomerization, and racemization. Truncated and/or post-translationally modified peptides have been shown to be modulators of disease progression. For example, treatment of mice with an inhibitor of glutaminyl cyclase, the enzyme responsible for the formation of pyroglutamate-modified Aβ (AβpE3-42), in AD mouse models results in reduced $A\beta_{40}$ and $A\beta_{42}$ levels, reduced plaque levels, and improvement in tests for context memory and spatial learning (Schilling *et al.*, 2008; Kummer & Heneka, 2014).

AD is a polyproteinopathy which, in addition to the presence of amyloid plaques, is characterized by abnormal aggregation of hyperphosphorylated tau in the form of the aforementioned neurofibrillary tangles (Huang & Mucke, 2012). The neurofibrillary tangles are composed of paired fibrils wound in a helix, the so called paired helical filaments (Perl, 2010). The major constituent of neurofibrillary tangles, tau, is a protein that is relatively abundant in neurons and commonly known to promote the assembly and the maintenance of microtubules, the assembly function being dependent on the phosphorylation status of the protein (Lindwall & Cole, 1984; Castellani *et al.*, 2008; Wang *et al.*, 2013). Except for some special cases, tau in the normal brain has two or three moles of phosphate per one mole of tau while in the AD brain the phosphorylation of tau is approximately three-fold higher (Wang *et al.*, 2013). Thus, in AD, the hyperphosphorylation of tau causes the dissociation of tau from the microtubules and its ectopic accumulation in perykaria and dendrites (Minati *et al.*, 2009).

Since its postulation in the beginning of the 1990s up until now, the amyloid cascade hypothesis has been the most popular hypothesis used to explain AD pathogenesis. During these decades, while preserving its name, the hypothesis has undergone significant changes as a result of constantly emerging data (Pimplikar, 2009). Briefly, a postulation of the hypothesis from 2010 states that accumulation and aggregation of the Aβ peptide in the brain, resulting from an imbalanced production and/or clearance of the peptide, triggers a pathological

cascade that includes amyloid deposition, inflammation, oxidative stress, neuronal injury and loss (Lemere & Masliah, 2010; Herrup, 2015). This hypothesis is supported by a variety of genetic, biochemical, and neuropathological studies but is mainly supported by the fact that all the mutations associated with familial AD result in a deviation of the processing of APP, which leads to an increased production of Aβ or to increased $A\beta_{42}$ levels relative to $A\beta_{40}$ levels (Cavallucci *et al.*, 2012; Morris *et al.*, 2014).

A major issue in Aβ toxicity research is which form of Aβ assembly is most pathogenic. It has been shown that while the correlation between the levels of insoluble Aβ and cognitive impairment, neuronal and synaptic loss is poor, the levels of soluble Aβ oligomers correlate well with the disease progression (McLean *et al.*, 1999; Cavallucci *et al.*, 2012). Thus, a variety of studies have tried to elucidate the role of Aβ oligomers in neurotoxicity. In spite of the assumption that Aβ oligomers are the main form contributing to neurotoxicity, the neurotoxicity of amyloid plaques cannot be completely rejected. Neuritic alterations have, indeed, been demonstrated immediately adjacent to senile plaques (Huang & Mucke, 2012; Mucke & Selkoe, 2012).

Another major question concerning Aβ toxicity is the role of extracellular vs. intracellular Aβ as a trigger of the pathogenic cascade. A plethora of studies on post-mortem AD brains and transgenic mouse brain have revealed the accumulation of intraneuronal Aβ. For example, Oddo and collaborators demonstrated that in triple transgenic mice expressing mutant APP, PS1 and tau, the appearance of intraneuronal Aβ precedes the formation of amyloid plaques and neurofibrillary tangles. Notably, in this mouse model, synaptic dysfunction was documented before plaques and tangles became obvious and it was shown to correlate with intraneuronal Aβ accumulation (Oddo *et al.*, 2003; Cavallucci *et al.*, 2012). The intracellular Aβ is thought to be either produced intracellularly or to be internalized after being secreted (Sakono & Zako, 2010). Despite many studies claiming the presence of intraneuronal Aβ accumulation, the actual presence and importance of it has been a matter of argument. A major reason for the debate is the cross-reactivity of Aβ antibodies with APP, which could lead to a misinterpretation of the results (Wirths & Bayer, 2012).

Notably, due to the fact that in AD synapse loss correlates better with cognitive decline when compared to neuron loss, many research groups have focused their attention on the mechanisms through which Aβ contributes to synapse dysfunction rather than studying the relation between Aβ and neuronal loss (Huang & Mucke, 2012; Mucke & Selkoe, 2012). Different studies have shown that one of the ways by which Aβ can lead to synaptic dysfunction is related to the connection between Aβ and ion channels (Cavallucci *et al.*,

2012). Several studies have examined the effect of Aβ on NMDA receptors function and Ca^{2+} influx. Aβ has been also shown to bind the α7 nicotinic acetylcholine receptor (Wang *et al.*, 2000; Cavallucci *et al.*, 2012). Interplay between AMPA receptors and Aβ has also been shown. It has been reported that the removal of AMPA from synapses is triggered by Aβ (D'Amelio *et al.*, 2011; Cavallucci *et al.*, 2012).

Mitochondrial dysfunction is a characteristic of many neurodegenerative diseases, including AD. Interestingly, Aβ has been found to be localized within mitochondria. Since synapses are characterized by high energy demand and constant calcium fluctuations, mitochondria are essential for proper synaptic functioning. Accumulation of Aβ in synaptic mitochondria has been shown by Du and collaborators in the transgenic mouse model Tg2576 expressing APP bearing the Swedish mutation (K670N, M671L). These mitochondria exhibited decreased mitochondrial respiration, decreased activity of key respiratory enzymes, increased oxidative stress, and defects in calcium handling. Importantly, synaptic mitochondria showed earlier Aβ accumulation and dysfunction when compared to non-synaptic mitochondria (Du *et al.*, 2010; Cavallucci *et al.*, 2012).

Besides its contribution to synaptic dysfunction, Aβ can induce cellular damage independently of synapse damage. For example, Aβ oligomers have been shown to induce cell death which is mediated by nerve growth factor receptor (NGFR) (Yamamoto *et al.*, 2007; Sakono & Zako, 2010). Moreover, it has been also shown that Aβ oligomers can trigger destabilization of the cellular membrane by formation of pores, which leads to abnormal flow of ions such as Ca^{2+} (Valincius *et al.*, 2008; Sakono & Zako, 2010).

Over the last years, in the field of AD pathogenesis, increasing attention has been put on spreading AD pathology through cell-to-cell spreading of Aβ and tau with toxic conformations. The so-called seeds are thought to interact with normal peptides and induce toxic conformations, analogous to prion disorders. The nature of those toxic conformations has not been fully elucidated (Huang & Mucke, 2012; Scheltens *et al.*, 2016).

One aspect of the amyloid hypothesis is that the formation of neurofibrillary tangles is preceded by Aβ pathology initiation. Support for this assumption has come from genetic studies demonstrating that while mutations in APP and presenilins lead to AD with amyloid plaques and neurofibrillary tangles, mutations in tau result in neurofibrillary tangle formation but not in senile plaques appearance (Huang & Mucke, 2012). Analogous to Aβ, soluble hyperphosphorylated tau oligomers rather than insoluble neurofibrillary tangles have been the most popular candidates for mediating neurotoxicity. Due to the essential function of tau in the assembly and maintenance of microtubules, hyperphosphorylated tau compromises

intracellular trafficking upon its dissociation from microtubules. Another way through which tau has been proposed to exert its toxicity is by disrupting protein turnover pathways – the proteasomal, the lysosomal and the autophagosomal function. Ren and collaborators found, for example, that in HEK293 cells hyperphosphorylation of tau inhibits the proteasome (Ren *et al.*, 2007; Gendreau & Hall, 2013; Wang *et al.*, 2013).

Interestingly, the amyloid cascade hypothesis is also supported by the fact that apoE has an Aβ-dependent role in AD pathogenesis. It has been shown that human apoE induces Aβ clearance in human APP transgenic mice and notably, apoE2 and apoE3 are able to clear more Aβ when compared to apoE4 (Holtzman *et al.*, 1999; Holtzman *et al.*, 2000; Bales *et al.*, 2009; Huang & Mucke, 2012).

Despite the enormous evidence supporting the well-known amyloid cascade hypothesis, in the last years some reports have provided evidence that the validity of the hypothesis cannot be unequivocally accepted. One of the arguments against the hypothesis is that amyloid burden can be seen in cognitively normal individuals (Morris *et al.*, 2014; Herrup, 2015). Another argument against the hypothesis originates from the fact that apart from its Aβ-dependent role in AD pathogenesis, ApoE can also have an Aβ-independent role. It has been shown that apoE4 can undergo proteolytic cleavage, which generates C-terminally truncated neurotoxic fragments that could trigger neuronal dysfunction and neurodegeneration. Interestingly, those fragments have been shown to increase tau phosphorylation and the formation of neurofibrillary tangles, which could be the reason for their neurotoxicity (Huang & Mucke, 2012).

1.4.5. Mouse models of Alzheimer's disease

Research on AD pathogenesis has involved many approaches to model the disease - ranging from *in vitro* assays to the development of elaborate rodent models of AD. Transgenic mouse models of AD, based on information about the genetics of rare inherited forms of AD, have been particularly popular and useful for the elucidation of the mechanisms of disease pathogenesis (Spires & Hyman, 2005). A variety of such transgenic mouse models of AD rely on the expression of wild type APP or APP bearing familial AD (FAD) mutations. The first convincing model based on this approach was published in 1995 by Games and collaborators, the PDAPP transgenic mouse model, which overexpresses human APP bearing a FAD-associated mutation (V717F) in neurons. Notably, the levels of APP in this mouse line are ten times higher than the endogenous levels of APP. This mouse model reproduces many features of AD pathology, such as extracellular thioflavin S-positive Aβ deposits, dystrophic neurites,

gliosis, and reduced synapse density (Games *et al.*, 1995; Spires & Hyman, 2005; Elder *et al.*, 2010). In 1996, Hsiao *et al*. described another APP transgenic mouse model, named Tg2576, which overexpresses human APP bearing the Swedish FAD-associated mutation (K670N, M671L) in neurons. Like the PDAPP mice, these mice also develop amyloid plaques along with dystrophic neurites and gliosis (Hsiao *et al.*, 1996; Spires & Hyman, 2005; Elder *et al.*, 2010).

Besides overexpression of wild type or mutant APP, another strategy employed in the field is the combination of APP transgenes with PS1 or PS2 transgenes in an attempt to enhance AD-related pathology. Indeed, in 1997, Borchelt and collaborators showed that mice coexpressing a PS1 variant bearing an FAD-linked mutation and a chimeric mouse/human APP bearing the Swedish mutation exhibit amyloid deposition earlier than mice expressing mutant APP or mutant PS1 alone (Borchelt *et al.*, 1997; Spires & Hyman, 2005).

Another model that combines the presence of APP and PS1 mutant transgenes is the model used in this study - 5xFAD (Oakley *et al.*, 2006). 5xFAD is a mouse model expressing APP695 and PS1 bearing five familial AD-related mutations in total. APP bears three FAD-associated mutations - the Swedish mutation (K670N, M671L) increases the total levels of Aβ, while the Florida (I716V) and the London (V717I) mutations increase the levels of $A\beta_{42}$. The mutations in PS1 (M146L and L286V) also increase the levels of $A\beta_{42}$. The transgenes are expressed under the control of the Thy1 promoter, which drives expression in neurons. The concentration of five FAD-associated mutations in the mouse model results in a highly accelerated development of AD pathology, with an accumulation of $A\beta_{42}$ starting within neuronal somata and neurites and preceding the formation of amyloid plaques at the age of one and a half months. Amyloid deposits, which appear at 2-month-old animals, are accompanied by gliosis - activated astrocytes and microglia surround the plaques - and spread from deeper cortical layers and the subiculum to later occupy large parts of the cortex, subiculum and hippocampus. Additionally, the 5xFAD model shows decreased levels of various synaptic markers. In comparison to other transgenic mouse models of AD, the 5xFAD mice are one of the few models that exhibit neuronal loss. Interestingly, the 5xFAD mice develop spatial memory deficits as measured in the Y-maze by the age of four to five months (Oakley *et al.*, 2006).

Notably, APP overexpressing AD model mice do not exhibit neurofibrillary tangles although many of them show substantial tau hyperphosphorylation. In order to model the formation of neurofibrillary tangles, tau transgenic models have been developed, which entail the overexpression of tau alone or in combination with other transgenes. For example, in

2003, Oddo and collaborators reported the generation of a triple transgenic mouse model characterized by overexpression of APP bearing the Swedish mutation, PS1 bearing the M146V mutation, and tau bearing the P301L mutation. Besides amyloid pathology, this mouse model also exhibits neurofibrillary tangles (Oddo *et al.*, 2003; Spires & Hyman, 2005; Morrissette *et al.*, 2009).

Despite the enormous usefulness of transgenic mouse models for the elucidation of mechanisms of AD pathogenesis, they have received criticism due to the possibility of overexpression artifacts. To avoid such off-target effects of overexpression, Saito and collaborators reported knock-in mouse lines which bear the Swedish and Beyreuther/Iberian mutations with or without the Arctic mutation in the APP gene. The mice exhibited Aβ pathology, neuroinflammation and memory impairment (Saito *et al.*, 2014).

1.5. SUMO in Alzheimer's disease

Over the past few years, an increasing number of studies have proposed a link between the post-translational modifier SUMO and AD pathology. This cannot be considered as unexpected, taking into account the large number of neuronal proteins that were shown or predicted to be SUMOylated (Lee *et al.*, 2013). However, the corresponding literature is still very sketchy and controversial.

1.5.1. SUMOylation of APP

In 2005, Gocke and collaborators described an *in vitro* expression cloning approach for the identification of putative SUMO1 substrates. Among the identified putative SUMO1 substrates was APP (Gocke *et al.*, 2005). Subsequently, conjugation of SUMO1 and SUMO2 to APP in HeLa cells was proposed, partly based on studies in which lysines 587 and 595 in APP were mutated to arginine (K587R, K595R). The authors also claimed that endogenous APP is SUMOylated in the mouse brain. To support their hypothesis, the authors intended to prove the presence of Ubc9 in the ER, the compartment in which APP was thought to become SUMOylated (Zhang & Sarge, 2008a). However, others failed to show conjugation of SUMO2 to APP in HEK293T cells (Li *et al.*, 2003) indicating that the SUMOylation of APP is still an unresolved matter.

1.5.2. Effect of SUMO on APP processing and Aβ levels

With the intention of developing new therapeutic approaches to modulate Aβ levels, several studies have explored the influence of SUMOylation on Aβ levels and APP

processing. However, the results obtained in the corresponding studies are very controversial and thus, the issue remains far from being resolved (Lee *et al.*, 2013).

In 2003, the first report exploring this issue was published, indicating that coexpression of SUMO2 and APP in HEK293T cells results in decreased Aβ levels as compared to control, and favours the nonamyloidogenic processing of APP. Interestingly, the authors claimed that poly-SUMO2 conjugation, in contrast to mono-SUMO2 or lowered SUMO2 conjugation, reduced Aβ production. Further analyses indicated that coexpression of both wild type and non-conjugatable SUMO2 increased the levels of APP and BACE1. Ultimately, the authors claimed that the turnover of APP was unchanged (Li *et al*., 2003; Lee *et al*., 2013). Unfortunately, the SUMO2 conjugates involved in the decreased Aβ levels were not identified. In support of the study from Li *et al.* (2003), Zhang and Sarge (2008) showed that increasing the SUMOylation machinery in cells causes decreased levels of Aβ aggregates and argued that increased levels of SUMOylated APP might be involved.

However, other studies contradicted these observations (Dorval *et al.*, 2007; Yun *et al.*, 2013). Although there is a certain ambiguity regarding the nomenclature of SUMO variants used, Dorval *et al*. (2007) showed that coexpression of SUMO2 and APP in HEK293 cells leads to a significant increase in the $A\beta_{40}$ and $A\beta_{42}$ levels. In contrast to the study of Li *et al*. (2003), this effect did apparently not require the covalent attachment of SUMO2 to substrates, supporting the hypothesis that the modulation of Aβ levels by SUMO2 does not require conjugation of SUMO2 to substrates. Notably, as in the study from Li *et al*. (2003), SUMO2 overexpression also lead to increased levels of APP and BACE1, but here, the authors claimed that the half-life of APP was altered. Thus, the results of Dorval *et al*. (2007) indicate that overexpression of SUMO2 monomers, and not SUMO2 conjugation, upregulates APP and BACE1 levels, thereby enhancing the formation of Aβ (Dorval *et al.*, 2007; Lee *et al.*, 2013).

In 2013, Yun and collaborators showed that coexpression of APP with either SUMO1, SUMO2 or SUMO3 in cells stably expressing Myc-tagged BACE1 (HBmg) resulted in increased levels of full length APP and of Aβ. Interestingly, this effect did not require covalent binding of SUMOs (Yun *et al.*, 2013). In a follow-up study, the group argued that SUMO1 regulates autophagy-dependent Aβ production (Cho *et al.*, 2015a). Additionally, Yun *et al.* (2013) showed that overexpression of all three SUMO isoforms increased the levels of BACE1 in HBmg cells and primary cortical neurons, and that this effect is abolished when a SIM-like motif is mutated in BACE1. While Yun *et al*. (2013) showed that the increased BACE1 levels are not caused at the transcriptional level, Fang and collaborators reported that

overexpression of SUMOs inhibits the BACE1 gene promoter activity (Fang *et al.*, 2011). Finally, in a recent study, Lee and collaborators showed in Tg2576 hippocampal slices that increasing SUMOylation does not affect $A\beta_{40}$ and $A\beta_{42}$ levels while it rescues Aβ-induced deficits in learning and memory (Lee *et al.*, 2014).

The main problem in interpreting the studies described above is the variety of the cell systems or AD transgenic mice used to study the link between SUMOylation and APP processing and Aβ levels, which makes it difficult to put the entirety of these into perspective. However, independently of whether Aβ levels are increased or decreased by SUMOylation, the corresponding studies establish a link between protein SUMOylation and APP processing, but the exact molecular mechanisms that cause these effects remain unidentified.

1.5.3. Effect of Aβ levels on SUMO

Besides studying the influence of protein SUMOylation on APP processing and Aβ levels, researchers have also addressed the question as to whether Aβ levels can modulate SUMOylation. Using predominantly transgenic mouse models of AD that overexpress APP, several groups intended to study how increased Aβ levels might influence the levels of free and/or conjugated SUMOs, producing again highly controversial and incomplete results.

Using a Western blot approach, McMillan and collaborators described in 9-month-old Tg2576 mice that the total levels of SUMO1 and SUMO2/3 conjugates do not differ significantly from control mice in cortex, hippocampus, or cerebellum, with the exception of two high molecular weight SUMO2/3 conjugate bands in the cortex. Additionally, the levels of Ubc9 and SENP1 proteins did not show any changes in any of the brain regions explored (McMillan *et al.*, 2011).

Furthermore, Nistico *et al*. (2014) found the levels of SUMO1 conjugates to be increased and the SUMO2/3 conjugate levels to be unchanged in the cortex and the hippocampus of 3-6 months old transgenic Tg2576 animals. Interestingly, the authors observed increased SUMO1 mRNA levels in transgenic Tg2576 animals at the age of 6 moths in both brain regions tested. At the age of 17 months, the levels of SUMO1 conjugates had returned to basal levels, while SUMO2/3 conjugate levels were reduced in cortex and hippocampus. Furthermore, Ubc9 and SENP1 proteins levels were increased in these brain regions at 6 months of age (Nistico *et al.*, 2014).

Finally, a third group studied SUMO conjugate levels in the Tg2576 model and described minimal changes in the levels of Ubc9 and SUMO1 conjugates at 1-2-, 7-8- and 13-

14- months in hippocampus, while SUMO2/3 conjugate levels were decreased in 7-8-, 13-14- and 24-26-month-old animals in the same brain region (Lee *et al.*, 2014).

In summary, three independent groups studied by Western blotting the levels of SUMO conjugates, and two of them the SUMOylation enzymes in the Tg2576 model, and reached different conclusions. A possible explanation for these discrepancies might be the use of different antibodies, partly of poor quality/specificity, and different ways of analysing Western blot data. Based on other mouse models of AD, several studies described increased levels of SUMO1 or of SUMO1 conjugates at various disease stages and in various brain regions, but here again, the corresponding data are poorly quantified (Yun *et al.*, 2013; Zhao *et al.*, 2013; Cho *et al.*, 2015a).

In light of the various AD mouse models used, the various brain regions and ages studied, and the various tools used to detect SUMOs, it is very difficult to draw any clear conclusions regarding the putative interplay between SUMO levels, aging, and AD.

Apart from the use of transgenic mice, the influence of increased Aβ levels on SUMO levels has also been studied in cell culture systems. Interestingly, Yun and collaborators described that treatment of primary cortical neurons and HBmg cells with $A\beta_{1-40}$ increases the levels of both, free and conjugated SUMO1. This effect was also observed after overexpression of GFP-$A\beta_{1-42}$ in HBmg cells (Yun *et al.*, 2013). Interestingly, the opposite effect was described in primary astrocyte cultures, where SUMO1 levels and levels of SUMO1 conjugates were decreased upon Aβ treatment. Besides SUMO1 conjugates, the levels of Ubc9 were also reduced. Furthermore, the authors showed that overexpression of SUMO1 in astrocytes blocks the Aβ-induced reactivity of astrocytes, as indicated by upregulated GFAP expression and hypertrophy of cell bodies and processes (Hoppe *et al.*, 2013). Here, the contradicting results may not only be due to the different cell systems tested but to various ways of preparing Aβ peptide.

In acute hippocampal slices from wild type mice, Lee *et al.* (2014) described that induction of LTP leads to increased levels of SUMO2/3 conjugates. Interestingly, this effect was abolished in slices from Tg2576 mice, as well as in wild type slices treated with $A\beta_{42}$ oligomers, indicating that increased Aβ levels block LTP-induced increases in SUMO2/3 conjugation levels. Incubation of Aβ-treated slices with TAT-Ubc9 restored the activity-induced increase in SUMO2/3 conjugation. However, the SUMO2/3 conjugates involved in this phenomenon were not identified.

Transgenic mouse models of AD have been also utilized to study alterations in SUMO localization. SUMO1 is mainly found in cell nuclei, but several studies, using different AD

mouse models (aged between 12 and 26 months) have reported a localization of SUMO1 surrounding amyloid plaques and colocalization of SUMO1 with phospho-Tau or autophagy markers (Takahashi *et al.*, 2008; Yun *et al.*, 2013; Zhao *et al.*, 2013; Cho *et al.*, 2015a). In addition to SUMO1 surrounding plaques, some SUMO1 labelling within plaques was observed (Yun *et al.*, 2013; Zhao *et al.*, 2013). However, it should be noted that in most of the studies mentioned above, the typical SUMO1 staining as a ring representing the nuclear membrane was not observed, which raises doubts about the specificity of the SUMO1 detection tools used.

1.5.4. SUMO and tau

Several studies have indicated a link between SUMOs and tau, another major player in AD pathogenesis. In 2006, Dorval and Fraser demonstrated SUMOylation of tau in HEK293 cells, with a preference for SUMO1 conjugation. In this study, lysine 340 appeared to be the dominant acceptor lysine. Interestingly, tau SUMOylation was decreased upon proteasome inhibition. Finally, the authors demonstrated that tau SUMOylation was increased upon treatment with the phosphatase inhibitor okadaic acid and the microtubule depolymerizing agent colchicine. Since tau binding to microtubules is negatively influenced by phosphorylation, the study indicates that SUMOs preferentially conjugate to the free soluble pool of tau, i.e. the pool that is not bound to microtubules (Dorval & Fraser, 2006).

Another recently published report extensively explored the downstream effects of tau SUMOylation. In an overexpression approach in HEK293 cells, the authors confirmed that tau is modified by SUMO1 at lysine 340 and that this results in increased tau phosphorylation at various residues, indicating that SUMOylation of tau induces its hyperphosphorylation. Strikingly, the authors also observed that tau SUMOylation is also stimulated by tau phosphorylation, indicative of a positive regulatory loop between SUMOylation and phosphorylation of tau. Further, the authors described that tau SUMOylation decreases its solubility and counteracts its degradation, indicating that SUMOylation might compete with tau ubiquitination. Finally, in an attempt to examine the upstream factors that influence tau SUMOylation, the authors treated primary rat hippocampal cultures with $A\beta_{40.}$ This resulted in an increase in tau phosphorylation and tau SUMOylation (Luo *et al.*, 2014). These studies describe an interesting interplay between SUMOylation, phosphorylation, and ubiquitination of tau, and a link with its aggregation propensity.

A link between SUMO and tau *in vivo* has been proposed by the aforementioned studies from Takahashi *et al.* (2008) and Zhao *et al.* (2013) which demonstrated a

colocalization of SUMO1 with phospho-tau surrounding amyloid plaques in transgenic mouse models of AD. Colocalization of SUMO1 and phospho-tau was also seen in cortex and the hippocampal CA1 region in AD patients (Luo *et al.*, 2014). However, these studies were done using anti-SUMO antibodies that did not show the typical nuclear SUMO1 staining, which raises concerns regarding the validity of the relevant studies.

1.5.5. SUMO in Alzheimer's disease patients

The use of transgenic mice, cell cultures, and *in vitro* systems to demonstrate a link between AD and SUMOylation has been complemented by analyses of samples from AD patients. Evidence that the mechanism of SUMOylation is linked to AD came from two genetic association studies. Genome-wide association studies showed that the SNP rs6907175, located within a gene homologous to SUMO1 activating enzyme subunit 1, and a polymorphism in intron 7 of the SUMO conjugating enzyme Ubc9 are associated with late-onset AD (Grupe *et al.*, 2007; Ahn *et al.*, 2009; Lee *et al.*, 2013). Additionally, using microarray and real-time RT PCR analyses of parietal lobes of late-onset AD patients, non-AD demented patients, and non-demented controls, Weeraratna *et al.* (2007) reported a downregulation of sentrin-specific protease 3 (SENP3) in AD patients. While these studies may indicate a link between protein SUMOylation and AD, the underlying molecular mechanisms remain unknown.

In studies on AD patients, several additional pieces of evidence were provided that appear to link SUMOylation and AD. One study reported an increased level of SUMO1 in blood plasma from demented patients as compared to healthy controls (Cho *et al.*, 2015b). Another study indicated that SUMO2/3 might localize to both, neuronal somata and nuclei, under normal conditions, while SUMO2/3 appears to be exclusively somatic in more neurons in AD patients (Li *et al.*, 2003). Further, Luo *et al.* (2014) described that SUMO1 signals are increased in the cortex and the hippocampal CA1 region of AD patients, and that SUMO1 appears to colocalize with phosphorylated tau. Additionally, Lee *et al.* (2014) described a significant decrease in the levels of high molecular weight SUMO2/3 conjugates, but not of SUMO1 conjugates, in brains of AD patients. Here again, it is difficult to draw definitive conclusions from these correlative studies in human patients. There seems to be a link between SUMOylation and AD, but the underlying molecular mechanisms are unclear, as is the question as to whether the observed changes are causes or consequences of the neurodegenerative process.

1.5.6. Other links between SUMO and Alzheimer's disease

SUMOylation has been implicated in the regulation of a variety of processes related to AD pathogenesis. For example, mitochondrial dysfunction is a major feature of various neurodegenerative diseases, including AD. Two studies have shown a dysregulation of DRP1, a GTPase required for mitochondrial fission, in brains of AD patients (Wang *et al.*, 2009; Manczak & Reddy, 2012). Interestingly, DRP1 was shown to be a SUMO substrate, and SUMOylation of DRP1 influences its function during mitochondrial fragmentation (Harder *et al.*, 2004; Figueroa-Romero *et al.*, 2009; Lee *et al.*, 2013; Martins *et al.*, 2016).

Further, a possible link between AD and kainate receptor signalling has been proposed. Kainate receptor binding is significantly increased in the frontal cortex of AD patients, and kainate binding sites being proportional to the plaque abundance in deep cortical layers has been described in AD (Chalmers *et al.*, 1990; Lee *et al.*, 2002; Martins *et al.*, 2016). In this context, it has also been proposed that SUMOylation of the kainate receptor subunit GluK2 favours its endocytosis (Martin *et al.*, 2007a). Thus, impaired SUMOylation of GluK2 in AD might increase its abundance at the neuronal cell surface.

Other interesting SUMO targets that could be investigated with relation to AD pathogenesis include the transcription factor MEF2 (Shalizi *et al.*, 2006), the RNA-binding protein La (van Niekerk *et al.*, 2007), the protein kinase CASK (Chao *et al.*, 2008), the cAMP-responsive element binding protein (CREB) (Comerford *et al.*, 2003), and the K2P1 potassium channel (Rajan *et al.*, 2005; Lee *et al.*, 2013).

1.6. Investigating SUMOylation

The identification of endogenous SUMO substrates has long been hampered due to a variety of reasons. Even though SUMOs are often conjugated to a ψKxD/E motif, SUMOylation sites cannot be reliably predicted by bioinformatics. Furthermore, SUMOylation is a transient modification due to isopeptidases that efficiently reverse SUMOylation. In addition, at any given time only a small percentage of a given protein is SUMOylated. Also, reliable antibodies for affinity purification of endogenous SUMO substrates have long been missing. Finally, one problem that particularly concerns the study of SUMO2 and SUMO3 conjugation stems from the close resemblance of SUMO2 and SUMO3 so that no currently available antibody can distinguish them (Tirard *et al.*, 2012; Yang & Paschen, 2015).

In attempts to overcome these difficulties, researchers have employed various approaches. One of these is the expression of tagged SUMOs in a wild type background

(Tirard *et al.*, 2012). A large number of studies reported on the expression of tagged SUMOs in mammalian cell cultures. Especially important in the SUMOylation research are proteomics analyses, the goal of which is the large-scale identification of candidate SUMO substrates by affinity purification followed by mass spectrometry, and the identification of the SUMO-targeted lysines using proteomics tools. Thus, a variety of proteomics studies were performed based on expressing tagged SUMOs in mammalian cell cultures (Vertegaal *et al.*, 2004; Rosas-Acosta *et al.*, 2005; Vertegaal *et al.*, 2006; Blomster *et al.*, 2009; Golebiowski *et al.*, 2009; Tatham *et al.*, 2011; Tirard *et al.*, 2012). For example, the first study that aimed to identify SUMO2 substrates at a large-scale was published by Vertegaal *et al.* (2004). Due to the already mentioned differences in the nomenclature used by some groups and by the existing databases, here SUMO2 actually means SUMO3. The study reported the use of a HeLa cell line stably expressing His_6-SUMO3 to pull down SUMOylated proteins by Ni^{2+}-nitriloacetic acid-agarose beads, which were then subjected to mass spectrometry analysis (Vertegaal *et al.*, 2004; Yang & Paschen, 2015). Apart from cell cultures, tagged SUMOs were also expressed *in vivo.* Proteomic studies with tagged SUMOs were performed, for instance, in *Trypanosoma cruzi* (Bayona *et al.*, 2011), *Toxoplasma gondii* (Braun *et al.*, 2009), *Drosophila melanogaster* (Nie *et al.*, 2009; Tirard *et al.*, 2012). Recently, a study reported the generation of a transgenic mouse in which the expression of His-SUMO1, HA-SUMO2 and FLAG-SUMO3 is Cre-dependent. In the same study, the authors describe the use of the transgenic mice for the proteomic examination of changes in SUMO3 conjugation upon ischemia (Yang *et al.*, 2014). Thus, proteomics could not only be used under normal physiological conditions but also to identify changes in SUMO conjugation upon different pathological events. In spite of the usefulness of the expression of tagged SUMOs in a wild type background, a key disadvantage of this approach are possible overexpression artifacts, e.g. by off-target SUMOylation (Tirard *et al.*, 2012).

Other groups have attempted to affinity purify endogenous SUMO conjugates. A purification approach for the enrichment of endogenous polySUMOylated proteins was published by Bruderer *et al.* (2011). The purification approach makes use of the four SIMs present on a fragment of RNF4, which allow it to bind to polySUMO chains. This strategy was employed to identify polySUMOylated proteins upon heat shock in HeLa cells (Bruderer *et al.*, 2011; Yang & Paschen, 2015). Yet another group also reported the purification of endogenous SUMO substrates with the use of monoclonal antibodies for immunoprecipitation and elution with epitope-specific peptides. The authors used this approach, combined with mass spectrometry analysis, to compare for the first time the endogenous SUMO1 and

SUMO2/3 conjugates in mammalian cells. Notably, the study also reported the enrichment of SUMO substrates from mouse liver (Becker *et al.*, 2013; Yang & Paschen, 2015).

Another approach that has been used in an attempt to facilitate the identification of novel SUMO targets is the exchange of endogenous SUMOs with affinity-tagged forms. This approach excludes the presence of overexpression artifacts as the tagged SUMOs are expressed at levels close to the endogenous ones (Tirard *et al.*, 2012). The use of substitution of the endogenous SUMO with tagged SUMOs for proteomics analysis has been reported in different organisms such as yeast (Panse *et al.*, 2004; Denison *et al.*, 2005; Hannich *et al.*, 2005), *Arabidopsis thaliana* (Miller *et al*., 2010), *Candida albicans* (Leach *et al*., 2011), and *Caenorhabditis elegans* (Kaminsky *et al*., 2009; Tirard *et al*., 2012). In 2012, Tirard *et al.* (2012) published the generation of the aforementioned SUMO1 knock-in mouse model, which expresses His_6-HA-SUMO1 instead of wild type SUMO1 under the control of the endogenous promoter. Apart from the identification and validation of SUMO substrates, this model is also extremely useful for studying the localization of free SUMO1 and SUMO1 conjugates. In comparison to previously published models, this knock-in model has several advantages. First, as was already mentioned, expression of tagged SUMO1 instead of the wild type protein excludes overexpression artifacts such as 'off-target' SUMOylation. Additionally, very reliable anti-HA antibodies for affinity purification and immunostaining exist. It should be also noted that wild type mice are ideal negative controls for the knock-in mice. The authors used this mouse model to explore for the first time the SUMO1 conjugates in the brain (Tirard *et al.*, 2012; Yang & Paschen, 2015). They performed anti-HA affinity purification to enrich SUMO1 conjugates from the brain, separated the eluates by SDS-PAGE and analysed the tryptically digested gel pieces by mass spectrometry. Using this approach, several hundreds of candidate SUMO1 substrates linked to various biological processes were identified. The candidate list included already known SUMO1 substrates, such as RanGAP1 and RanBP2, but also some novel candidate SUMO1 substrates such as Smchd1, Zbtb20, TIF1, and Ctip2. Some of the proteins from the candidate list were validated by Western blot analysis (Tirard *et al.*, 2012).

1.7. Aims of the present study

The first aim of the present study was the generation of a Strep-Myc-SUMO3 knock-in mouse line and its basic characterization. Analogous to the His_6-HA-SUMO1 knock-in model generated previously (Tirard *et al.*, 2012), we wanted to generate a reliable tool to study SUMO3 conjugation profile *in vivo* by the generation of a SUMO3 knock-in mouse

model. Our expectation is that this mouse line will be an excellent model to study SUMO3 localization and identify SUMO3 substrates. This would be extremely useful, given the high similarity between SUMO2 and SUMO3 that confounds the distinction between the two proteins using antibodies. Furthermore, we expect that the new mouse line will allow to investigate SUMO3 function in the context of different physiological and pathological conditions, which is important because it has been demonstrated that predominantly SUMO2/3 conjugation increases dramatically upon aberrant cellular conditions.

As has been mentioned above, a large number of studies indicate a link between SUMOylation and AD pathogenesis. Thus, the second aim of this study was to investigate SUMO1 conjugation profile in the presence of AD pathology by making use of His_6-HA-SUMO1 knock-in mice and 5xFAD mice as a model of AD. Using crossbred His_6-HA-SUMO1;5xFAD mice at different time points of disease progression, we aimed to identify changes in the localization of SUMO1 and in the global SUMO1 conjugation levels that might be associated with AD pathology. Our expectation was that these experiments would help to elucidate the molecular link between SUMO1 and AD pathogenesis.

2. Materials and Methods

2.1. Animals

All experiments including mice were performed in agreement with the guidelines for the welfare of experimental animals issued by the Federal Government of Germany and the Max Planck Society.

Table 2.1: Mouse lines used in this study

Mouse line	Description	Reference	Provider
His_6-HA-SUMO1 knock-in	SUMO1 knock-in mouse line expressing His_6-HA-tagged SUMO1 instead of wild type SUMO1 from the endogenous locus	(Tirard *et al.*, 2012)	Dr. M. Tirard
5xFAD	Double transgenic mice expressing human APP and PS1 bearing five familial AD-related mutations	(Oakley *et al.*, 2006)	Kindly provided by Prof. Dr. Thomas Bayer
Strep-Myc-SUMO3 knock-in	SUMO3 knock-in mouse line expressing Strep-Myc-SUMO3 instead of wild type SUMO-3		Created as a part of the PhD project

2.2. Molecular biology

2.2.1. Oligonucleotides

The oligonucleotides' Lab ID numbers and sequences are listed. Restriction sites which were used for cloning are underlined and in bold. The primers indicated with (1-8) were used for validation of positive ES cell clones and the ones indicated with (9-11) were used for genotyping of the Strep-Myc-SUMO3 knock-in mouse. All these numbers are used in Fig. 3.3.

Table 2.2: Primers used in this study

Primer ID	Sequence	Restriction site
29680	5'-CAGCGC**GCTAGC**CCCA -3'	NheI
29681	5'-**TGATCA**GCCAGTCAAGAGCACAGAATG -3'	BclI
29682	5'-A**GCTAGC**ATCTCCAAAGTGC -3'	NheI
29683	5'-**TGATCA**TTTAAGGCCACCTCCGCT -3'	BclI
30945	5'-CGAT**GTCGAC**TTGAGATAAGGAGTCTCCTC -3'	SalI
29685	5'-**GAATTCGCTAGC**GCGCTGCCCGGGGCGGAGT -3'	EcoRI, NheI
29686	5'-**ACTAGT**GTGACGCATTCGCAACCGT -3'	SpeI
29687	5'-**ACTAGT**GTACAAGTGTGTATCCACCTG -3'	SpeI
31653	5'-CATG**GAATTCGCTAGC**CCCACCCCCGGCT -3'	EcoRI, NheI
31654	5'-CGAT**GAATTCGCTAGC**ATCTCCAAAGTGC -3'	EcoRI, NheI
31738	5'-CATG**GGCGCC**TGACCCGCCCCGTGACGATTC -3'	NarI
31739	5'-ATGTGGTCACACCCGCAGTTTGAGAAGGAACAAAAACTTATTTCTGAAGAAGATCTGTCGGAAGAGAAGCCCAAGGTAAGCCCGG -3'	
31740	5'-CAGATCTTCTTCAGAAATAAGTTTTTGTTCCTTCTCAAACTGCGGGTGTGACCACATGGTTGCGCAGCGACGGCGGCGGCAAGCG -3'	
31741	5'-CATG**GCTAGC**GCGCTGCCCGGGGCGGAGTGCA -3'	NheI
31629 (1)	5'-GCCACCTAGTGGTTACTTTG -3'	
33462 (2)	5'-GCACCCTTCCTTTCTTGACTTTCC -3'	
22574 (3)	5'-CCTCTTGAAAACCACACTGCTCGACCT -3'	
33455 (4)	5'-CTTCTCAAACTGCGGGTGTGACCA -3'	
33456 (5)	5'-GGCTTACCTTGGGCTTCTCTTCCGA -3'	
33457 (6)	5'-GGCTTGCGTACCGGGCTTACCTTG -3'	
4174 (7)	5'-GGCTTGCGTACCGGGCTTACCTTG -3'	
33570 (8)	5'-CTGTCAAGACAGGTACGACTAGTGGGTTC -3'	
34055 (9)	5'-CGTGACTCGCCCGCTCCA -3'	
34056 (10)	5'-CCGGGTTCTCGAGCCGTG -3'	

16285 (11)	5'-TGAAAACCACACTGCTCGACC -3'	
31892	5'-CATG**AAGCTT**ATGTCCGAGGAGAAGCCCAAGGAG -3'	HindIII
31891	5'-CATG**AAGCTT**ATGTGGTCACACCCGCAGTTTGAGAAGGAACAAAAACTTATTTCTGAAGAAGATCTGTCCGAGGAGAAGCCCAAGGAG -3'	HindIII
30934	5'-CATG**AAGCTT**ATGGAACAAAAACTTATTTCTGAAGAAGATCTGTACCCATACGATGTTCCAGATTACGCTTCCGAGGAGAAGCCCAAGGAG -3'	HindIII
30935	5'-CAGT**GGATCC**CTAACCTCCCGTCTGCTGCTGG -3'	BamHI

2.2.2. Plasmids

Table 2.3: Plasmids used in this study

Name	Obtained from
pcDNA3	Invitrogen
pcDNA3.1 (-)	Invitrogen
pBluescript II SK (-)	Stratagene
pTKNeoLox	Kind gift from Prof. Dr. Thomas Südhof
pCRII-TOPO	Invitrogen
pCRII-TOPO + 5' miniarm for 5' homology arm (5' MA 5' HA pCRII-TOPO)	this work
pCRII-TOPO + 3' miniarm for 5' homology arm (3' MA 5' HA pCRII-TOPO)	this work
pCRII-TOPO + 5' miniarm for 3' homology arm (5' MA 3' HA pCRII-TOPO)	this work
pCRII-TOPO + 3' miniarm for 3' homology arm (3' MA 3' HA pCRII-	this work

TOPO)	
pBluescript II SK (-) + 5' and 3' miniarms for 5' homology arm (5', 3' MA 5' HA pBluescript II SK (-))	this work
pBluescript II SK (-) + 5' and 3' miniarms for 5' homology arm – MCS SpeI (5', 3' MA 5' HA – SpeI MCS pBluescript II SK (-))	this work
pBluescript II SK (-) + 5' homology arm (5' HA pBluescript II SK (-))	this work
pcDNA 3.1 (-) + 5' and 3' miniarms for 3' homology arm (5', 3' MA 3' HA pcDNA 3.1 (-))	this work
pBluescript II SK (-) + 5' and 3' miniarms for 3' homology arm (5', 3' MA 3' HA pBluescript II SK (-))	this work
pBluescript II SK (-) + 3' homology arm (3' HA pBluescript II SK (-))	this work
pTKNeoLox + 3' homology arm (3' HA pTKNeoLox)	this work
pCRII-TOPO + NarI-NheI segment with Strep-Myc-tagged exon1 (Strep-Myc-exon 1 pCRII-TOPO)	this work
pBluescript II SK(-) + 5' homology arm bearing Strep-Myc tag after the start codon of *SUMO3* (Strep-Myc-exon1 in 5' HA pBluescript II SK (-))	this work
pTKNeoLox + 5' homology arm bearing Strep-Myc tag after the start codon of *SUMO3* + 3' homology arm (Strep-Myc-exon1 in 5'HA, 3'HA pTKNeoLox)	this work
pCRUZ + HA-SUMO3 (HA-SUMO3 pCRUZ)	Kind gift from Prof. Dr. F. Melchior
pCRUZ + His_6-SUMO3 (His_6-SUMO3 pCRUZ)	Kind gift from Prof. Dr. F. Melchior
pCRII-TOPO + Myc-HA-SUMO3 (Myc-HA-SUMO3 pCRII-TOPO)	this work
pcDNA3 + Myc-HA-SUMO3 (Myc-HA-SUMO3 pcDNA3)	this work
pcDNA3 + SUMO3 (SUMO3 pcDNA3)	this work
pcDNA3 + Strep-Myc-SUMO3 (Strep-Myc-SUMO3 pcDNA3)	this work

Primers 30945 and 29687 were used to amplify the 5' miniarm for the recovery of the 5' homology arm of the Strep-Myc-SUMO3 knock-in targeting vector. As a template, BAC

DNA containing the *SUMO3* gene was used. The PCR product was inserted into pCRII-TOPO vector for the generation of the 5' MA 5' HA pCRII-TOPO plasmid.

Primers 29685 and 29686 were used to amplify the 3' miniarm for the recovery of the 5’ homology arm. The aforementioned BAC DNA was used as a template. The PCR product was inserted into pCRII-TOPO for the generation of 3' MA 5' HA pCRII-TOPO.

Primers 29680 and 29681 were used to amplify the 5' miniarm for the recovery of the 3' homology arm. The aforementioned BAC DNA was used as a template. The PCR product was inserted into pCRII-TOPO for the generation of 5’ MA 3' HA pCRII-TOPO.

Primers 29682 and 29683 were used to amplify the 3' miniarm for the recovery of the 3' homology arm. The aforementioned BAC DNA was used as a template. The PCR product was inserted into pCRII-TOPO for the generation of 3' MA 3' HA pCRII-TOPO.

5', 3' MA 5' HA pBluescript II SK (-) was obtained by digestion of 5' MA 5' HA pCRII-TOPO with SalI and SpeI, 3' MA 5' HA pCRII-TOPO with SpeI and EcoRI and pBluescript II SK (-) with SalI and EcoRI and subsequent triple ligation of the two miniarms into the pBluescript II SK (-) vector.

5', 3' MA 5' HA – SpeI MCS pBluescript II SK (-) was obtained by digestion of 5', 3' MA 5' HA pBluescript II SK (-) with XbaI and BamHI, incubation of the cut DNA with Klenow polymerase to create blunt ends and subsequent ligation.

5' HA pBluescript II SK (-) was generated by successful recombineering after transformation of 5', 3' MA 5' HA – SpeI MCS pBluescript II SK (-) in SW106 cells containing BAC DNA with the *SUMO3* gene. Before the transformation of the vector, it was linearized by SpeI and dephosphorylated.

5', 3' MA 3' HA pcDNA 3.1 (-) was obtained by digestion of 5' MA 3' HA pCRII-TOPO and 3' MA 3' HA pCRII-TOPO with NheI and BclI and pcDNA3.1. (-) with NheI followed by triple ligation of the miniarms into the pcDNA3.1 (-) vector. After digeston, pcDNA3.1 (-) was dephosphorylated.

Primers 31653 and 31654 were used to amplify the joined 5' and 3' miniarms for recovery of 3' homology arm. 5', 3' MA 3' HA pcDNA3.1 (-) was used as a template. The PCR product was cut with EcoRI. pBluescript II SK (-) was also cut with EcoRI and dephosphorylated. This was followed by ligation of the joined miniarms into pBluescript II SK (-) to obtain 5', 3' MA 3' HA pBluescript II SK (-).

3' HA pBluescript II SK (-) was generated by successful recombineering after transformation of 5', 3' MA 3' HA pBluescript II SK (-) in the aforementioned SW106 cells. Before the transformation of the vector, it was linearized with BclI and dephosphorylated.

For the generation of 3' HA pTKNeoLox, 3' HA pBluescript II SK (-) was cut with NheI, while pTKNeoLox was cut with XbaI and then dephosphorylated. This was followed by a ligation reaction.

A segment containing the Strep-Myc tag placed after the starting codon of *SUMO3* was generated by overlap PCR using the primers 31738, 31739, 31740 and 31741. 5' HA pBluescript II SK (-) was used as a template. The PCR product was then cloned in pCRII TOPO to obtain Strep-Myc-exon 1 pCRII-TOPO.

Strep-Myc-exon1 in 5' HA pBluescript II SK (-) was obtained by digestion of Strep-Myc-exon 1 pCRII-TOPO and 5' HA pBluescript II SK (-) with NarI and NheI and ligation leading to the exchange of the wild type segment with the Strep-Myc tag-containing segment in 5' HA pBluescript II SK (-).

Strep-Myc-exon1 in 5' HA, 3' HA pTKNeoLox (the final targeting vector) was generated by digestion of Strep-Myc-exon1 in 5' HA pBluescript II SK (-) and 3' HA pTKNeoLox with SalI and NheI and subsequent ligation of the Strep-Myc tag-containing 5' homology arm in pTKNeoLox.

Myc-HA-SUMO3 pCRII-TOPO was obtained by PCR amplification of Myc-HA-SUMO3 using primers 30934 and 30935. As a template, HA-SUMO3 pCRUZ was used. This was followed by ligation of the PCR product in pCRII-TOPO.

Myc-HA-SUMO3 pcDNA3 was generated by digestion of Myc-HA-SUMO3 pCRII-TOPO and pcDNA3 with HindIII and BamHI followed by ligation of Myc-HA-SUMO3 in pcDNA3.

SUMO3 pcDNA3 was generated by PCR amplification of SUMO3 with the primers 31892 and 30935 followed by digestion of the PCR fragment and pcDNA3 with BamHI and HindIII and subsequent ligation of SUMO3 in pcDNA3. As a template, HA-SUMO3 pCRUZ was used.

A fragment containing Strep-Myc-SUMO3 was PCR amplified by the use of the primers 31891 and 30935. Then the PCR fragment and pcDNA3 were digested with BamHI and HindIII, which was followed by ligation of Strep-Myc-SUMO3 in pcDNA3 to generate Strep-Myc-SUMO3 pcDNA3. As a template, HA-SUMO3 pCRUZ was used.

2.2.3. Bacterial strains

Table 2.4: Bacterial strains used in this study

Bacterial strain	Source
E. coli XL1-Blue	Stratagene
E. coli Electro10-Blue	Stratagene
E. coli SW106	Biological Resources Branch, DCTD NCI-Frederick Cancer Research and Development Center
E. coli XL2-Blue	Stratagene
E. coli One Shot TOP10	Invitrogen
E. coli JM110 (dam-/dcm-)	Stratagene
E.coli DH10B	Source BioScience, UK

2.2.4. Bacterial transformation

For electroporation, up to 1 μl ligation reaction or 0.5 μl plasmid DNA were in most cases added to thawed electrocompetent cells. The mixture of cells and DNA was pipetted in a precooled cuvette. The cuvette was subjected to a 1.8 kV electrical pulse. This was followed by resuspension of the bacteria in 1 ml LB or 200 μl SOC medium and their transfer into Eppendorf tubes or 14 ml Falcon tubes. Bacteria were then incubated for approximately 1 hour at 37°C with moderate shaking. For plating ligation reactions, bacteria were concentrated and after that plated on LB agar plates containing the appropriate antibiotic. For plating plasmid retransformations, bacteria were not pelleted and only a part of them was plated on LB agar plates with the appropriate antibiotic. Plates were kept overnight at 37°C.

For electroporation of BAC DNA, two colonies from a plate containing SW106 bacteria were picked, inoculated in 5 ml LB and left shaking overnight at 32°C. After that, the overnight cultures were diluted with a ratio 1:30 (1 ml in 29 ml LB) and were kept shaking at 32°C until the OD reached 0.6. The Erlenmeyer flasks containing the cultures were cooled on ice for several minutes and then their content was transferred into 15 ml Falcon tubes. Bacteria were spun down for 10 min, which was followed by removal of the supernatant and turning the tubes upside down on a paper towel. The pellet was then resuspended in 10 ml ice-cold ddH_2O by slowly pipetting up and down. Then, cells were spun down again for 10 min, the supernatant was removed and cells were resuspended again as before. Cells were spun

down once more and the pellet was resuspended in the leftover water (total volume around 100 μl). 50 μl of bacteria were placed in a pre-cooled Eppendorf tube and 0.5, 1, 1.5 and 2 μl of BAC minipreps with concentration 3726 and 5208 μg/ml were added to the bacteria. DNA was electroporated in the bacteria, they were resuspended in 1 ml LB and left to recover at 32°C shaking for 1 hour in 14 ml Falcon tubes. 100 μl from each tube were plated on chloramphenicol plates. The rest of the tube was spun for 10 sec, most of the supernatant was removed and the rest was plated again on chloramphenicol plates. The chloramphenicol plates were kept for approximately 24 hours at 32°C.

For transformation in XL2 bacteria, the procedure from the manufacturer's protocol was followed. 14 ml round-bottom Falcon tubes were placed on ice and NZY+ medium was placed at 42°C. Then, bacteria were thawed, transferred to the falcon tubes and 2 μl β-mercaptoethanol were pipetted to each bacterial aliquot. After that, the tubes were gently swirled and placed on ice for 10 min with gentle swirling every 2 min. To the tubes were added 10 μl DNA, they were swirled and placed on ice for 30 min. The tubes were incubated in 42°C water bath for 30 sec and then incubated on ice for 2 min. This was followed by addition of 0.9 ml of NZY+ medium and one hour incubation at 37°C with moderate shaking. After spinning down and resuspension of the cells in 200 μl NZY+, 150 μl and 50 μl bacteria were plated. Plates were kept overnight at 37°C.

2.2.5. Plasmid DNA preparation

For purification of small amounts of DNA for sequencing, analytical restriction digestion and PCR, PureLink Quick Plasmid Miniprep Kit from Invitrogen was utilized according to the manufacturer's protocol. Sometimes for testing a big number of colonies DNA was obtained by a boiling miniprep method. 1.5 ml bacterial culture was spun down. The bacterial cells were resuspended in 250 μl STET buffer and vortexed. 25 μl of freshly prepared 10 mg/ml lysozyme was pipetted into each tube and the tubes were vortexed again. Samples were boiled for 45 sec at 100°C and centrifuged at 13000 rpm for 10 min. The cell debris was then discarded with the use of a toothpick. 50 μl 7.5 M NH_4-acetate and 500 μl 100 % ethanol were added to the tubes which were then vortexed again. The tubes were centrifuged at 13000 rpm for 30 min. The supernatant was removed and 500 μl 70% ethanol were added. The samples were centrifuged at 13000 rpm for 5 min. The supernatant was discarded again, the pellet was air-dried and then resuspended in 50 μl of TE buffer. For

restriction digestion analysis of the obtained DNA, 5 μl DNA were used for 50 μl total volume including 0.5 μl of RNAse.

To obtain higher amounts of plasmid DNA, PureLink HiPure Plasmid Filter Midiprep Kit from Invitrogen was used according to the manufacturer's protocol. In order to obtain pure endotoxin-free plasmid DNA for electroporation in ES cells, EndoFree Plasmid Maxi Kit from Qiagen was used according to the manufacturer's protocol.

Sometimes TempliPhi preparation of DNA was used for screening colonies. A colony was picked and placed in 5 μl TempliPhi Denature buffer and then in a copy plate containing 100 μl LB. The plate with the Denature buffer was heated to 95°C for 3 min and cooled down. 5 μl TempliPhi Premix were added and the samples were incubated for 18 hours at 30°C. After that, they were heated to 65°C for 10 min and cooled down to 10°C. Before using the reaction for restriction digestion, 20 μl of water were added.

2.2.6. BAC DNA preparation

The bacteria containing BAC DNA were inoculated in 5 ml LB + chloramphenicol and left shaking overnight at 32°C. The cultures were spun down for 15 min. After the removal of the supernatant, bacteria were resuspended in 250 μl P1 buffer (Qiagen). Cells were then lysed by the addition of 250 μl P2 buffer (Qiagen) which was followed by turning the Eppendorf tubes upside down 5-6 times and 5 min incubation at RT. Then, 350 μl P3 buffer (Qiagen) were added and the content of the tubes was carefully mixed. The tubes were centrifuged for 4 min at 11000 rpm. The supernatant was transferred to a 2 ml Eppendorf tube and the tube was centrifuged again for 4 min at 11000 rpm. The supernatant was again transferred to a new tube and 750 μl isopropanol were added to it. The tubes were then incubated for 10 min at RT. DNA was pelleted by 10 min centrifugation at 13000 rpm and the supernatant was removed. DNA was washed by addition of 1 ml 70% ethanol. This was followed by 10 min spinning down at 13000 rpm and removal of the supernatant. The pellet was air-dried and resuspended in 50 μl 10 mM Tris.

Buffer P1 (resuspension buffer) – 50 mM TrisCl, pH 8.0; 10 mM EDTA; 100 μg/ml RNAse A

Buffer P2 (lysis buffer) – 200 mM NaOH, 1% SDS

Buffer P3 (neutralization buffer) – 3.0 M potassium acetate, pH 5.5

2.2.7. DNA extraction from agarose gel

For extraction of DNA fragments from agarose gel, in some cases a PureLink Quick Gel Extraction Kit from Invitrogen was used. This was done according to the manufacturer's protocol. In other cases, phenol/chloroform extraction of the DNA fragments was performed. The DNA band of interest was cut and crushed. 1 ml phenol solution was added and the tube was vortexed for 1 min. This was followed by incubation of the tube overnight at -80°C. The tube was then spun for 30 min at 15000 rpm. The upper phase was put in another tube, the same volume of phenol:chloroform (1:1) was added, the tube was then vortexed for 1 min and spun for 5 min at 15000 rpm. The upper phase was again taken and the same volume of chloroform was added to it followed by vortexing the tube for 1 min. The tube was then spun for 3 min at 15000 rpm. The upper phase was put again in a new Eppendorf tube. DNA was precipitated, washed with 70% ethanol and resuspended in water.

2.2.8. Phenol/chloroform extraction of the targeting vector

The linearized Strep-Myc-SUMO3 knock-in targeting vector was purified by phenol/chloroform extraction. An equal amount of phenol/chloroform (1:1) was added to the digestion reaction and the tubes were shaken gently. They were centrifuged at 15000 rpm for 15 min. The upper phase was placed in a new tube. This procedure was repeated again twice. After that, the procedure was repeated once only with chloroform. Sodium acetate was added to a final concentration of 0.25 M and the solution was mixed. 2 volumes of 100% ethanol were also added. The solution was mixed and was left at -20°C for at least one hour. This was followed by centrifugation for 15 min at 15000 rpm. From this point on, the steps were performed in the tissue culture hood. The DNA pellet was washed twice with 1 ml 70% ethanol and let to air-dry. After that, the pellet was resuspended in 50 μl sterile 0.1x TE buffer and all the aliquots were put together.

2.2.9. Recombineering

Two colonies of SW106 bacteria containing BAC DNA with the *SUMO3* gene were inoculated in 5 ml LB with chloramphenicol and left shaking overnight at 32°C. 30-40 ml of LB with chloramphenicol were inoculated with 1 ml of the overnight culture and left shaking at 32°C until the OD reached 0.6. At this point, 15 ml of the culture were placed in a 100 ml Erlenmeyer flask and incubated for 15 min at 42°C in a shaking waterbath. Another 15 ml of the culture were incubated shaking at 32°C serving as an uninduced control. Then, electrocompetent bacteria were prepared from the induced and uninduced cultures. Bacteria

were spun down for 10 min, resuspended in 1 ml ice-cold water and then the falcon was filled up to 10 ml with ice-cold water and was inverted several times. These steps were repeated two more times. Finally, cells were spun again, the supernatant was removed and cells were resuspended in the remaining water. The linearized and dephosphorylated vector was electroporated in the induced and uninduced bacterial cells. Bacteria were then resuspended in 1 ml LB and left shaking for 1 hour at 32°C. They were concentrated, plated on ampicillin plates and left at 32°C overnight.

2.2.10. Agarose gel electrophoresis

DNA samples were loaded on agarose gels with different percentage depending on the purpose. To run the DNA, 1x TBA buffer was used. For the visualization of the DNA in the gel, ethidium bromide or GelRed were used.

2.2.11. TOPO cloning

TOPO cloning was performed using the TOPO TA cloning kit according to the manufacturer's protocol. When the generated PCR product did not have 3'-A overhangs, it was additionally incubated with RedTaq polymerase.

2.2.12. Standard cloning procedures

All other standard cloning procedures (including restriction digest, ligation, dephosphorylation, PCRs, generation of blunt ends with Klenow polymerase) were carried out as described previously (Sambrook & Russell, 2001) and according to manufacturer's protocols.

2.3. Cell cultures

2.3.1. Mouse embryonic fibroblasts

2.3.1.1. Mouse embryonic fibroblasts culture

Mouse embryonic fibroblasts (MEFs) were grown in medium made by mixing 500 ml KO-DMEM, 95 ml FBS, 6ml MEM non-essential amino acids, 6 ml Glutamine, 6 ml 10 mM β-mercaptoethanol, and 3 ml Pen/Strep.

Before use, the flasks and the dishes for growing MEFs were coated with gelatin. 0.1% gelatin was placed in the flasks and dishes and incubated for minimum one hour at room temperature (RT). The gelatin was removed just before plating the MEFs.

For passaging MEFs, cells were washed once with PBS which was followed by addition of 0.05% Trypsin which is enough to cover the surface. Cells were incubated for 3-5 min at 37°C until they detach. An equal volume of medium was added, cells were triturated and then transferred to new flasks with sufficient amount of medium.

For freezing MEFs, cells were washed with PBS and 0.05% Trypsin was added. Cells were then incubated for several min at 37°C until they detach. An equal amount of medium was added and cells were triturated. Cells were spun for 7 min, the supernatant was discarded and they were resuspended in MEF medium. An equal amount of 2x Freezing medium was added dropwise. Cells were then aliquoted in cryovials and frozen overnight in a freezing box at -80°C.

2x Freezing medium: 60% DMEM, 20% FBS, 20% DMSO

2.3.1.2. Inactivation of MEFs

For inactivation of MEFs, cells were incubated for 2.5 hours with 10 μg/ml mitomycin C at 37°C. They were then washed 3-4 times with PBS. 0.05% Trypsin was added which was followed by incubation for several min at 37°C until cells detach. An equal amount of medium was added, cells were triturated, if needed resuspended in appropriate volume of M15 medium and plated.

2.3.2. Embryonic stem cells

2.3.2.1. Embryonic stem cells culture

Embryonic stem (ES) cells were grown in M15 medium made by mixing 500 ml KO-DMEM, 95 ml FBS, 6 ml MEM non-essential amino acids, 6 ml glutamine, 6 ml 10 mM β-mercaptoethanol, 3 ml Pen/Strep, and 65 μl LIF. ES cells were plated on feeder plates (containing inactivated MEFs).

The thawing of ES cells was performed by first putting the vial quickly in a 37°C water bath. Then, cells were diluted with 12 ml M15 medium in a 15 ml Falcon tube, the first 3-4 ml of the M15 medium being added dropwise. Cells were mixed and spun for 7 min. The su-

pernatant was discarded, cells were resuspended in 6 ml M15 medium and then plated on feeder plates.

Cells needed to be fed 3-4 hours before splitting. Cells were washed twice with PBS, 0.25% Trypsin was added and they were incubated at 37°C for 10-15 min until they detach. M15 medium was added, cells were triturated and then plated.

ES cells needed to be fed 3-4 hours before freezing. Cells were washed once with PBS, 0.25% Trypsin was added and they were incubated for 10-15 min at 37°C. An equal amount of M15 medium was added and cells were triturated. Cells were spun for 7 min, the supernatant was discarded and they were resuspended in M15 medium. An equal amount of 2x Freezing medium was added dropwise. After every drop, the tubes were mixed. Cells were then placed in cryovials which were put in a freezing container and frozen overnight at -80°C.

2.3.2.2. Electroporation of embryonic stem cells

Cells were fed 3-4 hours before electroporation. One 10 cm dish was trypsinized with 0.25% Trypsin, cells were incubated at 37°C for 10-15 min, an equal amount of M15 medium was added and trituration was performed. Then, cells were transferred into a Falcon tube, spun for 7 min and resuspended in PBS. After that, the concentration of the cells was adjusted to 11 million cells per ml. 0.9 ml of the cells were mixed with 25 μg (25 μl) vector. 0.9 ml of the cells and DNA mixture were transferred to an electroporation cuvette and electroporation was performed with the BioRad GenePulser set at 230 V, 500 μF. The cuvette was then incubated at RT for 5 min and cells were plated on 10 cm feeder plates. From the following day on, cells were subjected to positive selection by supplementing the M15 medium with G418 with a final concentration of 180 μg/ml. Between the third and the fifth days after the electroporation, the medium was also supplemented with ganciclovir at final concentration of 2 μM.

2.3.2.3. Picking embryonic stem cell colonies

20-25 μl of 0.25% Trypsin were added into the wells of 96-well round bottom plate and the plates were kept on ice. The medium from the petri dishes containing the ES cells was substituted with 30 ml PBS. Colonies were picked and transferred into the plates containing Trypsin. After the completion of a plate, it was incubated for 10-15 min at 37°C. After the incubation time was over, 35 μl of M15 medium containing G418 were added per well and cells were gently triturated. Cells were then transferred to 96-well feeder plates which con-

tained 100 µl of M15 medium with G418. After a few days, cells were split onto two feeder plates and two gelatinized plates.

2.3.2.4. Freezing 96-well plates with embryonic stem cells

Cells were fed 3-4 hours before freezing. Cells were washed twice with PBS, 50 µl 0.25% Trypsin were added and they were incubated at 37°C for approximately 15 min. After that, 50 µl of 2x Freezing medium were pipetted in each well and cells were triturated. 100 µl of filter-sterilized light paraffin oil were placed in each well. The plates were then closed, sealed with parafilm, placed in a polystyrene box and put in the -80°C freezer.

2.3.2.5. Isolating embryonic stem cell DNA and validation of positive embryonic stem cell clones

Stem cell DNA was isolated from the ES cell clones grown on gelatine. ES cells were washed twice with PBS and subjected to lysis with 50 µl of lysis buffer. The 96-well plates were then incubated overnight in a humidified chamber. On the next day, a fresh solution of 75 mM NaCl in ethanol was prepared by adding 150 µl of 5 M NaCl to 10 ml of cold absolute ethanol and mixing well. 100 µl of this solution were added per well and the plates were incubated at RT for approximately 15-60 min. To pour off the solution, the plates were inverted while the DNA sticked to the plate. The plates were then washed three times with 70% ethanol and stored at -20°C in the last ethanol wash.

Lysis buffer: 10 mM Tris pH 7.5, 10 mM EDTA pH 8.0, 10 mM NaCl, 0.5% Sarcosyl, 1 mg/ml proteinase K which is added fresh each time

For validation of positive ES cell clones, the plate was inverted to discard the ethanol and let to air-dry. DNA was then dissolved in 30 µl of 10 mM Tris (pH 8) and was used to perform diagnostic PCR as follows:
Diagnostic PCR of the 5' arm:
31629 (1) x 22574 (2) = 1155 bp
33662 (2) x 33455 (4) = 2923 bp
33462 (2) x 33456 (5) = 2924 bp
33462 (2) x 33457 (6) = 2991 bp

Diagnostic PCR of the 3' arm:
4174 (7) x 33570 (8) = 6603 bp

The primers are listed in Table 2.2. PCR was performed in duplicates. All PCR fragments were confirmed by sequencing. The PCR settings were the following:

1. 98.0°C 00:02:00
2. 98.0°C 00:00:30
3. 64.0°C 00:01:00
4. 72.0°C 00:03:00
5. go to 2 34x
6. 72.0°C 00:07:00
7. 12.0°C forever

2.3.3. HEK293FT cells

2.3.3.1. HEK293FT cells culture

HEK293FT cells were grown using standard cell culture techniques. The HEK cells medium was made by mixing 500 ml DMEM with GlutaMAX, 50 ml FBS and 5 ml Pen/Strep.

2.3.3.2. HEK293FT cells transfection

2.5 μg of each DNA construct were added to 100 μl Opti-MEM. Furthermore, 5 μl Lipofectamine were added to 100 μl Opti-MEM. The DNA-Opti-MEM mix was added to the Lipofectamine-Opti-MEM mix. The mixtures were then incubated for approximately 20 min under the hood and added dropwise to the cells.

2.4. Generation of the Strep-Myc-SUMO3 knock-in mouse line and genotyping strategy

For the generation of Strep-Myc-SUMO3 knock-in mouse line, a positive ES cell clone was injected into C57 mice blastocysts. A PCR evaluation showed that chimeras transmitting the mutation via the germ line were obtained. Mice heterozygous for the mutated *SUMO3* gene, which were offspring of the chimeric mice, were crossed with EIIa-cre mice expressing the *cre* transgene in early embryonic stages, the transgene being under the control of the adenovirus EIIa promoter (Lakso *et al.*, 1996). PCR was used to evaluate germ line transmission of the Cre recombined gene. Heterozygous for the mutation mice were crossbred

for the generation of WT and KI littermates which were further used for the generation of separate WT and KI lines.

In order to perform genotyping, DNA was isolated from tail tips using Nextec kit. Diagnostic PCR was performed as follows:

34055 (9) x 34056 (10) = 339bp (SUMO3 WT)

34055 (9) x 16825 (11) = 368bp (SUMO3 KI)

34055 (9) x 34056 (10) = 463bp (SUMO3 KI with Neo cassette removed)

The primers are listed in Table 2.2. PCR reactions were set up in the following way:

MasterMix: MG143 UHF_HotStartPCR_biotool

0.8 µl water

10 µl 2xUniverse Buffer (CatNo. B21103, LotNo. 4209043)

4 µl dNTPs (Bioline # DM-515107)

0.2 µl Universe High-Fidelity Hot Start DNA Polymerase (CatNo. B21103, LotNo. 4209043)

4 µl 1 PrimerSet (1 pmol/µl each)

1-2 µl DNA

Total: 20 µl

The PCR settings were the following:

1. 96.0°C 00:03:00
2. 94.0°C 00:00:30
3. 62.0°C 00:01:00
3. 72.0°C 00:01:00
4. go to 2 32x
5. 72.0°C 00:07:00
6. 12.0°C forever

2.5. Biochemistry

2.5.1. Antibodies

Table 2.5. Antibodies used for biochemistry in this study

Antibody	Concentration	Company	Cat. No.
Primary antibodies			
Mouse monoclonal anti-HA.11 (clone 16B12) (quantitative Western blot of SUMO1 conjugation levels)	1:1000	Biolegend	901501
Mouse monoclonal anti-HA.11 (clone 16B12) (subcellular fractionation)	1:1000	Covance, Biolegend	MMS-101R-500
Mouse monoclonal anti-GluN1	1:1000	Synaptic systems	114 011
Mouse monoclonal anti-synaptophysin	1:1000	Synaptic systems	101 011
Mouse monoclonal anti-SUMO2/3	1:1000 (testing of tags) 1:1000 (basic characterization)	Hybridoma Bank	8A2
Rabbit polyclonal anti-Myc	1:1000	Sigma	C3956
Secondary antibodies			
Goat anti-mouse IgG HRP-conjugated	1:5000 (testing of tags)	Jackson	705-035-003
Goat anti-mouse IgG HRP-conjugated (H&L)	1:5000	BIO-RAD	172-1011
Goat anti-rabbit IgG HRP-conjugated (H&L)	1:5000	BIO-RAD	172-1019

2.5.2. Basic characterization of the Strep-Myc-SUMO3 knock-in mouse line

8-12-week-old mice were sacrificed by cervical dislocation, their brains were taken and flash frozen in liquid nitrogen. Brains were then reduced to powder with a porcelain mortar and pestle in a liquid nitrogen bath. Cold RIPA buffer (150 mM NaCl, 1% Triton X-100, 10 mM Tris, pH 7.4) containing protease inhibitors (1 μg/ml aprotinin, 0.5 μg/ml leupeptine,

17.4 μg/ml PMSF) and 20 mM NEM was used to resuspend the powder. The powder was then sonicated and ultracentrifuged at 100000 x g for 1 hour at 4°C. The supernatant was incubated then for 4 h at 4°C on a rotating wheel with 0.2 ml anti-Myc beads (Sigma or Biotool). Then, the beads were subjected to pelleting and washing several times in RIPA buffer. SDS-PAGE sample buffer was used to directly elute the bound material. Western blot analysis with anti-Myc (Sigma) and anti-SUMO2/3 (Hybridoma Bank) antibodies was performed with the input and the eluted material.

2.5.3. Quantitative Western Blots to investigate SUMO1 conjugation levels

Mice of different ages were sacrificed by cervical dislocation which was followed by dissection of hippocampi and cortices on ice. Tissue was lysed in 150 mM NaCl, 20 mM Tris pH 7.4 containing protease inhibitors (1 μg/ml aprotinin, 0.5 μg/ml leupeptine, 17.4 μg/ml PMSF) and 20 mM NEM in a small glass potter homogenizer. The protein concentrations of the samples were assessed using the BCA assay (Pierce). The samples were separated by SDS-PAGE with the use of commercially available 4%-12% Bis-Tris gradient gels from Invitrogen. This was followed by Western blot. Memcode assay (Pierce) was used to visualize the transferred on the membrane proteins. Anti-HA antibody from Biolegend was used and for developing, enhanced chemiluminiscence (GE Healthcare) was utilized, as the Odyssey method could not detect the weak signal. Labeling with Memcode and anti-HA was assessed by ImageJ. The values were divided by the Memcode value for the corresponding lane and after that normalized to the average sample value. Loading of the samples was done in three replicates at various positions on the gel. N=6

SDS-PAGE sample buffer: 2% SDS, 62.5 mM Tris, 10% glycerol, 1% β-mercaptoethanol, 0.01% bromphenol blue, pH 6.8

2.5.4. Subcellular fractionation of brain tissue

Subcellular fractionation was performed as described previously (Jones & Matus, 1974; Tirard *et al.*, 2012). Brains were subjected to homogenization in 10 ml 320 mM sucrose containing 4 mM HEPES pH 7.4, 20 nM NEM, and protease inhibitors (1 μg/ml aprotinin, 0.5 μg/ml leupeptine and 17.4 μg/ml PMSF) with a glass-Teflon homogenizer (900 rpm, 12 strokes). Homogenates (H) were spun at 1000 x g for 10 min at 4°C with an SS - 34 rotor (Sorvall). The supernatant (S1) was separated from the pellet (P1) and spun at 12500 x g for

15 min at 4°C with an SS - 34 rotor. The supernatant was discarded, 9 volumes of cold water were used to resuspend the synaptosome-enriched pellet (P2). The pellet was homogenized using a glass-Teflon homogenizer (1500 rpm, 10 strokes) and spun for 20 min at 4°C with an SS-34 rotor at 25000 x g. For the generation of fractions LP2 and LS2, the supernatant (LS1) was spun at 200000 x g for 2 h at 4°C. The pellet (LP1), on the other hand, was subjected to resuspension in 1 ml homogenization buffer and placed on top of a two-step sucrose gradient (1.2 M and 5 ml of 0.8 M sucrose, 4 mM HEPES, protease inhibitors as stated above). The resulting gradient was spun for 2 hours at 62000 x g at 4°C with an SW - 41Ti rotor (Beckman). Synaptosomes were present at the interface of 0.8 M and 1.2 M sucrose and recovered with a Pasteur pipette. For the generation of the SPM fraction, the recovered synaptosomal fraction was diluted 10-fold and pelleted at 37000 x g at 4°C for 20 min using SS – 34 rotor. H, homogenate; P, nuclear pellet; S1, supernatant after P1 sedimentation; P2, crude synaptosomal pellet; S2, supernatant after P2 sedimentation; LP1, lysed synaptosomal membranes; LS1, supernatant after LP1 sedimentation; LP2, synaptic vesicle-enriched fraction; LS2, supernatant after LP2 sedimentation; SPM, synaptic plasma membrane.

2.5.5. SDS-PAGE and Western blotting for testing SUMO3 tags

2.5.5.1. Sample preparation

On the day after the transfection, cells which were incubated at 37°C were washed once with PBS and resuspended in 250 µl Lysis buffer containing fresh 20 nM NEM and 1x protease inhibitors. To lyse the cells, they were left on ice for 10 min and inverted regularly. Then, samples were centrifuged at maximum speed for 15 min. Supernatant was placed in a new Eppendorf tube. The concentration of the protein samples was determined using the BCA assay (Pierce). Samples were diluted with Lämmli buffer containing appropriate amount of DTT for final concentration of 100 mM and boiled for several min.

Lysis buffer (RIPA) – 150 mM NaCl, 20 mM Tris pH 7.4, 1% Triton

2.5.5.2. SDS-PAGE and Western blotting

Samples were run on a commercially available 4%-12% Bis-Tris gel and transferred to a nitrocellulose membrane for 16 h at 45 mA. Equal loading of the samples was assessed by Ponceau staining. The nitrocellulose membrane was blocked for 1 hour in 5% milk in PBST. This was followed by 2-hour incubation with primary antibody (mouse monoclonal anti-

SUMO2/3) with a concentration 1:000 in 5% milk in PBST. The membrane was washed three times with 5% milk in PBST and incubated for 1 hour with secondary antibody at a dilution of 1:5000 in 5% milk in PBST. The membrane was washed again three times with 5% milk in PBST, twice with PBS and developed using the ECL kit.

2.6. Immunohistochemistry

2.6.1. Antibodies

Table 2.6. Antibodies used for immunohistochemistry in this study

Antibody	Concentration	Company	Cat. No.
Primary antibodies			
Mouse monoclonal anti-c-Myc (clone 9E10)	1:500, 1:1000 (Fig. 3.5. 1:1000 heterozygous mice, 1:500 homozygous mice)	Sigma	M5546
Rabbit polyclonal anti-c-Myc	1:1000, 1:500, 1:250 (Fig.3.6. 1:500 heterozygous, 1:250 homozygous)	Sigma	C3956
Rabbit polyclonal anti-c-Myc (A-14)	1:250	Santa Cruz Biotechnology	sc-789
Mouse monoclonal anti-c-Myc	1:250	Life Technologies	132500
Mouse monoclonal anti-c-Myc (clone 9E11)	1:250	Santa Cruz Biotechnology	sc-47694
Mouse monoclonal anti-Strep (StrepMAB-Classic)	1:1000, 1:500 (Fig. 3.9. 1:500)	Iba	2-1507-001
Goat polyclonal anti-HA	1:500	Novus Biologicals	NB600-362
Chicken polyclonal anti-MAP2	1:1000	Novus Biologicals	NB300-213
Mouse monoclonal anti-β-amyloid 1-16 (clone 9E10)	1:1000	Covance	SIG-39320
Mouse monoclonal anti-HA.11 (clone 16B12)	1:1000	Covance	MMS-101R-500
Mouse monoclonal anti-HA.11 (clone 16B12)	1:1000	BioLegend	901501

Rabbit polyclonal anti-$A\beta_{42}$	1:500	Synaptic Systems	218-703
Secondary antibodies			
Goat anti-mouse Alexa555	1:1000	Invitrogen	A21424
Goat anti-rabbit Alexa555	1:1000	Mobitec	A21429
Goat anti-chicken Alexa633	1:1000	Invitrogen	A-21103
Donkey anti-goat Alexa555	1:1000	Mobitec	A21432
Goat anti-rabbit Alexa488	1:1000	Invitrogen	A11008
Goat anti-mouse Alexa488	1:1000	Mobitec	A11029

2.6.2. Tissue preparation

Mice were anaesthetized with isofluorane and injected with avertin solution. Mice were then transcardially perfused with 4% PFA in phosphate buffer using the following perfusion protocol:

12 (speed of the pump) – 1 min

11 – 1 min

10 - 1 min

9 – 1 min

8 – 8 min

Depending on the perfusion quality, brains were postfixed at least for 1 hour in 4% PFA. After the postfixation, brains were moved sequentially in 10%, 20% and 30% sucrose in phosphate buffer. In order to proceed with placing the brains in a solution with higher sucrose concentration, brains needed to sink. Brains were incubated for at least 24 hours in 30% sucrose.

To prepare brains for cutting, they were cut in two sagittally and rolled on the surface of dry ice wrapped in aluminum foil. Then, brains were embedded in Tissue-Tek and kept in the Cryostat (Leica) for at least one hour. 35 μm sagittal brain sections were cut and stored in PBS with sodium azide at 4°C.

Avertin solution: 100 μl stock avertin, 400 μl 100% ethanol, 4.5 ml 0.9% NaCl

2.6.3. Immunostaining

For localizing Strep-Myc-SUMO3, sections were blocked with PBS containing 5-10% normal goat serum (NGS) or 5% horse serum, 0.3-0.5% Triton X-100 and in some cases 1% fish skin gelatin and 1% BSA. For labeling His_6-HA-SUMO1, sections were blocked with PBS containing 5% NGS or horse serum and 0.3% Triton X-100. The blocking step was performed for 1 hour at RT. The blocking solutions were also used for diluting the primary and secondary antibodies. Sections were incubated with the primary antibodies overnight at 4°C. On the next day, sections were washed three times with PBS. From this point on, the incubations were done in the dark. Sections were incubated for approximately 2 hours with a secondary antibody, washed three times with PBS and mounted using Vectashield containing DAPI. For staining His_6-HA-SUMO1 with goat anti-HA antibody, sections were incubated first with donkey anti-goat antibody for 2 hours, washed three times with PBS and then incubated for another 2 hours with goat anti-mouse and goat anti-chicken antibodies.

2.6.4. Image acquisition

Confocal microscopy was performed using Leica TCS-SP5. Single-plane images were taken with 40x oil objective. For some images, a zoom factor of 3 was used. For a given labeling, the gain and the offset were kept constant.

2.6.5. Figure preparation and image analysis

All the figures containing confocal images were created using Photoshop CS5.1. Readjustment of the tonal range of the images was the only change to which the original data was subjected.

For quantification of the nuclear anti-HA signal in His_6-HA-SUMO1 knock-in mice, ImageJ was utilized. Pyramidal neurons in cortical layer V were selected by location and/or size and/or shape. For choosing the appropriate neurons in the subiculum, a line was drawn separating the big pyramidal cells from the mostly small cells located in the deep subiculum. These deeply located cells were excluded from the analysis. For quantification of the anti-HA signal, a line surrounding the anti-HA labeled nuclei was drawn. This was followed by obtaining information about the mean intensity of the circled area by choosing Analyze $\rightarrow$ Measure. The average intensity from all the neurons in the examined section was then found which was followed by finding the average intensity of all the sections examined for a given mouse.

2.7. Statistics

For the comparison of the nuclear anti-HA signal in His_6-HA-SUMO1 knock-in 5xFAD and non-5xFAD mice, GraphPad was used to perform two-tailed unpaired Student's t-test.

For the quantitative Western blot, a 2-way ANOVA with genotype and age as factors was used to conduct statistical analysis for both hippocampal and cortical tissues. There was no significant main effect of genotype or genotype x age interaction. The age factor was significant for both hippocampus and cortex (hippocampus P=0.009, cortex P=0.01).

3. Results

3.1. Generation and basic characterization of a Strep-Myc-SUMO3 knock-in mouse line

3.1.1. Choosing the appropriate tag

The generation of a knock-in mouse model that can be reliably used for the localization of SUMO3 and the identification of SUMO3 substrates requires the choice of appropriate tags. An important characteristic of an appropriate tag is that it should not affect the function of the tagged protein. Thus, in order to facilitate the choice of the tag that should be incorporated in the SUMO3 knock-in mouse model, we cloned constructs encoding untagged SUMO3 or SUMO3 with Myc-HA and Strep-Myc tag. HA-SUMO2 and His_6-SUMO2 in pCRUZ were a kind gift from Prof. Dr. Frauke Melchior. We transfected the prepared plasmids into HEK293FT cells and performed SDS-PAGE and Western blot analysis of whole cell extracts with an anti-SUMO2/3 antibody in order to test if the tags affect the SUMO3 conjugation pattern (Fig. 3.1.). As a control, we transfected 'empty' pcDNA3 to be able to draw a comparison with endogenous SUMO2/3 conjugation. Notably, neither the overexpression of untagged SUMO3, nor the overexpression of SUMO3 with any of the tags resulted in obvious changes of the SUMO2/3 conjugation pattern. A drawback of this experiment was, though, that it was not possible to judge what percentage of the overexpressed SUMO3 remains free and what percentage is conjugated to proteins. Furthermore, as SUMO2 and SUMO3 cannot be distinguished by antibodies, in all the lanes endogenous SUMO2 is also detected.

Additionally, we wanted the chosen tag to be suitable for affinity purification and immunostaining and, ideally, to differ from the His_6-HA tag present in the SUMO1 knock-in mouse model. Thus, we chose the double tag Strep-Myc for the generation of the SUMO3 knock-in mouse model. A double tag allows alternative options for investigation and, additionally, allows the performance of a two-step affinity purification protocol.

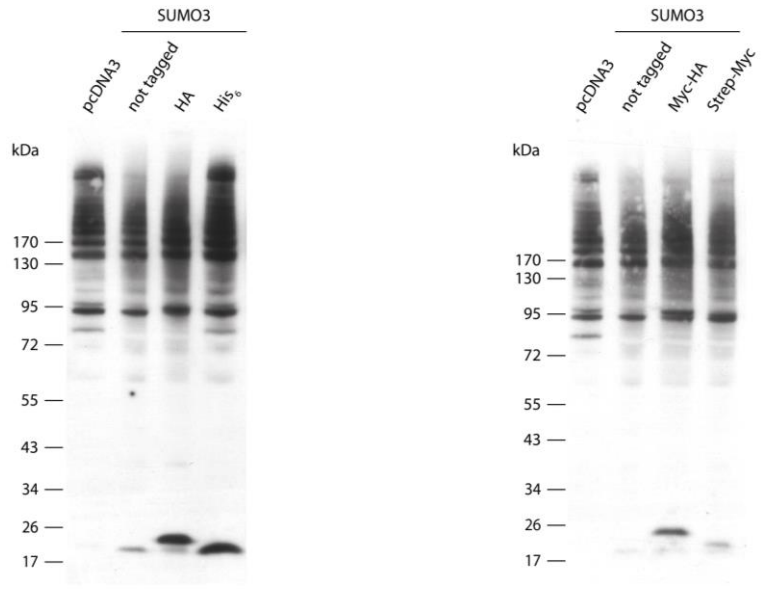

Fig. 3.1. Testing of SUMO3 tags for the generation of a SUMO3 knock-in mouse model.

HEK293FT cells were transfected with SUMO3, HA-SUMO3, His_6-SUMO3, Myc-HA-SUMO3, Strep-Myc-SUMO3 or with 'empty' pcDNA3 as a control. Whole cell extracts were analyzed by SDS-PAGE and Western blotting. Anti-SUMO2/3 antibody was used for probing the extracts. Note the endogenous SUMO2/3 and the transfected SUMO3 at the bottom part of the membranes.

3.1.2. Generation of the targeting vector

We decided to generate the SUMO3 knock-in mouse model using homologous recombination in mouse embryonic stem (ES) cells. Thus, the targeting vector had to contain two homology arms so that homologous recombination could take place. In addition, the 5' homology arm, which carried the exon 1 of the *SUMO3* gene, had to undergo insertion of the Strep-Myc tag after the start codon (ATG) of the *SUMO3* gene (Fig. 3.2.).

The first step in the generation of the SUMO3 knock-in targeting vector was the retrieval of the 5' and the 3' homology arms by a chromosome engineering approach called recombineering. This approach involves homologous recombination in *E.coli*, which is mediated by lambda phage-encoded Red proteins (Liu *et al.*, 2003). In order to retrieve the 5' homology arm, firstly, 5' and 3' miniarms were PCR-amplified from a BAC DNA containing the full sequence of the *SUMO3* gene. The amplified miniarms were then cloned into a TOPO vector. The 5' miniarm was excised from the TOPO vector with SalI and SpeI, while the 3' miniarm was excised with SpeI and EcoRI. The two inserts were then ligated with a triple ligation into pBluescript II SK (-) that had been digested with SalI and EcoRI.

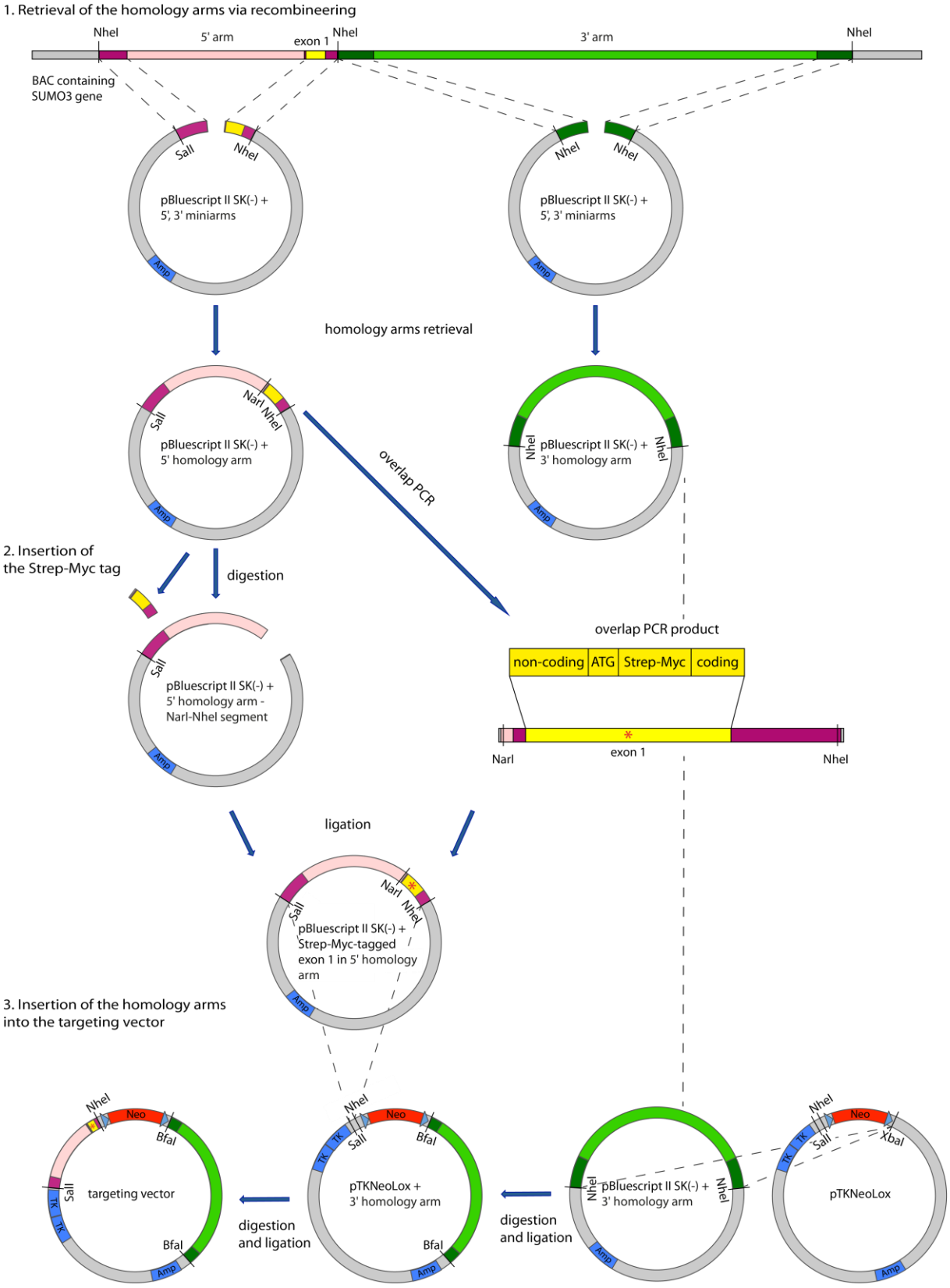
1. Retrieval of the homology arms via recombineering
NheI
5' arm
exon 1
NheI
3' arm
NheI
BAC containing SUMO3 gene
SalI
NheI
pBluescript II SK(-) + 5', 3' miniarms
Amp
NheI
NheI
pBluescript II SK(-) + 5', 3' miniarms
Amp
homology arms retrieval
SalI
NarI NheI
pBluescript II SK(-) + 5' homology arm
Amp
overlap PCR
NheI
pBluescript II SK(-) + 3' homology arm
NheI
Amp
2. Insertion of the Strep-Myc tag
digestion
SalI
pBluescript II SK(-) + 5' homology arm - NarI-NheI segment
Amp
overlap PCR product
non-coding
ATG
Strep-Myc
coding
NarI
exon 1
NheI
ligation
SalI
NarI NheI
pBluescript II SK(-) + Strep-Myc-tagged exon 1 in 5' homology arm
Amp
3. Insertion of the homology arms into the targeting vector
NheI
Neo
BfaI
SalI
targeting vector
TK
TK
BfaI
Amp
digestion and ligation
NheI
Neo
TK
TK
SalI
BfaI
pTKNeoLox + 3' homology arm
BfaI
Amp
digestion and ligation
NheI
pBluescript II SK(-) + 3' homology arm
NheI
Amp
NheI
Neo
TK
TK
SalI
XbaI
pTKNeoLox
Amp

Fig. 3.2. Cloning strategy for the generation of the Strep-Myc SUMO3 knock-in targeting vector.

1. Retrieval of the homology arms via recombineering. For the retrieval of the 5' and the 3' homology arms, 5' and 3' miniarms were amplified from a BAC DNA containing the *SUMO3* gene and inserted into pBluescript II SK (-) vectors. For the retrieval of the 5' homology arm, the vector was linearized with SpeI, while for the retrieval of the 3' homology arm, the corresponding vector was linearized with BclI. Recombineering was performed using the SW106 bacterial strain containing the aforementioned BAC DNA. **2. Insertion of the Strep-Myc tag**. With the use of overlap PCR, a small fragment that contains the Strep-Myc tag after the starting codon of exon 1 of *SUMO3* was generated. This fragment was used for the substitution of the wild type fragment in pBluescript II SK (-) that contains the retrieved 5' homology arm. **3. Insertion of the homology arms into the targeting vector.** The 5' and 3' homology arms were inserted into the backbone of pTKNeoLox using the SalI and NheI sites, and the XbaI site, respectively.

Importantly, the SpeI restriction site had then to be removed from the multiple cloning site of the pBluescript vector containing the miniarms. This was achieved by digestion of the plasmid with BamHI and XbaI, subsequent treatment with Klenow polymerase followed by ligation of the blunt ends. After that, in order to prepare for the recombineering, BAC DNA containing the *SUMO3* gene was electroporated in SW106 bacterial strain, which expresses lambda phage-encoded recombination proteins upon heat induction (Liu *et al.*, 2003). For the retrieval of the 3 kbp 5' homology arm, the pBluescript vector containing the miniarms was linearized with SpeI and dephosphorylated. Then the recombineering was performed and colonies with successful retrieval of the 5' homology arm were validated by restriction digestion analysis and sequencing.

In order to retrieve the 3' homology arm, 5' and 3' miniarms were again PCR amplified and cloned into TOPO vectors, which were amplified in Dcm^-/Dam^- bacteria. A triple ligation reaction was then performed after excision of the TOPO inserts with NheI and BclI and after digestion of pcDNA3.1 (-) with NheI. Later, the joined miniarms were PCR-amplified and subcloned in pBluescript II SK (-). For the recombineering, the pBluescript vector, which had been amplified in Dcm^-/Dam^- bacteria, containing both of the miniarms, was linearized with BclI and dephosphorylated. Successful retrieval of the 3' homology arm was validated by restriction digestion analysis and sequencing.

The second step of the generation of the targeting vector was the introduction of the Strep-Myc tag after the start codon of *SUMO3.* In order to achieve this, first, Strep-Myc tag was introduced by overlap PCR into a small fragment containing exon 1 of *SUMO3*. This fragment was then cloned into a TOPO vector. After that, the wild type fragment from the 5' homology arm was substituted with the fragment containing the tagged exon 1. This was

achieved by excising the respective insert from TOPO with NarI and NheI and cloning it into the respective sites of the pBluescript vector lacking the wild type fragment.

The final step in the generation of the targeting vector was the subcloning of the retrieved 5' and 3' homology arms from pBluescript II SK (-) to pTKNeoLox. Initially, the 3' homology arm was subcloned using the XbaI cloning site. This was followed by introduction of the tagged 5' homology arm using the SalI and the NheI cloning site. Besides with SalI and NheI, pBluescript containing the tagged 5' homology arm was also cut with XmnI.

3.1.3. Generation of the SUMO3 knock-in mouse line

The targeting vector was purified using the EndoFree Plasmid Maxi Kit from Qiagen. For the electroporation, the purified targeting vector was linearized with NotI and adjusted to a concentration of 1 µg/µl. The linearized targeting vector was electroporated into SV129/Ola ES cells. The clones were then subjected to positive and negative selection by using the antibiotic G418 and the antiviral drug ganciclovir, respectively. Cells containing the Neomycin cassette, which is located within the homology arms, are resistant to the antibiotic G418. In contrast, the herpes simplex virus thymidine kinase (HSV-TK) gene is located outside of the homology arms and its incorporation into the cells would signify a non-homologous insertion. The HSV-TK-containing cells are sensitive to ganciclovir (Dubey, 2014). Positive clones were validated by PCR using as a template DNA isolated from ES cells grown on gelatine. Then, injection of a positive clone into C57 mice blastocysts was performed. The goal was the generation of chimeric mice that are able to transfer the mutation to the next generation via the germ line. Later, mice heterozygous for the wanted mutation, which were offspring of the chimeras, were crossbred with EIIa-cre mice, which express Cre recombinase under the control of adenovirus EIIa promoter in early embryonic stages. PCR was used to detect the presence of germ line transmission of the Cre recombined gene (Lakso *et al*., 1996). Later, wild type and knock-in littermates were generated by crossing mutants heterozygous for the mutation. The wild type and knock-in mice were used for the generation of wild type and knock-in mouse lines. Tail tips were used for the preparation of DNA for genotyping. To prepare the DNA, the Nextec genomic isolation kit was used (Fig. 3.3.).

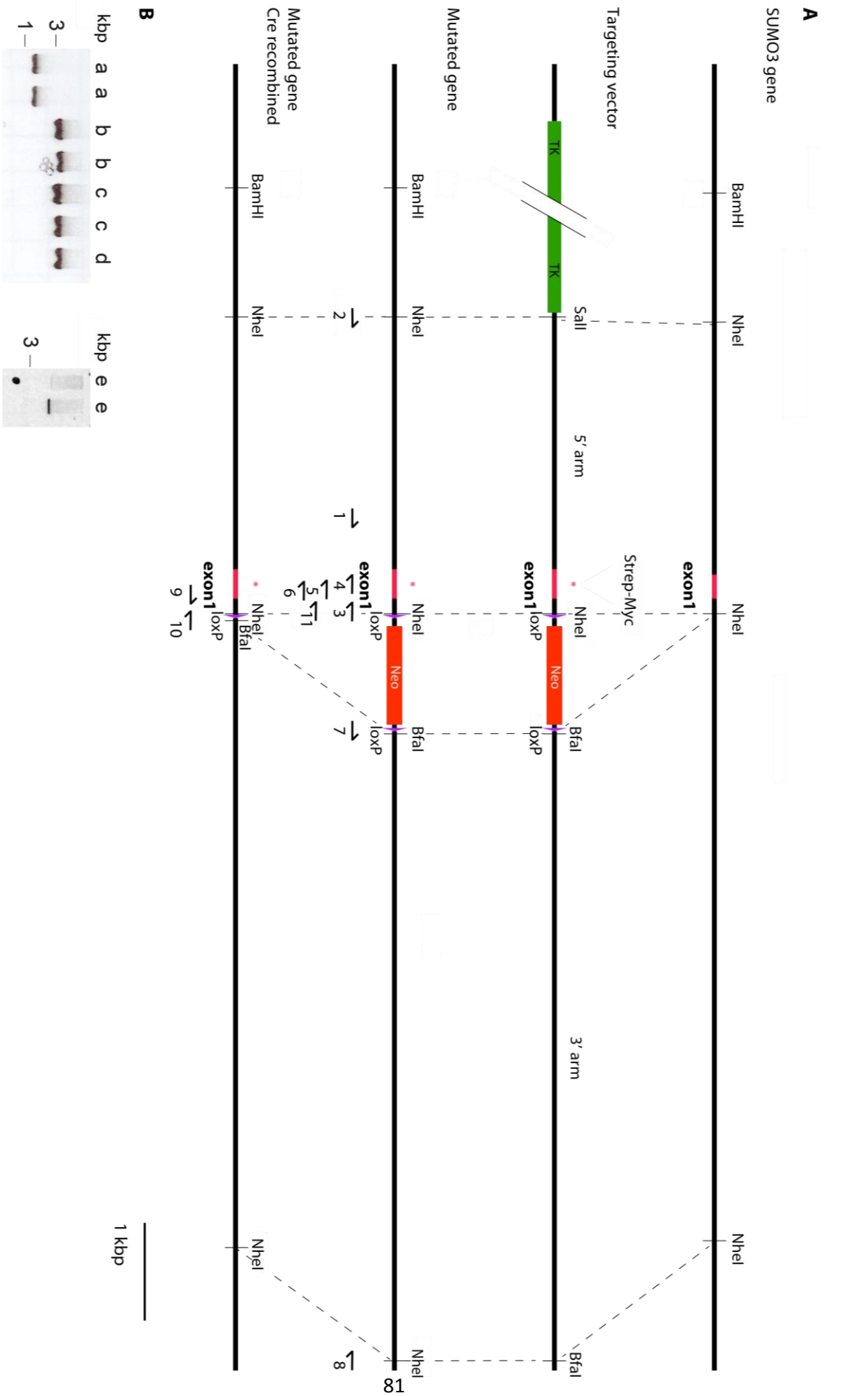
A
SUMO3 gene
BamHI
NheI
exon1
Targeting vector
TK
TK
SalI
5' arm
Strep-Myc
NheI
exon1
loxP
Neo
loxP
BfaI
3' arm
NheI
Mutated gene
BamHI
NheI
exon1
loxP
Neo
loxP
BfaI
NheI
Mutated gene
Cre recombined
BamHI
NheI
exon1
loxP
NheI
BfaI
NheI
1
2
3
4
5
6
7
8
9
10
11
B
kbp
a a b b c c d
3
1
kbp
e e
3
1 kbp

Fig. 3.3. Generation of the Strep-Myc-SUMO3 mouse line.

(**A**) Representation of the structure of the SUMO3 gene, the targeting vector, the mutated gene after homologous recombination and the mutated gene after Cre recombination. The primers used for validation of the positive clones (1, 2, 3, 4, 5, 6, 7, and 8) and for the genotyping (9, 10, and 11) are shown with numbers. Neo: neomycin resistance gene; TK: herpes simplex virus thymidine kinase gene. (**B**) PCR validation of positive clones after homologous recombination in ES cells. a: 1 x 3 = 1155 bp; b: 2 x 4 = 2923 bp; c: 2 x 5 = 2924 bp; d: 2 x 6 = 2991 bp, e: 7 x 8 = 6603 bp. (Data obtained in collaboration with Dr. M. Tirard)

3.1.4. Basic characterization of the SUMO3 knock-in mouse line

After the establishment of the Strep-Myc-SUMO3 knock-in mouse line, we wanted to prove the expression of the tagged SUMO3 and its conjugation to substrates. For this purpose, we employed anti-Myc immunoprecipitation using brain homogenates from knock-in and wild type mice and subsequent SDS-PAGE and anti-Myc and anti-SUMO2/3 Western blot (Fig. 3.4.). The mice were between 8 and 12 weeks old. Two different types of anti-Myc beads were tested. Thus, we were able to show the enrichment of Strep-Myc-SUMO3 conjugates in the eluate from the knock-in mice when compared to wild type mice. This enrichment was accomplished with both types of beads. Additionally, enrichment of free SUMO3 was seen in the knock-in eluate. It should be noted that the expression levels of SUMO2/3 seemed to be very similar between the wild type and the knock-in mice as could be seen from the anti-SUMO2/3 labelling of the two inputs. Thus, we were able to validate the newly generated mouse model demonstrating the expression of tagged SUMO3 and its ability to be conjugated to substrates. The successful enrichment of SUMO3 conjugates by anti-Myc immunoprecipitation also proved that the model can be used as a tool for affinity purification and subsequent identification of SUMO3 substrates.

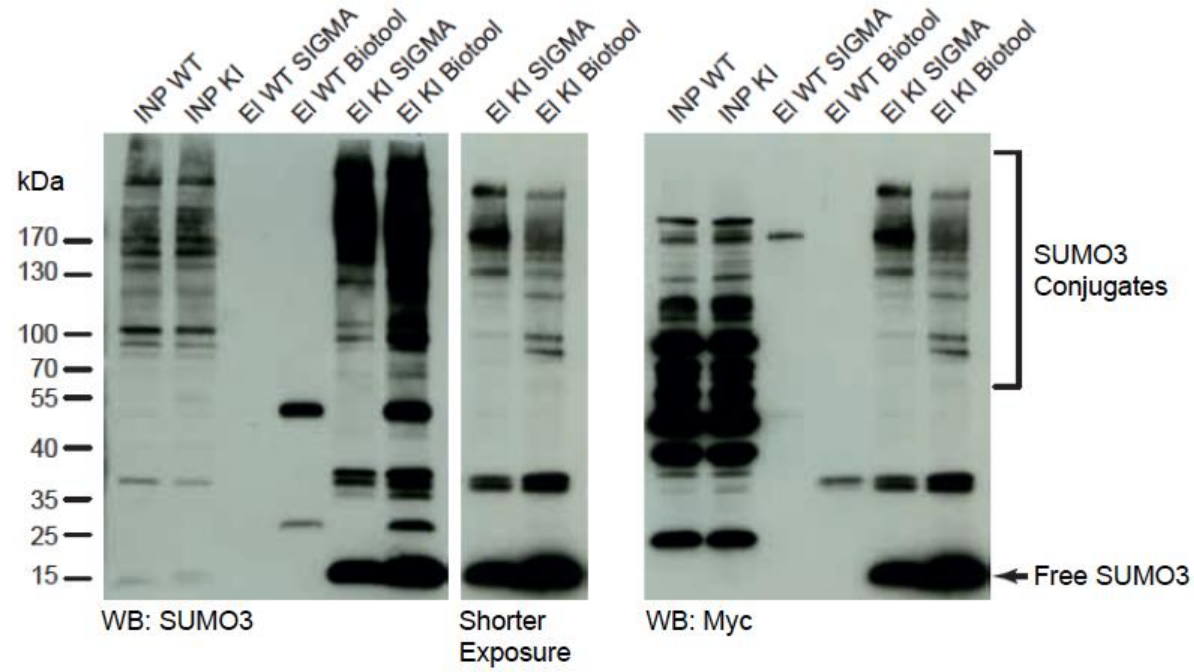

Fig. 3.4. Anti-Myc affinity purification of free Strep-Myc-SUMO3 and Strep-Myc-SUMO3-conjugated proteins from Strep-Myc-SUMO3 knock-in mice.

Brain homogenates from Strep-Myc-SUMO3 knock-in mice (KI) and wild type (WT) mice were subjected to anti-Myc affinity purification using two types of anti-Myc beads – Sigma and Biotool. The input (INP) and the eluate (El) were analysed by SDS-PAGE and Western blotting. Anti-SUMO2/3 and anti-Myc antibodies were used for probing the input and the eluate samples. Note the enrichment of Strep-Myc-SUMO3 conjugates and free Strep-Myc-SUMO3 in the eluate samples from the knock-in mice. (Data obtained in collaboration with Dr. M. Tirard and K. Hellmann)

In the scope of the basic characterization of the mouse line, we also wanted to explore its use as a tool for localization of SUMO3. More specifically, we wanted to focus on SUMO3 localization in the brain. For this purpose, we decided to employ anti-Myc and anti-Strep labelling of brain sections from 5-week-old heterozygous and 11- or 12-week-old homozygous SUMO3 knock-in mice using wild type mice as a negative control. All the mice were male except one 12-week-old homozygous mouse and one 12-week-old wild type mouse. In the following description of the used antibodies we focused on neuronal cells unless otherwise stated. Furthermore, even though specific brain regions were mentioned, this does not exclude the presence of labelling in other brain regions.

The use of a mouse anti-Myc antibody from Sigma (clone 9E10) resulted in pronounced neuronal somata cytoplasmic staining in a heterozygous SUMO3 knock-in mouse in the CA3 hippocampal region, subiculum and dentate gyrus (Fig. 3.5. A). Additionally, in the CA3 hippocampal region, the anti-Myc antibody also labelled the apical dendrites of the pyramidal neurons. Notably, the antibody showed weaker background cytoplasmic staining of

neuronal somata in brain sections from a wild type mouse in the same brain regions. Interestingly, the use of the same clone from a different company (Life Technologies) showed similar results in the upper cortical layers of heterozygous and wild type mice. Unexpectedly, when SUMO3 knock-in homozygous mice were used, two out of four mice exhibited cytoplasmic anti-Myc labelling in the deep cortical layers while in the rest of the mice in addition to weak somata cytoplasmic staining in some regions, the anti-Myc antibody labelled some structures resembling cells in a variety of brain regions (Fig. 3.5. B). The incubation of the wild type controls with the anti-Myc antibody resulted again in cytoplasmic staining that was in most but not all of the cases localized to neuronal somata. It could not be concluded if the cytoplasmic staining in the wild type mice was weaker than the one in the homozygous Strep-Myc-SUMO3 mice.

The next antibody that was used was a rabbit anti-Myc antibody from Sigma (Fig. 3.6.). Staining of brain sections from Strep-Myc-SUMO3 heterozygous mouse with this antibody generated both nuclear and cytoplasmic anti-Myc labelling in different brain regions examined such as CA3 hippocampal region, subiculum and parts of the cortex. The results were quite inconsistent. In most cases, the intensities of the cytoplasmic and the nuclear labelling did not differ much from each other. However, in some cases the cytoplasmic staining was clearly stronger than the nuclear. Differences in the staining pattern were seen even between different labellings of the same region. The cytoplasmic labelling seemed to be either restricted or not restricted to the soma. For example, in the CA3 hippocampal region, the apical dendrite was also labelled. The wild type mouse exhibited predominantly cytoplasmic background staining but sometimes also nuclear staining. Again, the part of the cytoplasm labelled by this unspecific staining varied. When Strep-Myc-SUMO3 homozygous mice were used, the observations were again inconsistent. While in the subiculum, for example, the anti-Myc cytoplasmic staining was comparable to the nuclear staining, this was not observed in other brain regions such as the CA3 hippocampal region where the cytoplasmic labelling was stronger than the nuclear (Fig. 3.6. B). Further, the staining seemed inconsistent even between the wild type controls.

The next antibody that we utilized in an attempt to study the localization of SUMO3 was a rabbit anti-Myc antibody from Santa Cruz (A-14) (Fig. 3.7.). In the CA3 hippocampal region, the wild type mouse showed diffuse cytoplasmic background staining, while in the heterozygote mouse a more pronounced cytoplasmic staining was detected. In both genotypes the cytoplasmic staining seemed to be localized to the neuronal somata.

Next, we used a mouse antibody from Santa Cruz (clone 9E11) (Fig. 3.8.). Incubation of the brain sections from the heterozygous and the wild type mice did not result in any differences between the two genotypes in dentate gyrus, upper cortical layers and subiculum. Both genotypes exhibited the same general and diffuse background staining.

Finally, we engaged in staining with a mouse anti-Strep antibody (Fig. 3.9.). In both the heterozygous and the wild type mice, the antibody mainly labelled the outline of the neuronal nuclei in different brain regions including CA3 hippocampal region and subiculum. Interestingly, while in the subiculum of the wild type mouse the antibody labelled only the nuclear outline, in the heterozygous mouse some neurons also exhibited anti-Myc staining within their nuclei.

In conclusion, despite the utilization of several different antibodies, we could not reach a definite conclusion regarding the subcellular localization of SUMO3 or compare SUMO3 presence between different brain regions. Some of the data indicate the presence of SUMO3 in the nucleus but the inconsistency of the results does not allow us to confirm this hypothesis.

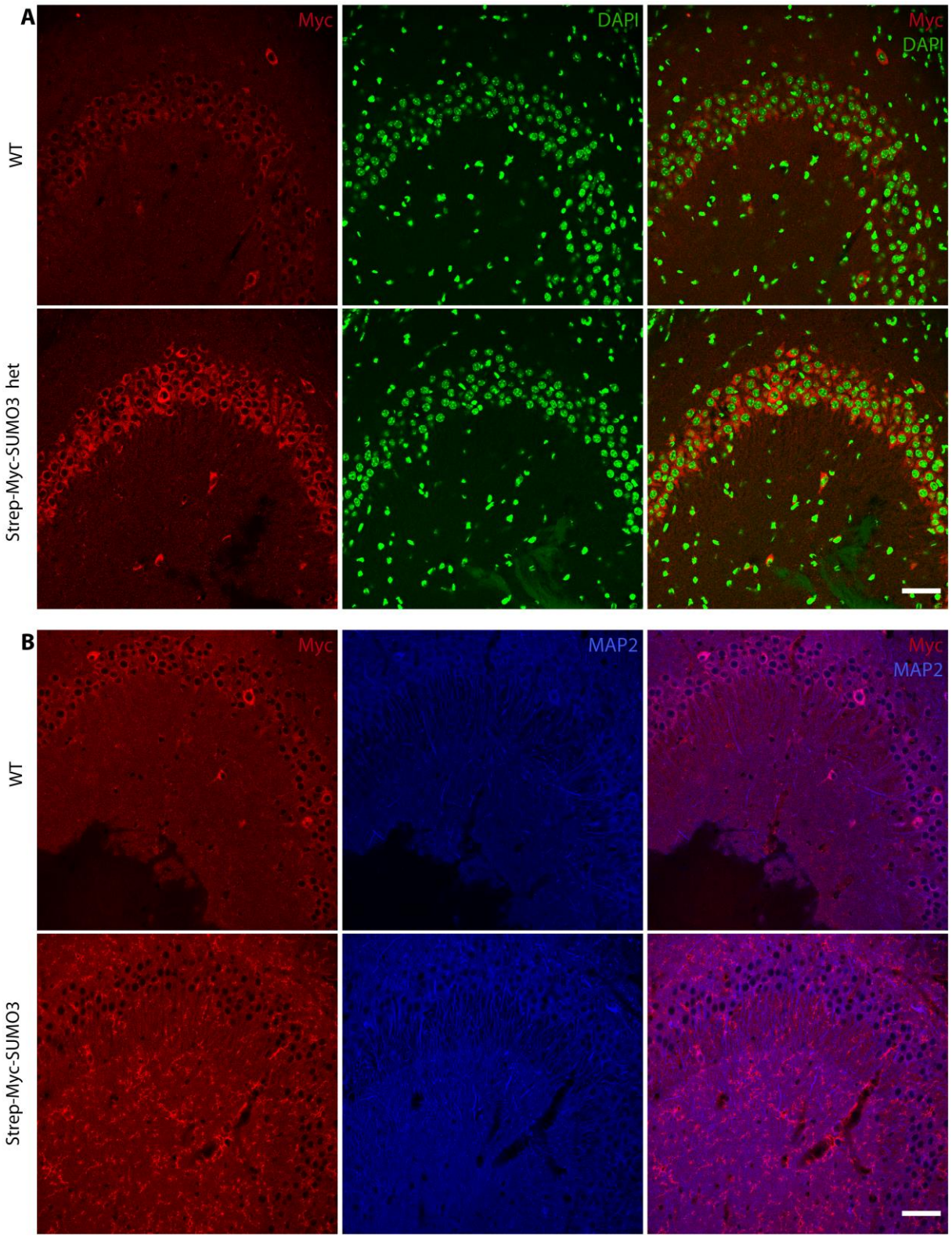

Fig. 3.5. Analysis of the localization of Strep-Myc-SUMO3 in brain sections from Strep-Myc-SUMO3 knock-in mice using a mouse anti-Myc antibody from Sigma (clone 9E10).

Sagittal brain sections from PFA-perfused Strep-Myc-SUMO3 heterozygous, Strep-Myc-SUMO3 homozygous and wild type (WT) mice were incubated with a mouse anti-Myc antibody from Sigma (clone 9E10) (red) and an anti-MAP2 antibody (blue). The images show CA3 hippocampal regions. (**A**) CA3 hippocampal regions from heterozygous Strep-Myc-

SUMO3 knock-in and wild type mice. Note the prominent anti-Myc cytoplasmic staining in the pyramidal neurons of the heterozygote animal and the weaker cytoplasmic staining in the wild type animal. Scale bar – 50 μm. (**B**) CA3 hippocampal region of homozygous Strep-Myc-SUMO3 knock-in mice and wild type mice. The wild type mice show again cytoplasmic staining, while half of the homozygous mice exhibit cell-like anti-Myc labelling. Scale bar – 50 μm.

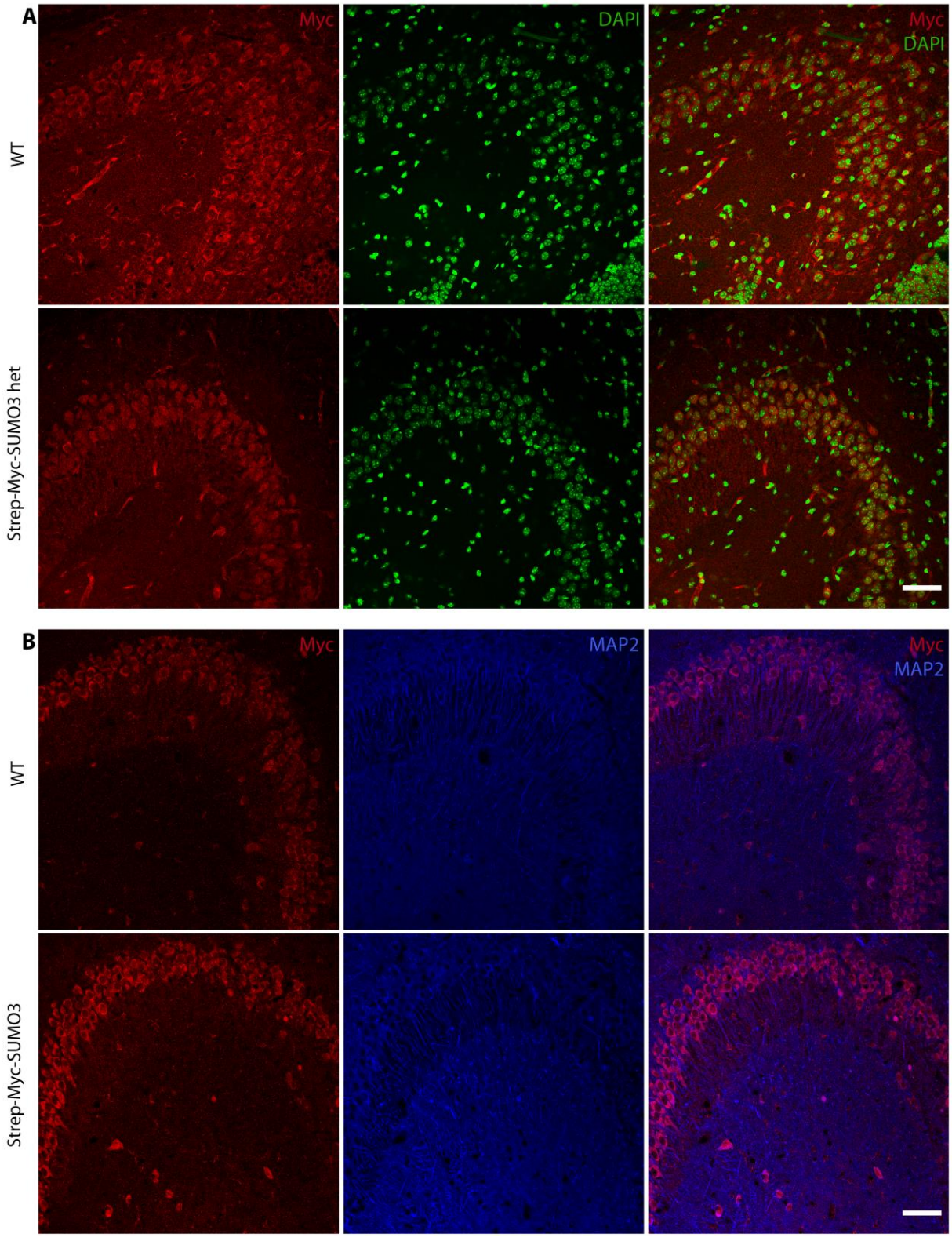

Fig. 3.6. Analysis of the localization of Strep-Myc-SUMO3 in brain sections from Strep-Myc-SUMO3 knock-in mice using a rabbit anti-Myc antibody from Sigma.

Sagittal brain sections from PFA-perfused Strep-Myc-SUMO3 heterozygous, Strep-Myc-SUMO3 homozygous and wild type mice were stained with a rabbit anti-Myc antibody from Sigma (red) and an anti-MAP2 antibody (blue). The images show CA3 hippocampal regions. (**A**) CA3 hippocampal regions from heterozygous Strep-Myc-SUMO3 knock-in and wild type mice. Note the lack of any visible difference between the intensities of the nuclear and the cytoplasmic anti-Myc labelling in the heterozygous mouse. Scale bar – 50 μm (**B**) CA3 hippocampal regions from homozygous Strep-Myc-SUMO3 knock-in and wild type mice. In contrast to the heterozygous mouse, in the homozygous mice the cytoplasmic labelling of the CA3 pyramidal neurons is much stronger than the nuclear staining. Scale bar – 50 μm.

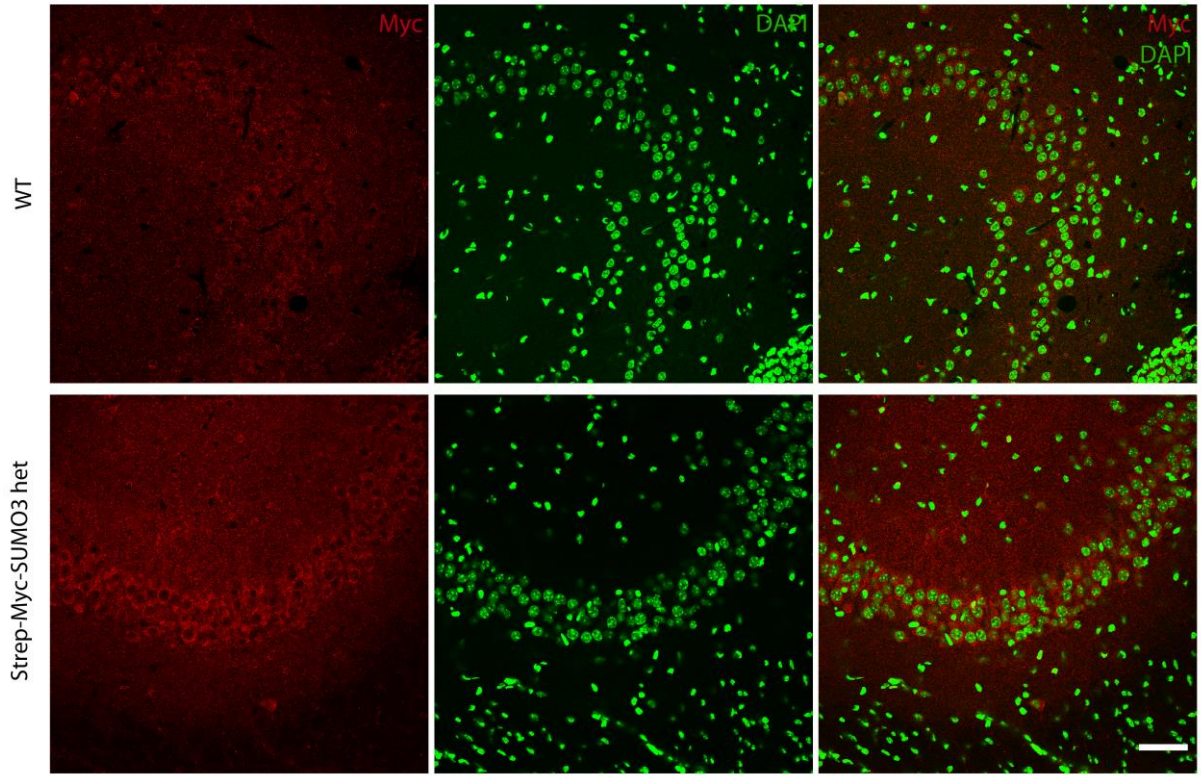

Fig. 3.7. Analysis of the localization of Strep-Myc-SUMO3 in brain sections from Strep-Myc-SUMO3 knock-in mice using a rabbit anti-Myc antibody from Santa Cruz.

Sagittal brain sections from PFA-perfused Strep-Myc-SUMO3 heterozygous and wild type mice were stained with a rabbit anti-Myc antibody from Santa Cruz (red) and an anti-MAP2 antibody (not shown). The images show CA3 hippocampal regions. Scale bar – 50 μm.

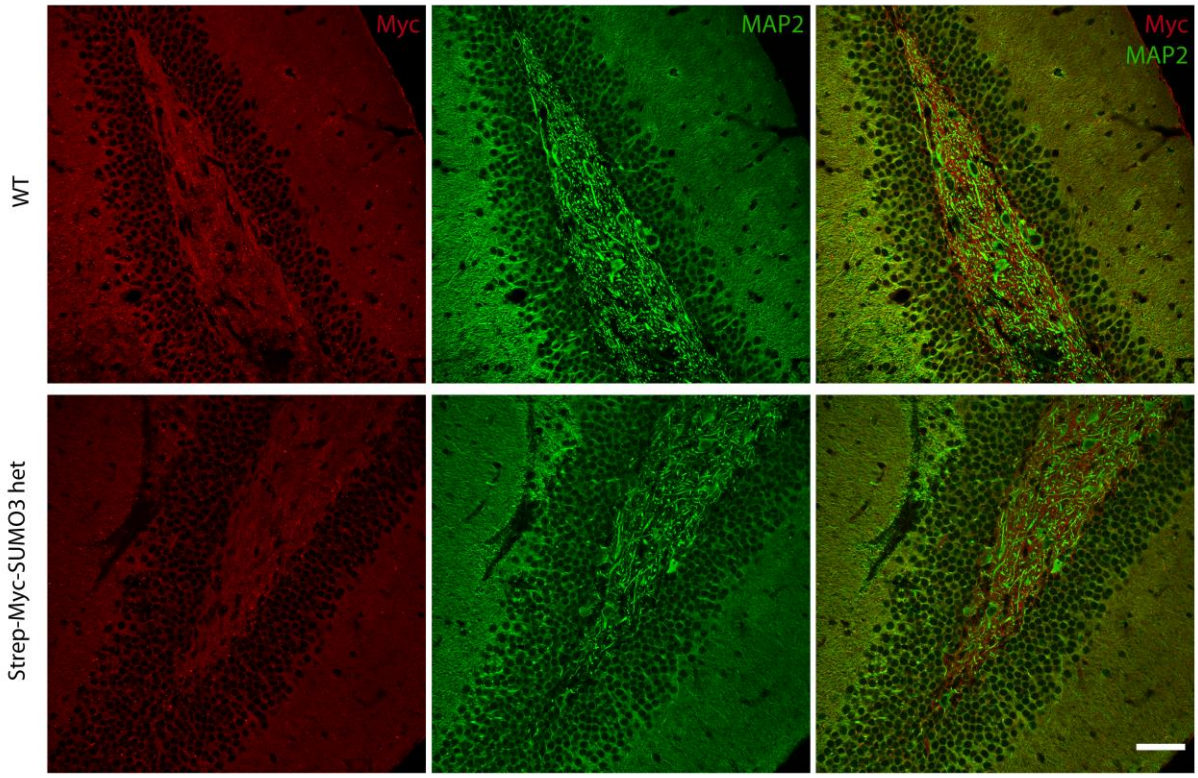

Fig. 3.8. Analysis of the localization of Strep-Myc-SUMO3 in brain sections from Strep-Myc-SUMO3 knock-in mice using a mouse anti-Myc antibody from Santa Cruz (clone 9E11).

Sagittal brain sections from PFA-perfused Strep-Myc-SUMO3 heterozygous and wild type mice were stained with a mouse anti-Myc antibody from Santa Cruz (clone 9E11) and an anti-MAP2 antibody (green). The images show dentate gyri. Scale bar – 50 μm.

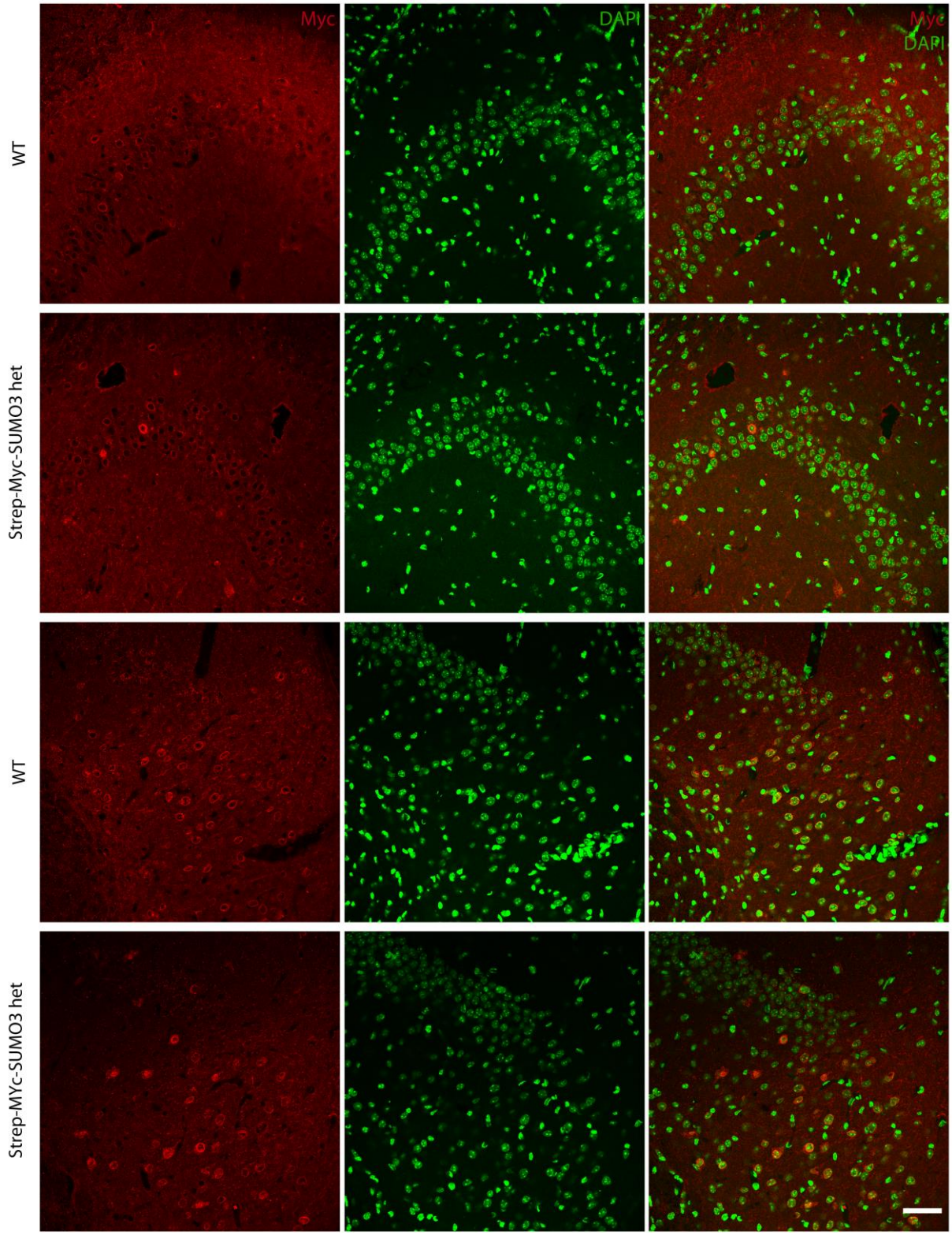

Fig. 3.9. Analysis of the localization of Strep-Myc-SUMO3 in brain sections from Strep-Myc-SUMO3 knock-in mice using a mouse anti-Strep antibody from Iba.

Sagittal sections from PFA-perfused Strep-Myc-SUMO3 heterozygous and wild type mice were stained with a mouse anti-Strep antibody from Iba (red) and an anti-MAP2 antibody (not shown). The first two rows show CA3 hippocampal regions and the last two rows show

subicular regions. Note the staining of the nuclear outline in the CA3 hippocampal regions of both the heterozygous Strep-Myc-SUMO3 knock-in mouse and the wild type mouse. In the subicular region of the wild type mouse the antibody labelled only the nuclear outlines of the neurons, while in the same region of the heterozygous mouse besides the nuclear outlines, the antibody also labelled the inner part of some nuclei. Scale bar – 50 μm.

3.2. Analysis of SUMO1 conjugation profile in a mouse model of Alzheimer's disease

3.2.1. Investigation of the localization of SUMO1 upon Alzheimer's disease pathology

A large number of studies have indicated an apparent link between SUMOylation and AD. Thus, in the second part of this work, our goal was to investigate SUMO1 conjugation profile during AD pathology by crossbreeding the His_6-HA-SUMO1 knock-in mice and the 5xFAD mice - a mouse model of AD.

Before engaging in description of the results, a question that should be discussed is whether the tagging of SUMO1 has an influence on AD pathology. We took the abundance of amyloid plaques as a readout of AD pathology (Fig. 3.10. and Fig. 3.11.). In 24-week-old mice, the plaque density in the subiculum and cortical layer V seemed to be comparable between His_6-HA-SUMO1;5xFAD mice and non-knock-in 5xFAD mice. In 12-week-old mice there seemed to be more plaques in the knock-in mice when compared to non-knock-in. 16-week-old mice did not show the same tendency as the 12-week-old ones and even seemed to show the opposite tendency in the cortical layer V. The similarity in the plaque abundance in the 24-week-old mice together with the low number of mice available do not speak in favour of big influence of SUMO1 tagging on AD pathology. The slight differences we observed are likely a result of interindividual variability.

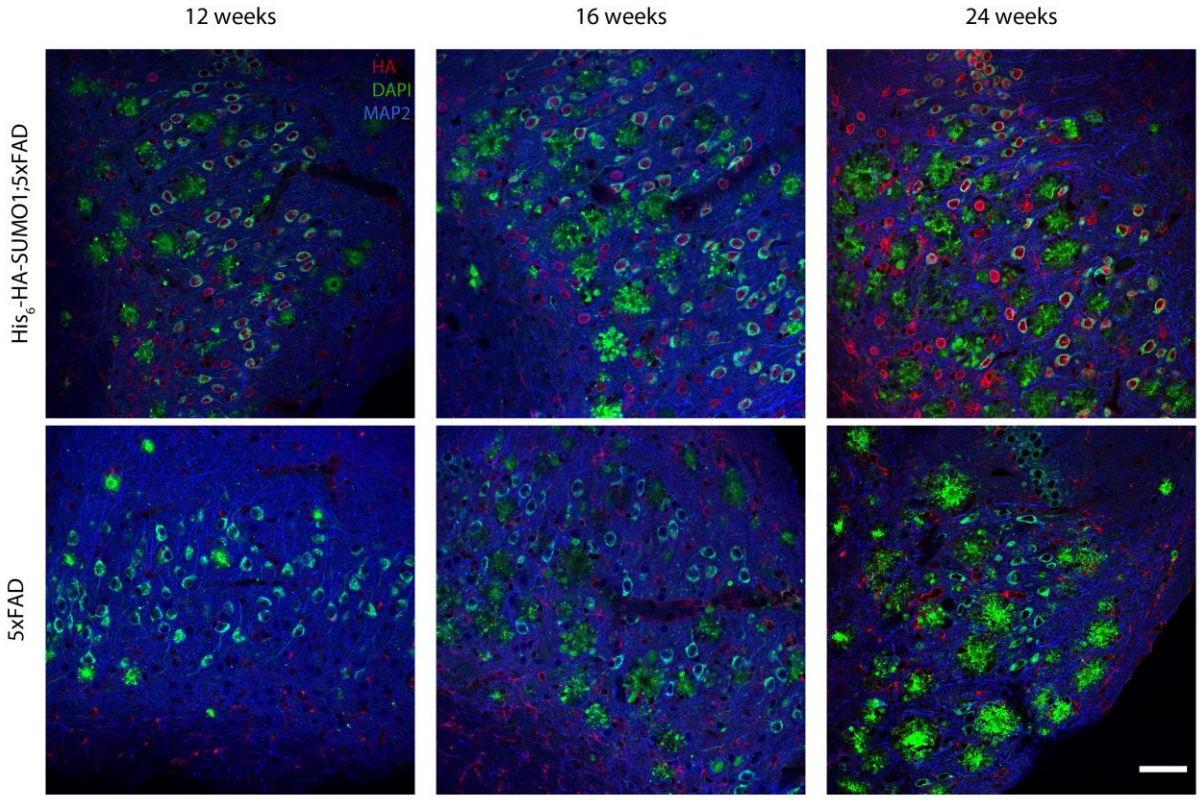

Fig. 3.10. Analysis of the influence of His_6-HA tagging of SUMO1 on Alzheimer's disease pathology in the subiculum of His_6-HA-SUMO1;5xFAD mice.

Sagittal brain sections from PFA-perfused His_6-HA-SUMO1;5xFAD and 5xFAD were stained with a goat anti-HA antibody (red), a mouse anti-Aβ antibody (green) and an anti-MAP2 antibody (blue). The images show subicular regions. AD pathology is represented by intraneuronal Aβ accumulation and extracellular amyloid plaques. Scale bar - 50 μm.

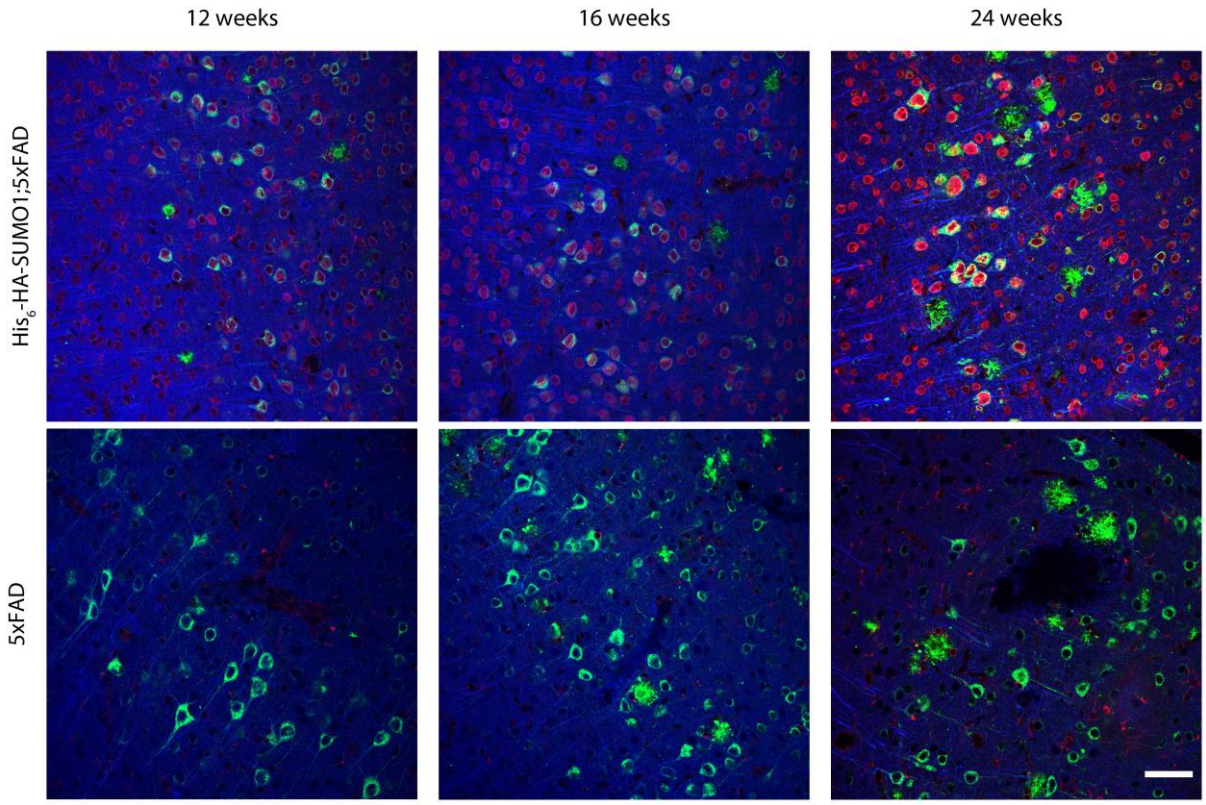

Fig. 3.11. Analysis of the influence of His_6-HA tagging of SUMO1 on Alzheimer's disease pathology in cortical layer V of His_6-HA-SUMO1;5xFAD mice.

Sagittal brain sections from PFA-perfused His_6-HA-SUMO1;5xFAD and 5xFAD were stained with a goat anti-HA antibody (red), a mouse anti-Aβ antibody (green) and an anti-MAP2 antibody (blue). The images show cortical layer V. AD pathology is represented by intraneuronal Aβ accumulation and extracellular amyloid plaques. Scale bar - 50 μm.

The first issue we wanted to address was whether SUMO1 undergoes changes in its subcellular localization in the context of AD pathology. For this purpose, we compared the subcellular localization of SUMO1 in anti-HA-labelled brain sections from His_6-HA-SUMO1;5xFAD mice and His_6-HA-SUMO1 mice. As controls, 5xFAD and wild type mice were used. In order to study differences in the SUMO1 localization at different stages of the disease progression, we utilized mice from different ages, i.e. 8-, 12-, 16-, 24- and approximately 48-week-old mice. We focused our investigation on two brain regions -

subiculum and cortical layer V - since intraneuronal Aβ is visible in these regions and amyloid plaques first appear there. Additionally, two different anti-HA antibodies were used. First, we will focus on the results from staining with a goat anti-HA antibody. Figure 3.12. and Figure 3.13. show examples of anti-HA immunolabelling of brain sections from 16-week-old His_6-HA-SUMO1;5xFAD, His_6-HA-SUMO1, 5xFAD and wild type mice. The AD pathology is visible in the His_6-HA-SUMO1;5xFAD mice and the 5xFAD mice as the presence of extracellular amyloid plaques and intraneuronal accumulation of Aβ. Analogous to what was shown by Tirard *et al*. (2012), in both cortical layer V and subiculum, SUMO1 showed predominantly nuclear localization in the neurons of His_6-HA-SUMO1 knock-in mice. Interestingly, in His_6-HA-SUMO1;5xFAD mice SUMO1 also showed pronounced nuclear localization. In both genotypes, especially pronounced was the staining of the nuclear envelope which results from the labelling of the extensively SUMOylated RanGAP1. Importantly, the nuclear anti-HA remained present in all the examined ages. In contrast, the non-knock-in mice did not show any anti-HA staining in the neuronal nuclei, which proves the specificity of the signal.

Apart from nuclear localization of the anti-HA signal, the crossbred His_6-HA-SUMO1;5xFAD mice exhibited non-nuclear anti-HA signals in the subiculum which seemed to be proportional to the abundance of amyloid plaques. We focused our analysis of this additional signal on the subiculum due to its high concentration of plaques. We examined 24-week-old mice since this age is characterized by a significant amount of senile plaques. This non-nuclear signal could be line-shaped and interestingly, some of the lines surrounded amyloid plaques (Fig. 3.14. yellow arrowheads). Additionally, some of this anti-HA signal looked like an amorphous mass (Fig. 3.14. yellow arrow). The specificity of this signal could be determined by examining the appropriate control – 5xFAD non-knock-in mice. Notably, the 5xFAD mice exhibited a similar type of anti-HA staining (Fig. 3.14. white arrowheads and arrows), which suggests that the observed non-nuclear signal is a non-specific background signal associated with Alzheimer's disease pathology. In addition, even the mice from the non-5xFAD genotypes sometimes showed significant background staining, probably resulting from poor perfusion which could mean that some of the non-nuclear signal in His_6-HA-SUMO1;5xFAD is just background not even related to Alzheimer's disease pathology.

Besides the goat anti-HA antibody, we also utilized a monoclonal mouse anti-HA antibody (Fig. 3.15.). Analogous to the goat antibody, His_6-HA-SUMO1 was observed in the neuronal nuclei in both of the knock-in genotypes. Interestingly, the use of this antibody resulted in a different type of non-nuclear anti-HA staining. His_6-HA-SUMO1;5xFAD mice

showed anti-HA signal localizing to the amyloid plaques (Fig. 3.15. yellow arrowheads). Importantly, a similar signal was observed again in the 5xFAD non-knock-in mice, which speaks against the specificity of the signal in the knock-in mice (Fig. 3.15. white arrowheads). Studying SUMO1 localization in the context of Alzheimer's disease pathology, several studies have reported the presence of SUMO1 around or within amyloid plaques (Takahashi *et al.*, 2008; Yun *et al.*, 2013; Zhao *et al.*, 2013; Cho *et al.*, 2015a). However, the similarity of the non-nuclear anti-HA signal observed in His_6-HA-SUMO1;5xFAD and 5xFAD mice did not allow us to confirm this observation.

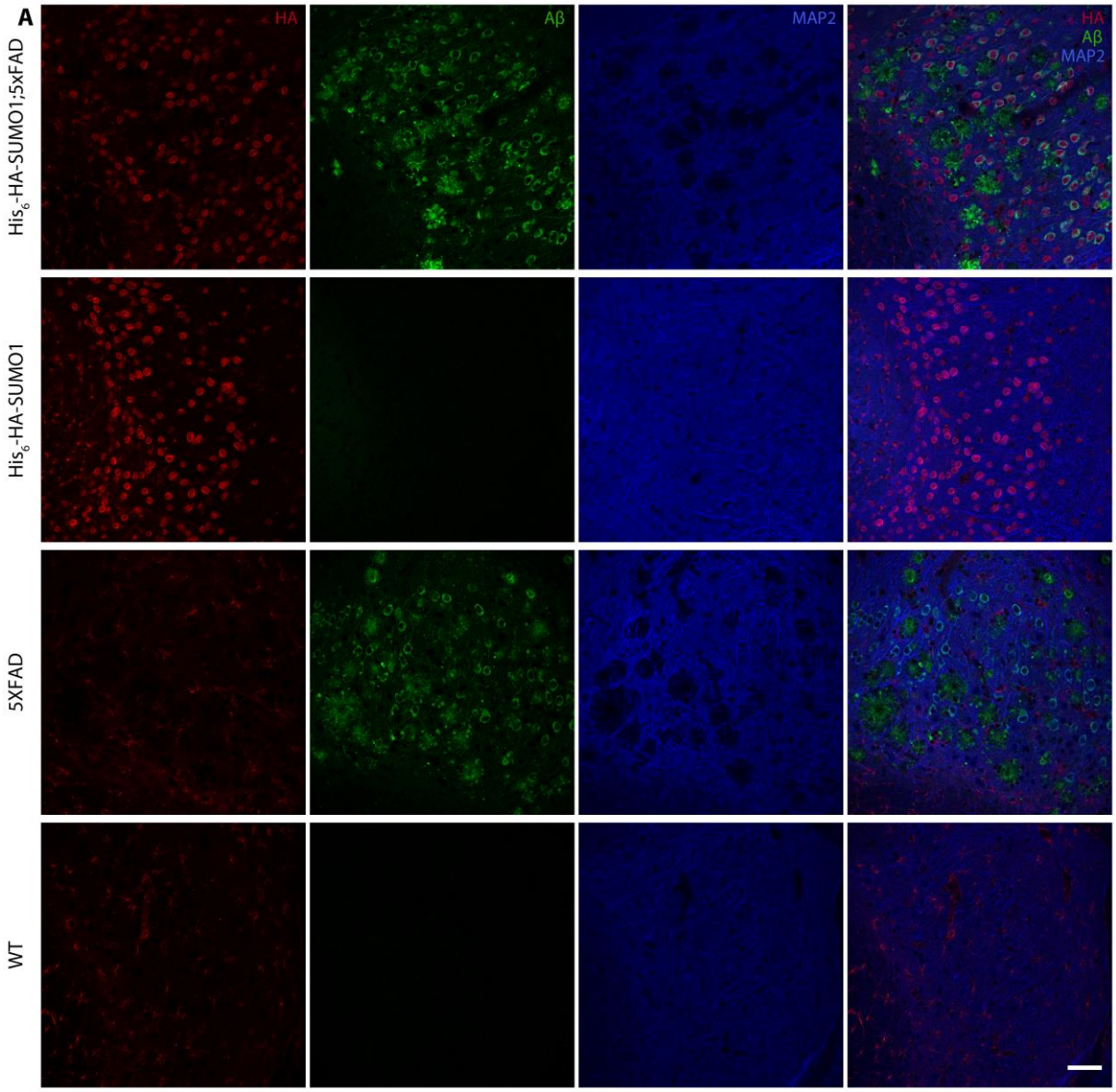

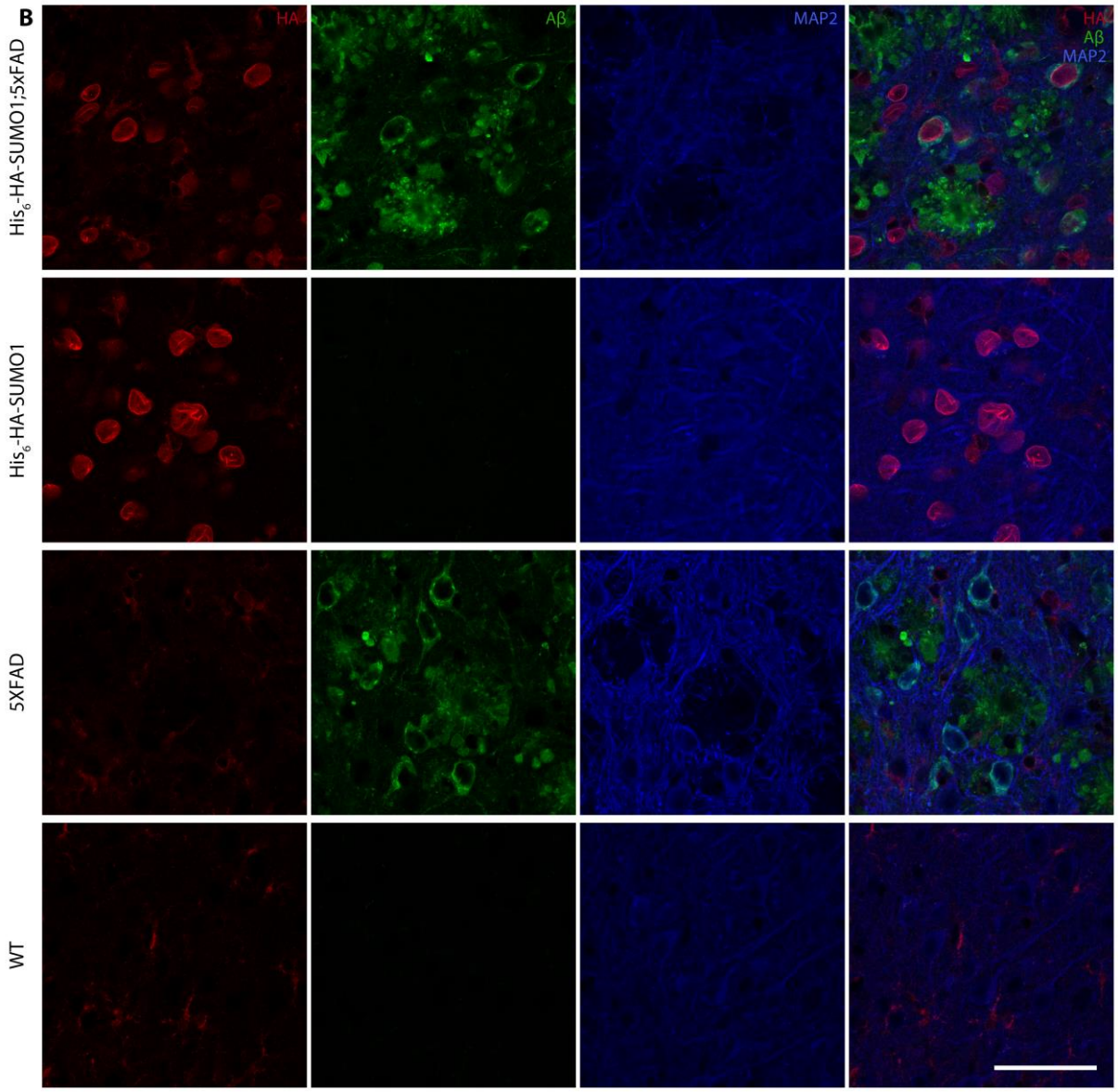

Fig. 3.12. Analysis of the localization of His_6-HA-SUMO1 in the subiculum of 16-week-old mice.

Sagittal brain sections from PFA-perfused His_6-HA-SUMO1, His_6-HA-SUMO1;5xFAD, 5xFAD and wild type mice were stained with a goat anti-HA antibody (red), a mouse anti-Aβ antibody (green) and an anti-MAP2 antibody (blue). The images show subicular regions. In (**B**) a higher magnification of the same regions is shown. Note the predominantly nuclear localization of the anti-HA signal in both His_6-HA-SUMO1 and His_6-HA-SUMO1;5xFAD mice. Extracellular amyloid plaques and intraneuronal accumulation of Aβ represent the AD pathology in His_6-HA-SUMO1;5xFAD and 5xFAD mice. Scale bar - 50 μm.

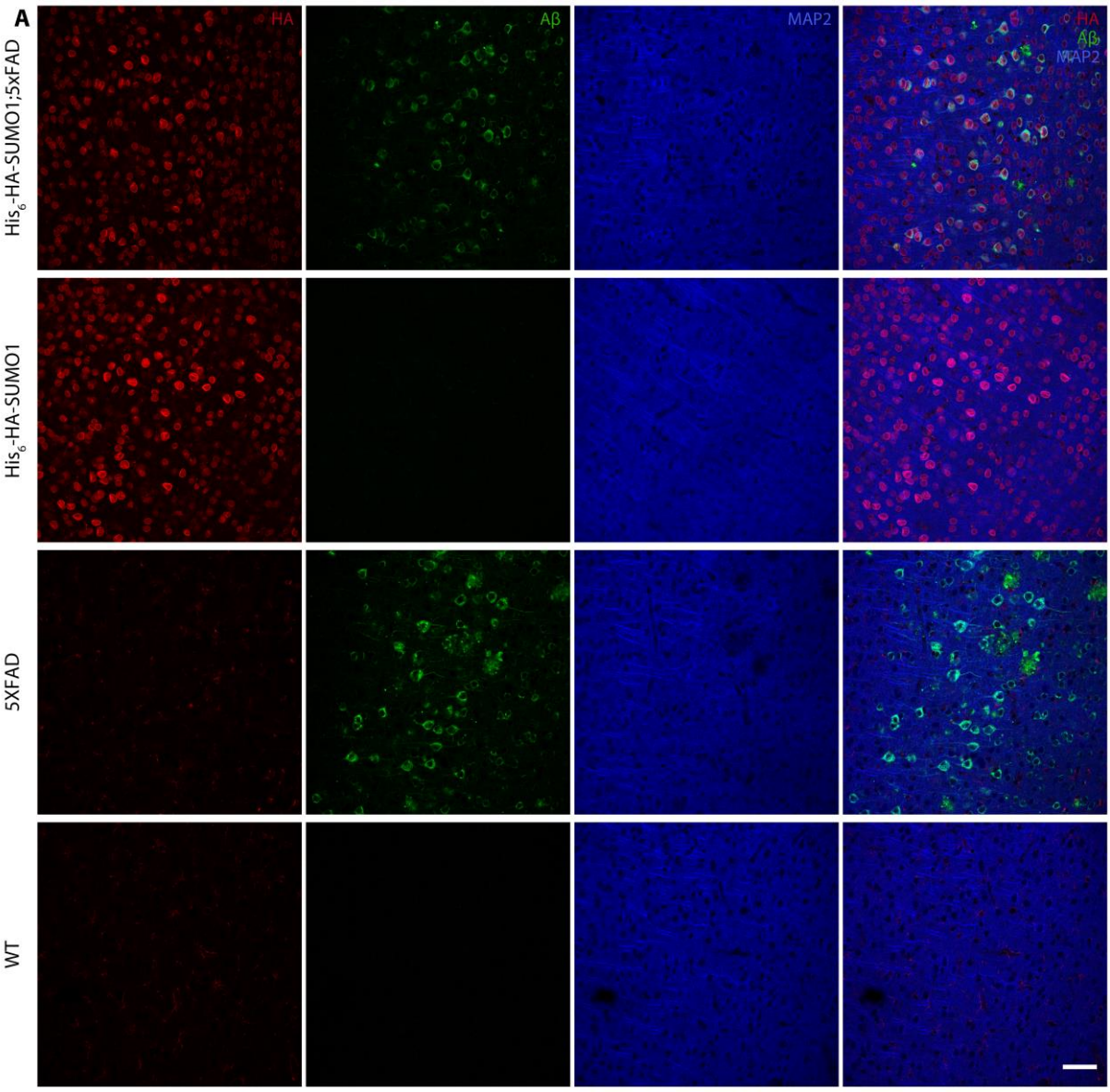
A
HA
Aβ
MAP2
HA
Aβ
MAP2
His6-HA-SUMO1;5xFAD
His6-HA-SUMO1
5XFAD
WT

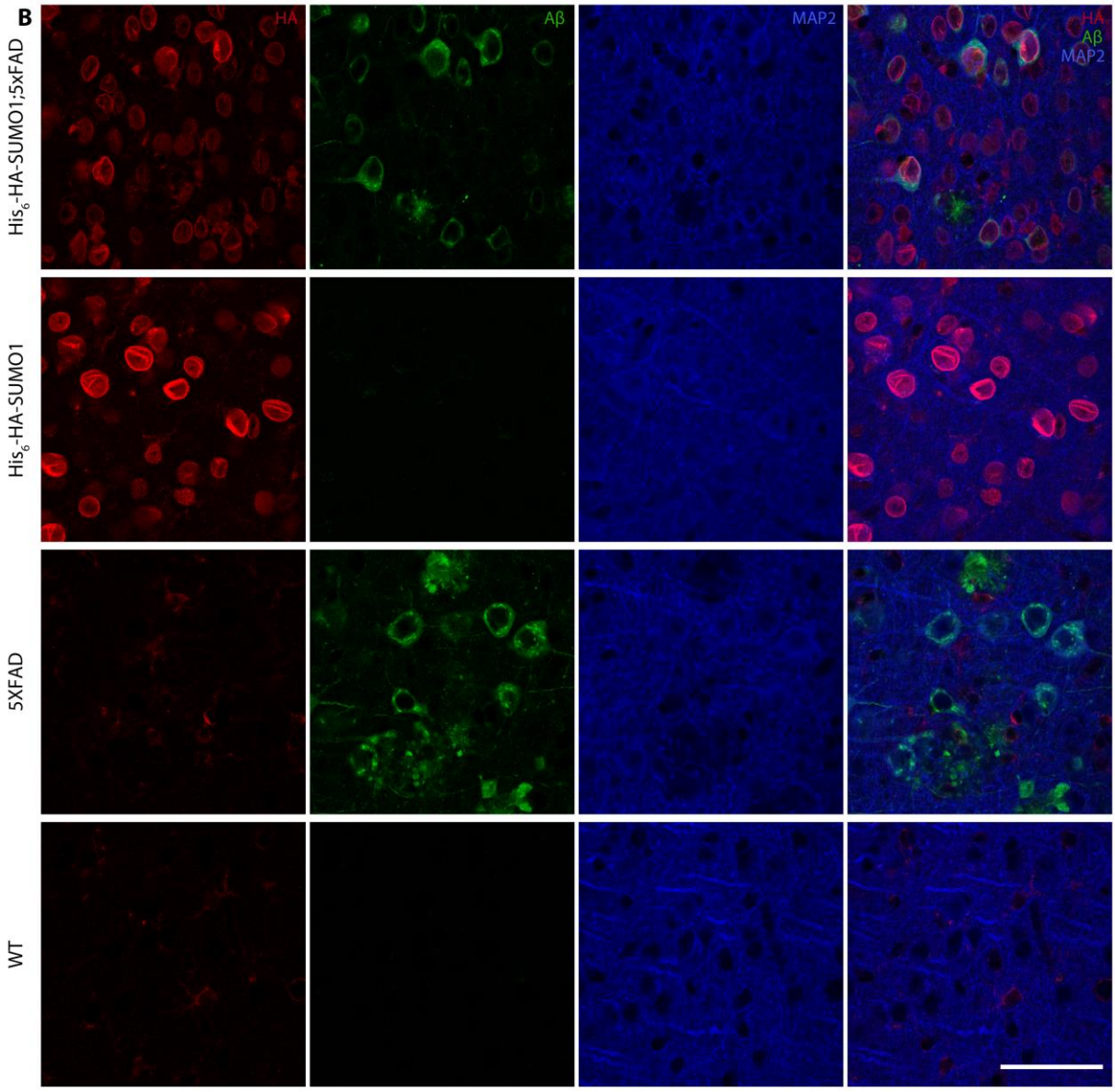

Fig. 3.13. Analysis of the localization of His_6-HA-SUMO1 in the cortical layer V of 16-week-old mice.

Sagittal brain sections from PFA-perfused His_6-HA-SUMO1, His_6-HA-SUMO1;5xFAD, 5xFAD and wild type mice were stained with a goat anti-HA antibody (red), a mouse anti-Aβ antibody (green) and an anti-MAP2 antibody (blue). The images show cortical layer V and its surrounding layers. In (**B**) a higher magnification of the same regions is shown. Note the predominantly nuclear localization of the anti-HA signal in both His_6-HA-SUMO1 and His_6-HA-SUMO1;5xFAD mice. Scale bar - 50 μm.

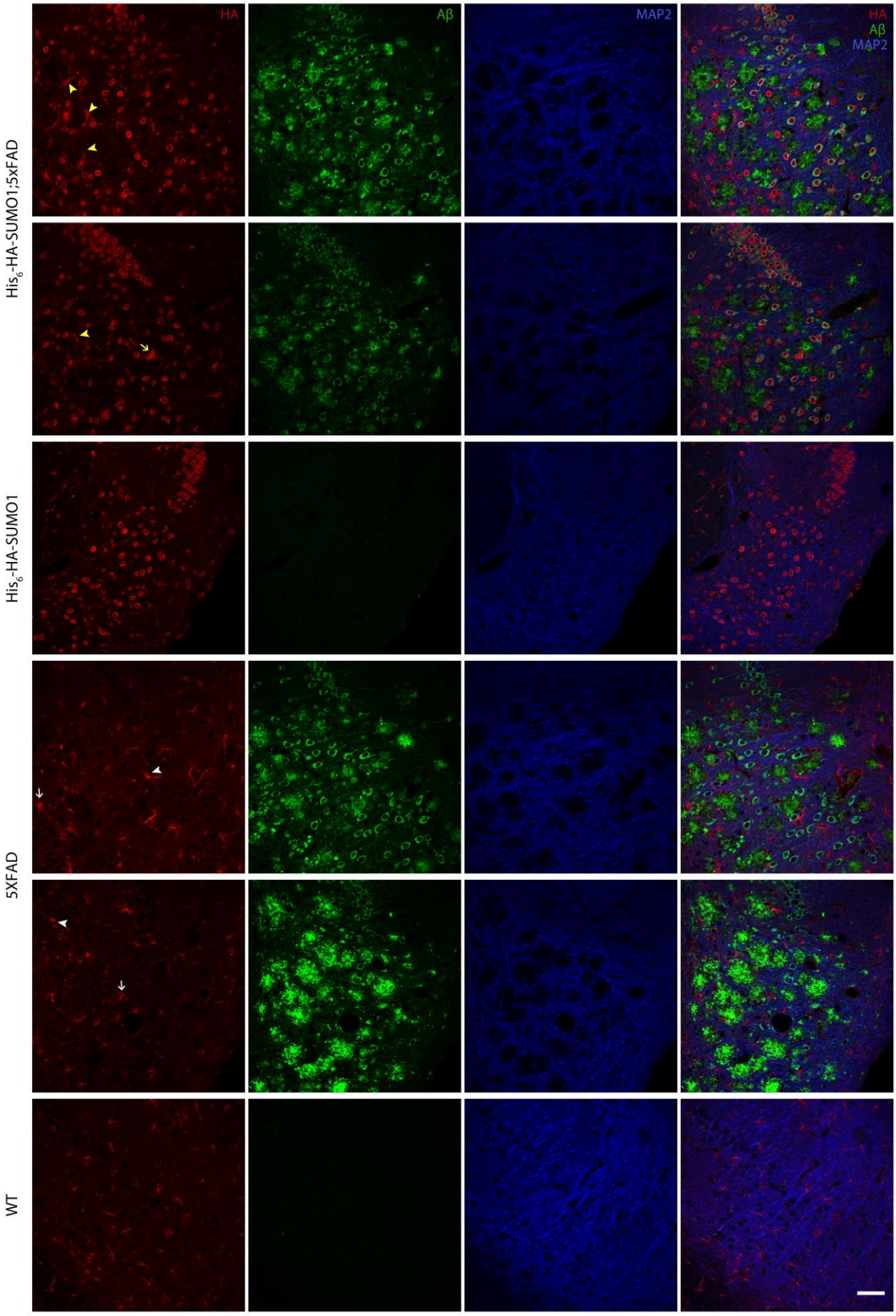
HA
Aβ
MAP2
HA
Aβ
MAP2
His6-HA-SUMO1;5xFAD
His6-HA-SUMO1
5XFAD
WT

Fig. 3.14. Analysis of the non-nuclear anti-HA signal produced by the goat anti-HA antibody in 24-week-old mice.

Sagittal brain sections from PFA-perfused His_6-HA-SUMO1, His_6-HA-SUMO1;5xFAD, 5xFAD and wild type mice were stained with a goat anti-HA antibody (red), a mouse anti-Aβ antibody (green) and an anti-MAP2 antibody (blue). The images show subicular regions. Note the presence of extranuclear line-shaped signal, some of which surrounds amyloid plaques (arrowheads) and extranuclear amorphous masses (arrows) in both His_6-HA-SUMO1;5xFAD and 5xFAD mice. WT: wild type. Scale bar - 50 μm.

In addition to immunostaining of brain sections, we decided to complement our analysis of SUMO1 localization in the context of AD pathology by performing SDS-PAGE and anti-HA Western blot of subcellular fractions from brains of His_6-HA-SUMO1 and His_6-HA-SUMO1;5xFAD mice (Fig. 3.16.). The age of the studied mice was 36 weeks. Both genotypes showed similar distribution of the anti-HA signal throughout the different subcellular fractions. As expected, the nuclear fractions exhibited the most prominent signal. Thus, the predominantly nuclear localization of His_6-HA-SUMO1 was also confirmed with this technique.

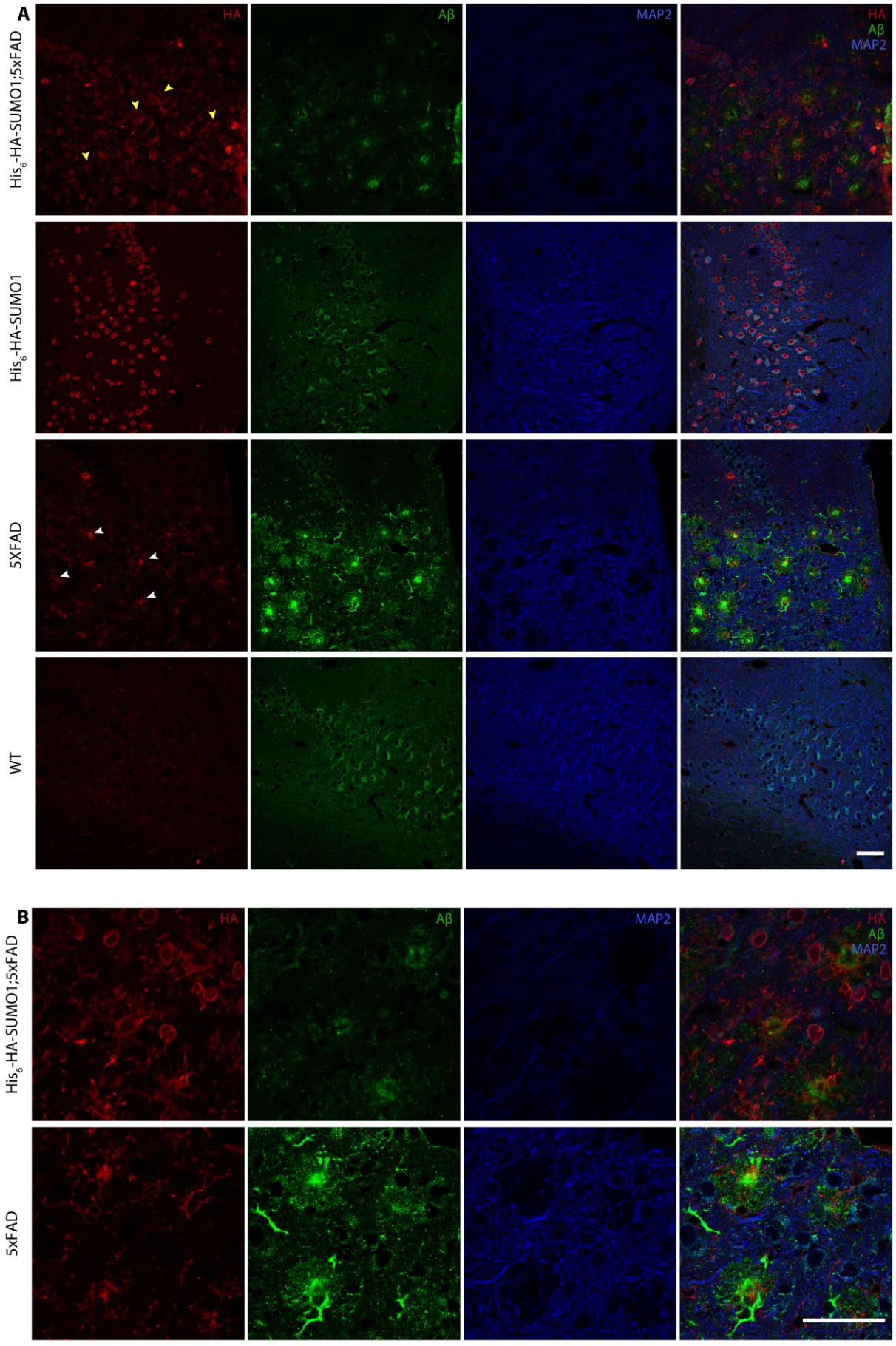
A
HA
Aβ
MAP2
HA
Aβ
MAP2
His6-HA-SUMO1;5xFAD
His6-HA-SUMO1
5XFAD
WT
B
HA
Aβ
MAP2
HA
Aβ
MAP2
His6-HA-SUMO1;5xFAD
5xFAD

Fig. 3.15. Analysis of the non-nuclear anti-HA signal produced by a mouse anti-HA antibody in 24-week-old mice.

Sagittal brain sections from PFA-perfused His_6-HA-SUMO1, His_6-HA-SUMO1;5xFAD, 5xFAD and wild type mice were stained with a mouse anti-HA antibody (red), a rabbit anti-$A\beta_{42}$ antibody (green) and an anti-MAP2 antibody (blue). The images show subicular regions. Note the presence of extranuclear anti-HA signal in the plaques in both His_6-HA-SUMO1;5xFAD (yellow arrowheads) and 5xFAD (white arrowheads) genotypes. In (**B**) a higher magnification of the same regions is shown. Scale bar - 50 μm.

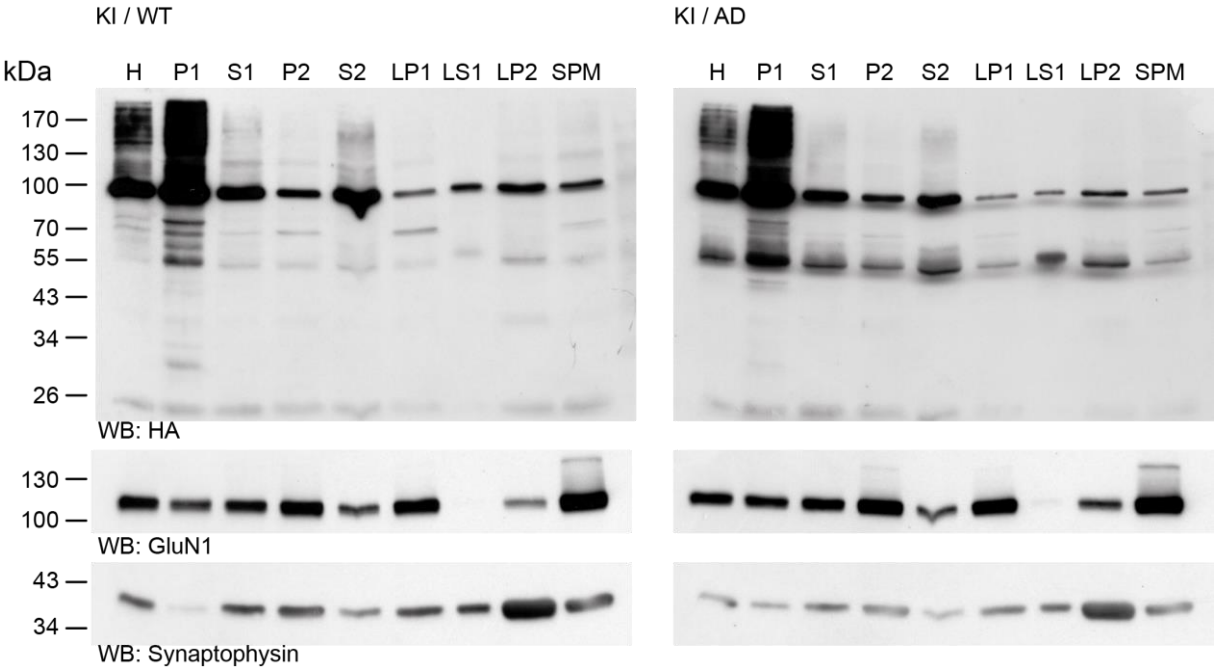

Fig. 3.16. Subcellular localization of His_6-HA-SUMO1 in the brain of 36-week-old mice.
Subcellular fractions from His_6-HA-SUMO1;5xFAD (KI/AD) and His_6-HA-SUMO1 (KI/WT) mouse brains were analysed by SDS-PAGE and Western blot using an anti-HA antibody to detect SUMO1, and anti-GluN1 and anti-synaptophysin antibodies to confirm accurate fractionation. The subcellular distribution of His_6-HA-SUMO1 is similar in both genotypes. Note that SUMO1 is most abundant in the nuclear fraction (P1). H, homogenate; P1, nuclear pellet; S1, supernatant after P1 sedimentation; P2, crude synaptosomal pellet; S2, supernatant after P2 sedimentation; LP1, lysed synaptosomal membrane; LS1, supernatant after LP1 sedimentation; LP2, synaptic vesicles-enriched fraction; SPM, synaptic plasma membrane. (Data obtained in collaboration with Dr. M. Tirard and K. Hellmann)

3.2.2. Investigation of SUMO1 conjugation levels upon Alzheimer's disease pathology

A significant number of studies have investigated the effect of increased amyloid burden on the levels of free SUMO or SUMO conjugates but the results have been very inconsistent (McMillan *et al.*, 2011; Hoppe *et al.*, 2013; Lee *et al.*, 2013; Yun *et al.*, 2013; Nistico *et al.*, 2014). Thus, we wanted to increase the current knowledge concerned in particular with SUMO1 conjugation levels in the context of AD pathology. For this purpose, we employed two approaches.

First, we engaged in quantitative comparison of the anti-HA signal intensity in the neuronal nuclei of His_6-HA-SUMO1;5xFAD and His_6-HA-SUMO1 mice from different ages - 8-, 12-, 16-, and approximately 48-week-old mice. For this purpose, for cortical layer V, we focused predominantly on the pyramidal neurons. Regarding the subiculum, the mainly smaller neurons residing deep in the subiculum were not included in the analysis. 8-, 12- and 16-week-old mice were female while approximately 48-week-old mice were male.

The quantification of the anti-HA signal intensity in the subiculum of 8-week-old His_6-HA-SUMO1;5xFAD and His_6-HA-SUMO1 mice did not reveal any significant difference between the two genotypes (Fig. 3.17. and Fig. 3.23. A and B). However, when we examined the pyramidal neurons of cortical layer V, the His_6-HA-SUMO1;5xFAD mice showed a significant increase in the signal intensity which amounted to 25.8% ($p=0.0205$) (Fig. 3.18. and Fig. 3.22. C and D).

The examination of 12-week-old mice revealed a slight increase in the signal in the crossbred His_6-HA-SUMO1;5xFAD mice in both subiculum and cortical layer V (Fig. 3.19., Fig. 3.20. and Fig. 3.23. E, F, G and H). However, as there were only two mice from the His_6-HA-SUMO1 genotype, no definite conclusion can be drawn from these data.

The quantification of the anti-HA signal in 16-week-old mice did not show any significant differences between the two genotypes in both brain regions examined (Fig. 3.12., Fig. 3.13. and Fig. 3.23. I, J, K and L). However, for His_6-HA-SUMO1;5xFAD mice the results displayed an almost significant decrease in the anti-HA signal in the cortical layer V.

Finally, the approximately 48-week-old His_6-HA-SUMO1;5xFAD and His_6-HA-SUMO1 did not show any significant differences in the signal intensity in both subiculum and cortical layer V (Fig. 3.21., Fig. 3.22. and Fig. 3.23. M, N, O and P).

Importantly, the results using this technique should be carefully interpreted with regard to SUMO1 conjugation levels since we cannot distinguish between free and conjugated SUMO and the examined SUMO is only the one residing in the nucleus.

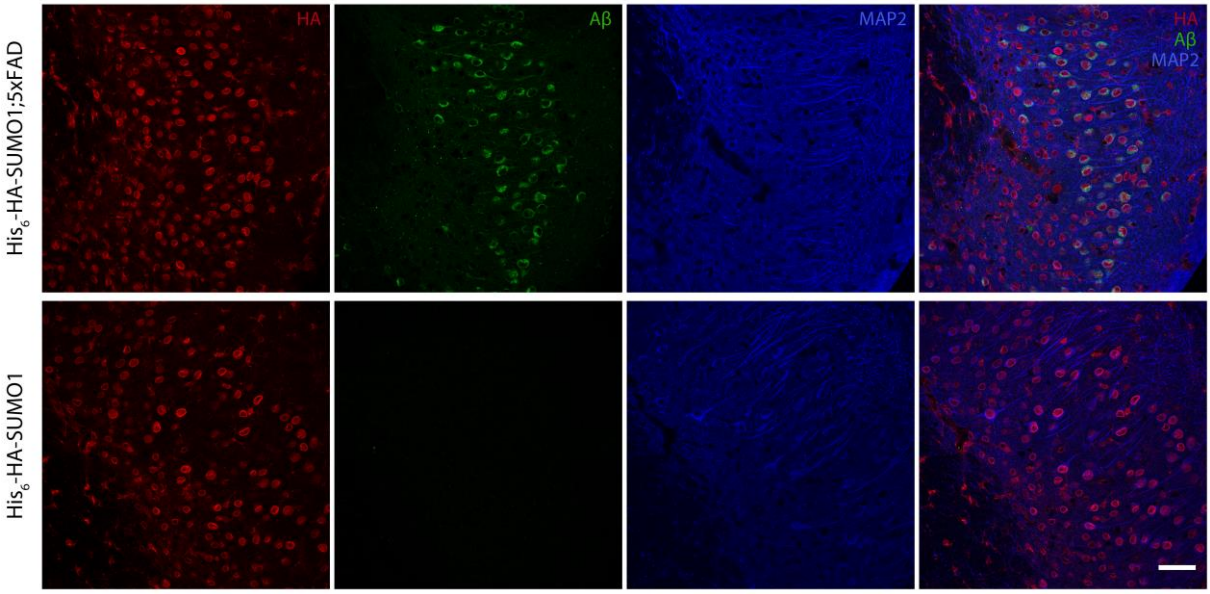

Fig. 3.17. Analysis of the nuclear anti-HA signal intensity in the subiculum of 8-week-old mice.

Sagittal brain sections from PFA-perfused His_6-HA-SUMO1;5xFAD and His_6-HA-SUMO1 mice were stained with a goat anti-HA antibody (red), a mouse anti-Aβ antibody (green) and an anti-MAP2 (blue) antibody. The images show subicular regions. Note the intraneuronal accumulation of Aβ in the His_6-HA-SUMO1;5xFAD mice. Plaques are rarely visible at this age. The mainly small cells deep in the subiculum were excluded from the analysis. Scale bar - 50 μm.

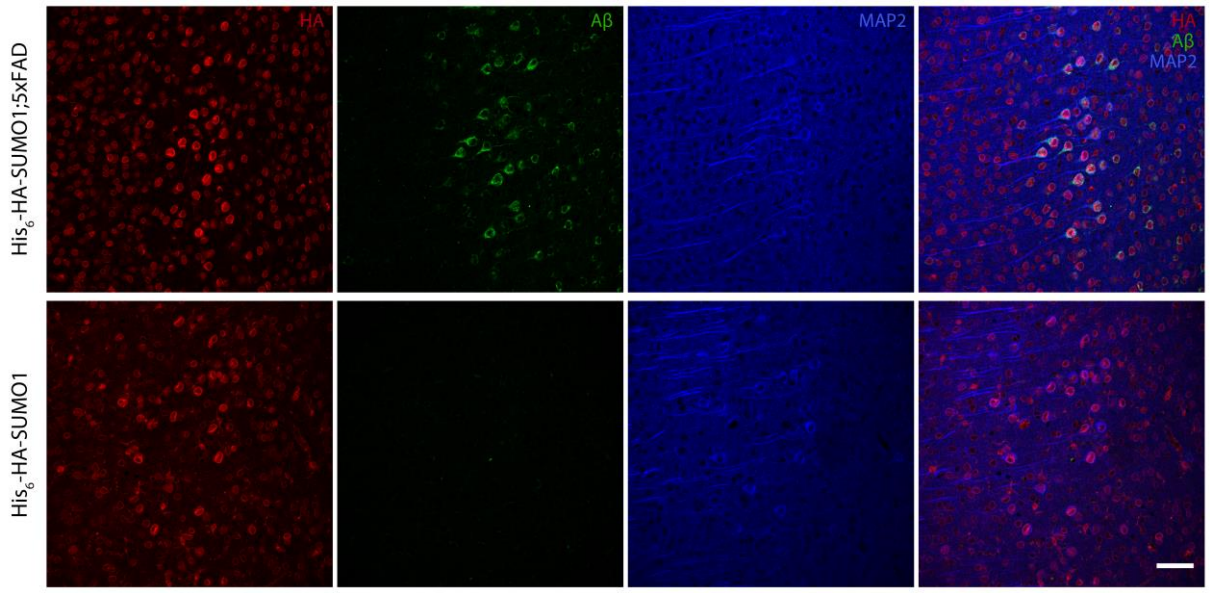

Fig. 3.18. Analysis of the nuclear anti-HA signal intensity in the cortical layer V of 8-week-old mice.

Sagittal brain sections from PFA-perfused His_6-HA-SUMO1;5xFAD and His_6-HA-SUMO1 mice were stained with a goat anti-HA antibody (red), a mouse anti-Aβ antibody (green) and an anti-MAP2 (blue) antibody. The images show cortical layer V and its surrounding layers. The signal from the pyramidal neurons of layer V was used for the quantification. Scale bar – 50 μm.

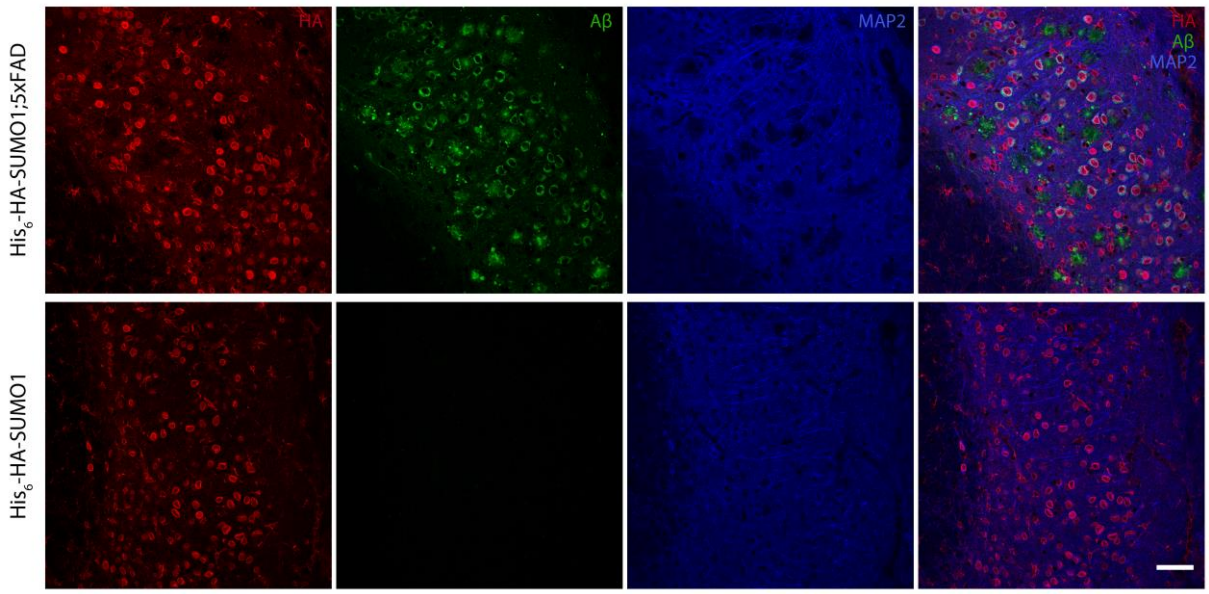

Fig. 3.19. Analysis of the nuclear anti-HA signal intensity in the subiculum of 12-week-old mice.

Sagittal brain sections from PFA-perfused His_6-HA-SUMO1;5xFAD and His_6-HA-SUMO1 mice were stained with a goat anti-HA antibody (red), a mouse anti-Aβ antibody (green) and an anti-MAP2 (blue) antibody. The images show subicular regions. Scale bar – 50 μm.

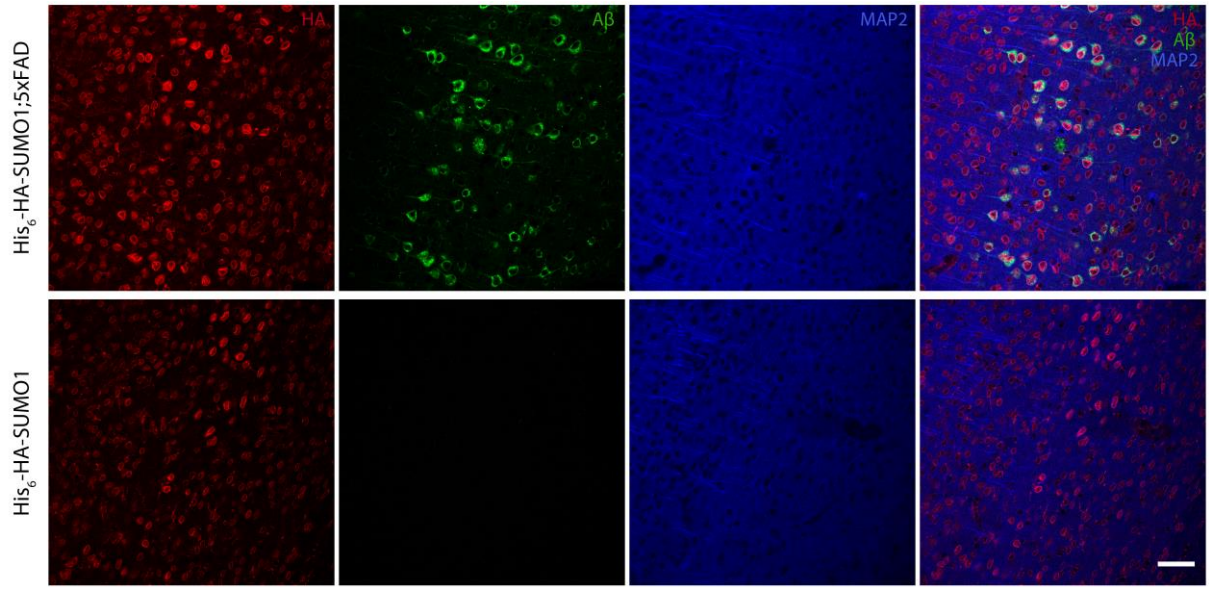

Fig. 3.20. Analysis of the nuclear anti-HA signal intensity in the cortical layer V of 12-week-old mice.

Sagittal brain sections from PFA-perfused His_6-HA-SUMO1;5xFAD and His_6-HA-SUMO1 mice were stained with a goat anti-HA antibody (red), a mouse anti-Aβ antibody (green) and an anti-MAP2 (blue) antibody. The images show cortical layer V and its surrounding layers. Scale bar – 50 μm.

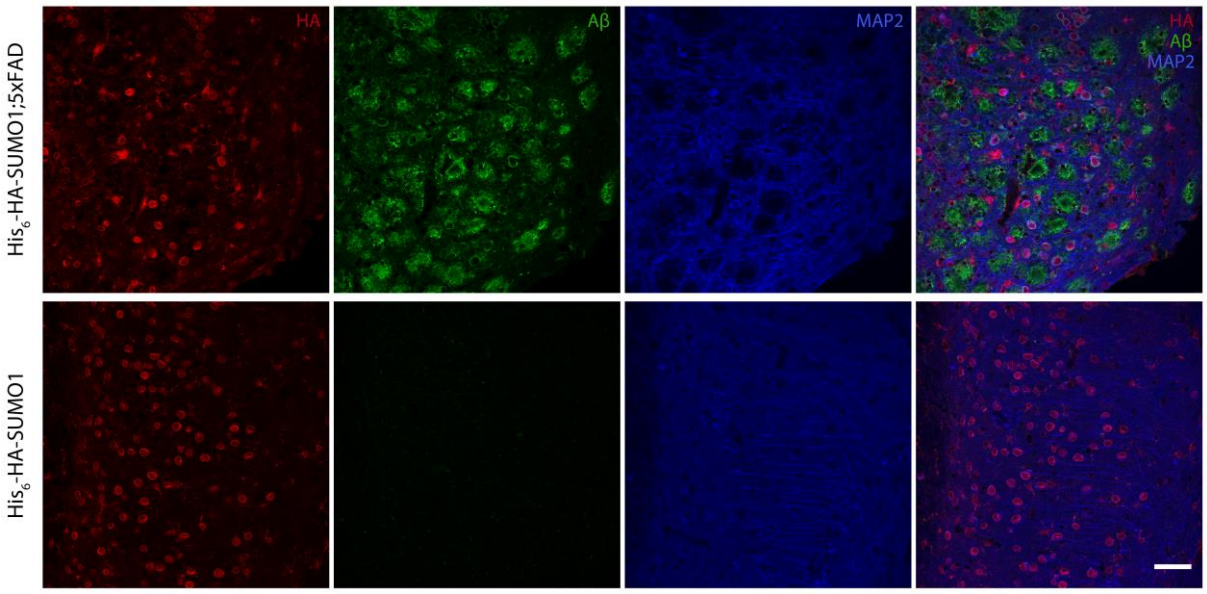

Fig. 3.21. Analysis of the nuclear anti-HA signal intensity in the subiculum of approximately 48-week-old mice.

Sagittal brain sections from PFA-perfused His_6-HA-SUMO1;5xFAD and His_6-HA-SUMO1 mice were stained with a goat anti-HA antibody (red), a mouse anti-Aβ antibody (green) and an anti-MAP2 (blue) antibody. The images show subicular regions. Scale bar – 50 μm.

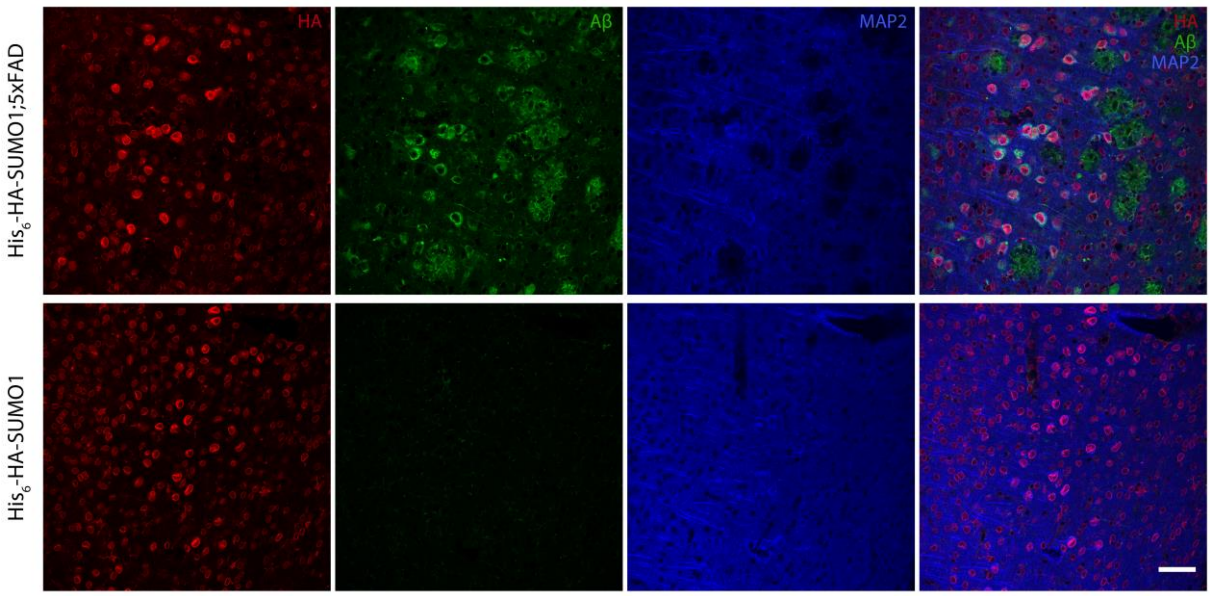

Fig. 3.22. Analysis of the nuclear anti-HA signal intensity in the cortical layer V of approximately 48-week-old mice.

Sagittal brain sections from PFA-perfused His_6-HA-SUMO1;5xFAD and His_6-HA-SUMO1 mice were stained with a goat anti-HA antibody (red), a mouse anti-Aβ antibody (green) and an anti-MAP2 (blue) antibody. The images show cortical layer V and its surrounding layers. Scale bar – 50 μm.

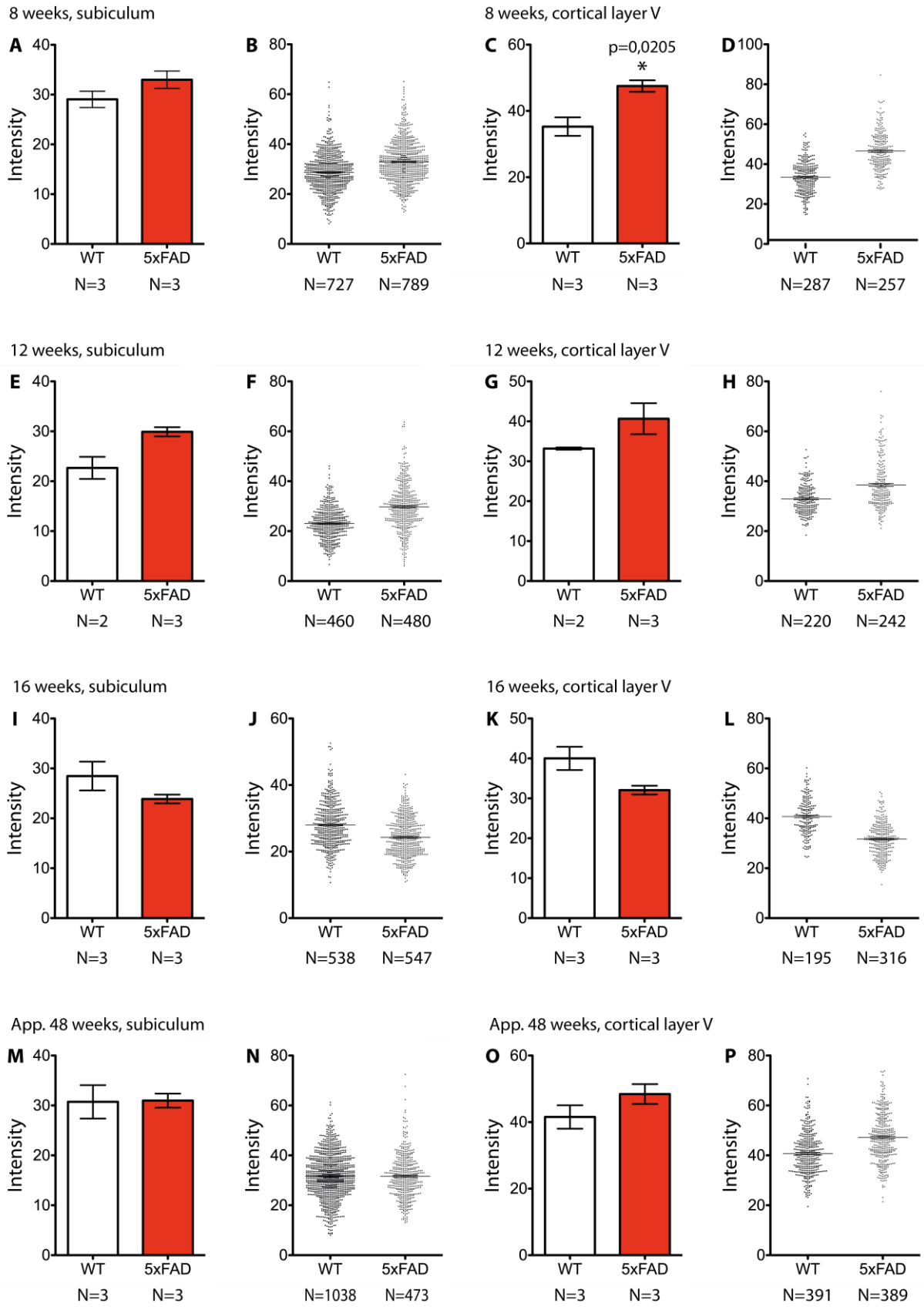
8 weeks, subiculum
8 weeks, cortical layer V
A
B
C
D
p=0,0205
*
Intensity
WT
5xFAD
N=3
N=3
N=727
N=789
N=3
N=3
N=287
N=257
12 weeks, subiculum
12 weeks, cortical layer V
E
F
G
H
N=2
N=3
N=460
N=480
N=2
N=3
N=220
N=242
16 weeks, subiculum
16 weeks, cortical layer V
I
J
K
L
N=3
N=3
N=538
N=547
N=3
N=3
N=195
N=316
App. 48 weeks, subiculum
App. 48 weeks, cortical layer V
M
N
O
P
N=3
N=3
N=1038
N=473
N=3
N=3
N=391
N=389

Fig. 3.23. Quantification of the nuclear anti-HA signal intensity in 8-, 12-, 16- and approximately 48-week-old mice.

(**A**) and (**B**) Quantification of the nuclear anti-HA signal intensity in the subiculum of 8-week-old His_6-HA-SUMO1 (WT) and His_6-HA-SUMO1;5xFAD (5xFAD) mice. (**A**) Mean anti-HA signal intensity of His_6-HA-SUMO1 (N=3) and His_6-HA-SUMO1;5xFAD (N=3) mice. No significant difference is seen between the two genotypes. p=0.1744. Data are represented as mean ± SEM. (**B**) Scatter plot graph including the anti-HA signal intensity values of all the examined neurons from the two genotypes - His_6-HA-SUMO1 (N=727) and His_6-HA-SUMO1;5xFAD (N=789). Mean ± SEM is shown. (**C**) and (**D)** Quantification of the nuclear anti-HA signal intensity in the cortical layer V of 8-week-old His_6-HA-SUMO1 and His_6-HA-SUMO1;5xFAD mice. (**C**) Mean anti-HA signal intensity of His_6-HA-SUMO1 (N=3) and His_6-HA-SUMO1;5xFAD (N=3) mice. His_6-HA-SUMO1;5xFAD mice show a 25.8% increase in the nuclear anti-HA signal intensity when compared to His_6-HA-SUMO1 mice. p=0.0205. (**D**) Scatter plot graph including the anti-HA signal intensity values of all the examined neurons from the two genotypes - His_6-HA-SUMO1 (N=287) and His_6-HA-SUMO1;5xFAD (N=259). (**E**) and (**F**) Quantification of the nuclear anti-HA signal intensity in the subiculum of 12-week-old His_6-HA-SUMO1 and His_6-HA-SUMO1;5xFAD mice. (**E**) Mean anti-HA signal intensity of His_6-HA-SUMO1 (N=2) and His_6-HA-SUMO1;5xFAD (N=3) mice. (**F**) Scatter plot graph including the anti-HA signal intensity values of all the examined neurons from the two genotypes - His_6-HA-SUMO1 (N=460) and His_6-HA-SUMO1;5xFAD (N=480). (**G**) and (**H**) Quantification of the nuclear anti-HA signal intensity in the cortical layer V of 12-week-old His_6-HA-SUMO1 and His_6-HA-SUMO1;5xFAD mice. (**G**) Mean anti-HA signal intensity of His_6-HA-SUMO1 (N=2) and His_6-HA-SUMO1;5xFAD (N=3) mice. (**H**) Scatter plot graph including the anti-HA signal intensity values of all the examined neurons from the two genotypes - His_6-HA-SUMO1 (N=220) and His_6-HA-SUMO1;5xFAD (N=242). (**I**) and (**J**) Quantification of the nuclear anti-HA signal intensity in the subiculum of 16-week-old His_6-HA-SUMO1 and His_6-HA-SUMO1;5xFAD mice. (**I**) Mean anti-HA signal intensity of His_6-HA-SUMO1 (N=3) and His_6-HA-SUMO1;5xFAD (N=3) mice. No significant difference is seen between the two genotypes p=0.2025. (**J**) Scatter plot graph including the anti-HA signal intensity values of all the examined neurons from the two genotypes - His_6-HA-SUMO1 (N=538) and His_6-HA-SUMO1;5xFAD (N=547). (**K**) and (**L**) Quantification of the nuclear anti-HA signal intensity in the cortical layer V of 16-week-old His_6-HA-SUMO1 and His_6-HA-SUMO1;5xFAD mice. (**K**) Mean anti-HA signal intensity of His_6-HA-SUMO1 (N=3) and His_6-HA-SUMO1;5xFAD (N=3) mice. An almost significant decrease is observed in His_6-HA-SUMO1;5xFAD mice. p=0.0624. (**L**) Scatter plot graph including the anti-HA signal intensity values of all the examined neurons from the two genotypes - His_6-HA-SUMO1 (N=195) and His_6-HA-SUMO1;5xFAD (N=316). (**M**) and (**N**) Quantification of the nuclear anti-HA signal intensity in the subiculum of approximately 48-week-old His_6-HA-SUMO1 and His_6-HA-SUMO1;5xFAD mice. (**M**) Mean anti-HA signal intensity of His_6-HA-SUMO1 (N=3) and His_6-HA-SUMO1;5xFAD (N=3) mice. No significant difference was observed between the two genotypes. p=0.9452. (**N**) Scatter plot graph including the anti-HA signal intensity values of all the examined neurons from the two genotypes - His_6-HA-SUMO1 (N=1038) and His_6-HA-SUMO1;5xFAD (N=473). (**O**) and (**P**) Quantification of the nuclear anti-HA signal intensity in the cortical layer V of approximately 48-week-old His_6-HA-SUMO1 and His_6-HA-SUMO1;5xFAD mice. (**O**) Mean anti-HA signal intensity of His_6-HA-SUMO1 (N=3) and His_6-HA-SUMO1;5xFAD (N=3) mice. No significant difference is observed between the two genotypes. p=0.2089. (**P**) Scatter plot graph including the anti-HA signal intensity values of all the examined neurons from the two genotypes - His_6-HA-SUMO1 (N=391) and His_6-HA-SUMO1;5xFAD (N=389). App. - approximately

The second approach employed to detect changes in the SUMO1 levels relied on SDS-PAGE and quantitative anti-HA Western blot (Fig. 3.24.). The levels of His_6-HA-SUMO1 conjugates in hippocampus and cerebral cortex were compared between His_6-HA-SUMO1;5xFAD and His_6-HA-SUMO1 mice. Mice from different ages were again used – 8-, 12-, 16-, 24-, and 36-week-old mice. Analogous to most of the results from the immunostaining experiments, there was no significant difference in the His_6-HA-SUMO1 conjugation levels between the two genotypes in the hippocampus and cortex at any of the investigated ages in both hippocampus and cortex. Only minor trends were observed. For example, in the cortex of His_6-HA-SUMO1;5xFAD 16-week-old mice there is a trend towards an increase when compared to His_6-HA-SUMO1 mice. However, overall amyloid pathology does not influence SUMO1 conjugation. Further, a slight decrease in SUMO1 conjugation levels was observed with increasing age, at least in hippocampus. This effect was independent of the 5xFAD genotype, indicating a general age-dependent reduction of SUMO1 conjugation.

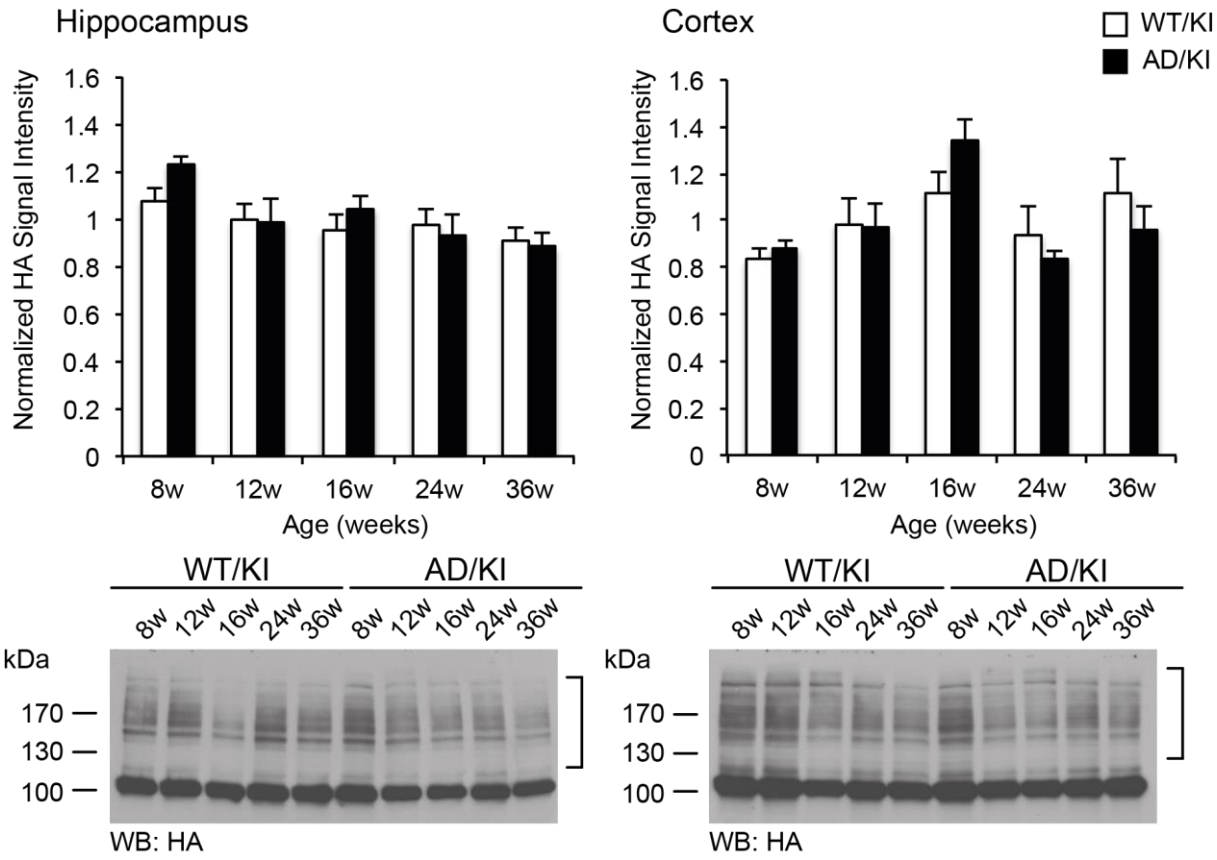

Fig. 3.24. Quantitative Western blot of global His_6-HA-SUMO1 conjugation levels in hippocampus and cortex.

Hippocampal and cortical tissue extracts from His_6-HA-SUMO1;5xFAD (AD, black bar) and His_6-HA-SUMO1 mice (WT, white bar) were subjected to SDS-PAGE and quantitative anti-HA Western blot. The mice were 8 (8w), 12 (12w), 16 (16w), 24 (24w) and 36 (36w) weeks of age. The bracket indicates the quantified SUMO1 conjugates. No significant differences in the His_6-HA-SUMO1 conjugation values were observed between the two genotypes at any of the examined ages in both cortex and hippocampus. (Data obtained in collaboration with Dr. M. Tirard and K. Hellmann)

4. Discussion

4.1. Generation and basic characterization of a Strep-Myc-SUMO3 knock-in mouse line

Studying SUMOylation has long been hampered by a number of difficulties - the lack of reliable antibodies, the transient nature of the post-translational modification, the fact that only a small fraction of a certain protein is SUMOylated at a given time. In an attempt to facilitate the study of SUMOylation, Tirard *et al.* (2012) generated a His_6-HA-SUMO1 knock-in mouse expressing the double-tagged SUMO1 protein under the control of the endogenous SUMO1 promoter. This proved to be a reliable model for the localization of SUMO1 and the identification of SUMO1 substrates. Analogous to that, in the course of my doctoral work, we generated a Strep-Myc-SUMO3 knock-in mouse line expressing Strep-Myc-tagged SUMO3 instead of wild type SUMO3. Importantly, a successfully generated mouse would allow to distinguish SUMO3 from SUMO2 as till now, due to their high sequence similarity, no antibody can distinguish between them. Additionally, the choice of tags different from His_6 and HA would allow a direct comparison of the localization of SUMO1 and SUMO3. Furthermore, besides studying SUMO3 under normal conditions, the mouse model would make it possible to investigate SUMO3 in the context of different pathologies since predominantly SUMO2/3 conjugation has been shown to change dramatically in response to aberrant cellular conditions both in cell cultures (Saitoh & Hinchey, 2000; Golebiowski *et al.*, 2009; Castoralova *et al.*, 2012; Cimarosti *et al.*, 2012; Guo *et al.*, 2013) and *in vivo* (Lee *et al.*, 2007; Cimarosti *et al.*, 2008; Yang *et al.*, 2008a; b; Yang *et al.*, 2009; Wang *et al.*, 2012; Yang *et al.*, 2014).

4.1.1. Strep-Myc-SUMO3 mouse line as a model for identification of SUMO3 substrates

After the generation of the Strep-Myc-SUMO3 mouse line, we wanted to test if the line could be used as a model for the identification of SUMO3 substrates. By performing anti-Myc affinity purification of brain homogenates from wild type and Strep-Myc-SUMO3 mice, we were able to show the enrichment of free and conjugated Strep-Myc-SUMO3 in the eluate from the knock-in mice (Fig. 3.4.). Thus, we proved that by performing anti-Myc affinity purification and subsequent mass spectrometry analysis, the mouse line can be used as a model for identifying SUMO3 substrates. Notably, the presence of a double tag after the start codon of the *SUMO3* gene presents the opportunity for a two-step affinity purification, which would increase the stringency of the purification procedure. For this purpose, the anti-Strep

affinity purification still needs to be optimized. Furthermore, Fig. 3.4. shows comparable expression levels of SUMO2/3 in the knock-in and the wild type mice. Unfortunately, the lack of SUMO3-specific antibody does not allow us to compare the expression of SUMO3 between knock-in and wild type mice.

4.1.2. Strep-Myc-SUMO3 mouse line as a model for localization of SUMO3

A look at the literature shows that even though some studies have focused on SUMO2 and SUMO3 localization in the brain, endogenous SUMO2 and SUMO3 have always been studied together owing to the fact that no antibody can distinguish between them (Li *et al.*, 2003; Yang *et al.*, 2008a; Yang *et al.*, 2009; Wang *et al.*, 2012; Hasegawa *et al.*, 2014; Wang *et al.*, 2014). This makes the examination of SUMO3 localization in the brain of Strep-Myc-SUMO3 mice very interesting.

However, in contrast to the successful affinity purification of free Strep-Myc-SUMO3 and Strep-Myc-SUMO3 conjugates, we could not achieve much in revealing the localization of SUMO3 in the brain both on subcellular and regional level. The utilization of several different anti-Myc and one anti-Strep antibody resulted in very different types of staining in the knock-in mice, which was accompanied by different types of background staining in the wild type mice. A likely reason for this failure is the methodology that was used. Indeed, some antibodies work well for staining cell cultures but fail to give a good signal in brain sections. Furthermore, optimization of the conditions could be required, such as changing the fixation method. Another likely reason for the inability to localize Strep-Myc-SUMO3 is low expression levels of SUMO3. Indeed, in 2014 Wang and collaborators provided evidence that SUMO2 is the predominant SUMO isoform in both embryonic and adult tissues. While SUMO3-/- mice were viable, SUMO2-/- embryos died around the age of E10.5. Using quantitative RT-PCR, the authors showed very low expression levels of SUMO3 in contrast to SUMO2. At embryonic day 7.5 and 8.5 SUMO3 was only 2 and 3%, respectively, from all the SUMO isoforms while SUMO2 was 80 and 75%. Notably, in adult tissue SUMO3 expression increased to 20% of all isoforms. Besides quantitative RT-PCR, the authors also used Western blot to determine the relative abundance of SUMO2 and SUMO3 in both embryonic and adult tissue. In E8.5 embryos, the levels of SUMO2/3 conjugated proteins were decreased in SUMO2-/- mice compared to SUMO2+/- and SUMO2+/+, while there were no significant differences in the levels of SUMO2/3 conjugated proteins between SUMO3-/-, SUMO3+/- and SUMO3+/+. The results were similar when brains, hearts and kidneys from adult mice were used with the difference that the levels of free SUMO2/3 were compared since in adult

animals there were few SUMO2/3 conjugates (Wang *et al.*, 2014). Finally, another, albeit unlikely, reason for the failure to properly localize Strep-Myc-SUMO3 could be that the protein is present in brain regions that were not examined in the present study.

In essence, some of the used antibodies indicated nuclear localization of SUMO3 while others indicated that SUMO3 resides in the cytoplasm. However, it is really difficult to draw any conclusions since the results varied not only when different antibodies were used but also between homozygous and heterozygous mice. A possible though unlikely explanation for these discrepancies between homozygous and heterozygous mice could be the differences in the mice age.

To summarize, the generation of the Strep-Myc-SUMO3 knock-in mouse model proved to be successful in providing a tool for the enrichment and identification of SUMO3 substrates. Regarding the localization of SUMO3, given all the controversial results obtained by now, further work is needed to draw a definite conclusion.

4.2. Analysis of SUMO1 conjugation profile in a mouse model of Alzheimer's disease

Different reports implicated SUMOylation in the pathogenesis of different neurodegenerative diseases. For example, key players in AD pathology, APP and tau, were suggested to be SUMO-modified (Gocke *et al.*, 2005; Dorval & Fraser, 2006; Zhang & Sarge, 2008a; Luo *et al.*, 2014). Furthermore, different groups reported dysregulation of SUMO conjugation levels in mouse models of AD (Zhao *et al.*, 2013; Lee *et al.*, 2014; Nistico *et al.*, 2014). Some of the observations, however, are highly controversial requiring additional investigations to shed light on the matter. Thus, in a second project, our goal was to examine SUMO1 in the context of AD pathology using a mouse model of AD. This included checking for differences in SUMO1 localization and conjugation levels between His_6-HA-SUMO1 mice and crossbred His_6-HA-SUMO1;5xFAD mice. Mice from different ages were used in order to identify any changes between different stages of the disease progression.

Regarding the localization of SUMO1, the nuclear localization was evident in both His_6-HA-SUMO1 and His_6-HA-SUMO1;5xFAD mice in both of the brain regions examined - subiculum and cortical layer V - and at any of the ages examined. Furthermore, additional anti-HA signal was observed in His_6-HA-SUMO1;5xFAD, the abundance of which correlated with the abundance of amyloid plaques. The examination of the non-nuclear signal was done in the subiculum due to the high concentration of amyloid plaques. However, this does not exclude the presence of this signal in other brain regions. The signal had either the shape of a line or of an amorphous mass. Some of the line-shaped signal surrounded amyloid plaques.

However, similar staining was also observed in 5xFAD non-knock-in mice which does not speak in favour of specific anti-HA signal in His_6-HA-SUMO1;5xFAD mice. A different anti-HA antibody, raised in mouse, in addition to nuclear anti-HA signal, produced a different type of non-nuclear staining in the subiculum of His_6-HA-SUMO1;5xFAD mice. This antibody labelled the amyloid plaques. Again, non-knock-in 5xFAD mice exhibited a similar type of signal. Apart from immunostaining, the nuclear localization of SUMO1 was confirmed using subcellular fractionation and subsequent SDS-PAGE and Western blot. His_6-HA-SUMO1 resided predominantly in the nuclear fraction in both 5xFAD and non-5xFAD mice.

With regard to SUMO1 conjugation levels upon AD pathology, using anti-HA Western blot, we did not observe any significant differences in the SUMO1 conjugation levels between His_6-HA-SUMO1 and His_6-HA-SUMO1;5xFAD mice in both cortex and hippocampus at any of the ages examined – 8-, 12-, 16-, 24- and 36-week-old mice. Similarly, quantification of the anti-HA signal intensity in the nuclei of His_6-HA-SUMO1 and His_6-HA-SUMO1;5xFAD mice in both cortical layer V and subiculum did not reveal any substantial differences between the two genotypes. A significant but small increase which accounted for 25.8% was observed in the cortical layer V of 8-week-old His_6-HA-SUMO1;5xFAD mice when compared to His_6-HA-SUMO1 mice. In 12-week-old mice there may be small differences but the number of mice did not allow us to perform statistics. Opposite to 8- and 12-week-old mice, the cortical layer V of His6-HA-SUMO1;5xFAD 16-week-old mice showed almost significant decrease in the nuclear anti-HA signal.

4.2.1. 5xFAD as a model to study Alzheimer's disease

AD research is based on an enormous amount of experimental models with transgenic mouse models constituting a big part of them. The mouse model which was used in our study is 5xFAD – the mice bear five familial AD-related mutations in APP and PS1 (Oakley *et al.*, 2006).

Supposedly the most important advantage of the 5xFAD mouse model is the fast development of AD-like pathology, owing to the compound mutations. Indeed, while in the very popular mouse model Tg2576 amyloid plaques do not appear before 9 months of age (Hsiao *et al.*, 1996; Spires & Hyman, 2005), in 5xFAD mice the amyloid plaques are visible in 2-month-old mice (Oakley *et al.*, 2006). Furthermore, the 5xFAD mouse model exhibits neuronal loss – an important characteristic of AD pathology. In contrast, many of the other transgenic mouse models of AD fail to reproduce this feature (Oakley *et al.*, 2006).

Despite the enormous usefulness of the 5xFAD mouse model, certain limitations should also be mentioned. Some of those limitations are shared by AD transgenic mouse models or even by all transgenic mouse models. One of the problems is the non-physiological level of expression of the transgenes (Elder *et al.*, 2010). Furthermore, a main issue for all AD transgenic mouse models is the inability to reproduce all the features that characterize human AD pathology (Elder *et al.*, 2010). For example, 5xFAD mice do not develop neurofibrillary tangles despite the fact that neurofibrillary tangle development is believed to be downstream with regard to Aβ pathology as postulated by the amyloid hypothesis (Oakley *et al.*, 2006). Another major problem regarding transgenic mouse models of AD is that they are based on mutations exhibited in a very small percentage of AD patients. As Elder and collaborators argue in their review paper about transgenic mouse models of AD from 2010, such mutations can result in introduction of effects which are not present in sporadic AD (Elder *et al.*, 2010). Furthermore, most transgenic mouse models, including 5xFAD, utilize heterologous promoters, which results in different patterns of temporal and spatial expression when compared to human AD (Kitazawa *et al.*, 2012). Notably, the integration of the transgene may result in disruption of an endogenous gene (Onos *et al.*, 2016). Finally, in their original paper describing the generation of 5xFAD mice, Oakley and collaborators state two important limitations of the mouse model with regard to studying AD in humans. First, AD in humans is never caused by multiple mutations and thus, the authors speculate about occurrence of some unpredicted changes in APP processing in the 5xFAD mouse model. Second, the $A\beta_{42}/A\beta_{40}$ ratio is higher than the one in humans which could lead to a higher $A\beta_{42}$ toxicity in the 5xFAD mice (Oakley *et al.*, 2006).

4.2.2. Investigation of the localization of SUMO1 upon Alzheimer's disease pathology

Interestingly, several studies have reported the presence of SUMO1 surrounding or within amyloid plaques using anti-SUMO1 antibodies for staining brain sections of different AD mouse models. First, in 2008, Takahashi and collaborators reported the colocalization of SUMO1 with phospho-Tau positive puncta around amyloid plaques in Tg2576 mice (Takahashi *et al.*, 2008). Later, in 2013, Zhao and collaborators using an APP/PS1 transgenic mouse model reported the colocalization of SUMO1 with AT8 stained phospho-tau in dystrophic neurites around amyloid plaques and furthermore, the presence of diffuse SUMO1 signal in the centre of some plaques (Zhao *et al.*, 2013). In 2013 again, Yun *et al*. used APP/PS1ΔE9 transgenic mice to report SUMO1 surrounding and partially colocalizing with

amyloid plaques. Finally, the same group using the same mouse model reported colocalization of SUMO1 with autophagy markers surrounding amyloid plaques (Cho *et al.*, 2015a).

In contrast to those studies, we could not find evidence of the presence of SUMO1 within or surrounding amyloid plaques and in general of a significant presence of SUMO1 outside the nucleus. The existence of similar non-nuclear signals in both knock-in 5xFAD and non-knock-in 5xFAD speaks strongly against the specificity of the signal in knock-in 5xFAD mice. Furthermore, the different plaque-related staining produced by the use of a different antibody strongly supports the lack of specificity hypothesis. The labelling around or within the plaques with the two antibodies could be a result of amyloid plaques acting as a trap for antibodies. Of course, we cannot completely rule out that there are differences between the non-nuclear staining in the two genotypes and thus the possibility of AD-related SUMO1 relocalization. Drawing a definite conclusion would require an even more thorough investigation including quantitative analysis. Notably, in our hands, none of the plaque-related signal had punctate appearance, which was, in contrast, predominantly seen in the aforementioned studies. Several reasons could account for the discrepancies between our results and the results obtained by the aforementioned groups. First, this could arise from differences in the model systems that were used. The colocalization of SUMO1 with phosphorylated tau in some of the studies could suggest distinct tau phosphorylation profiles in the different AD transgenic mouse models. Secondly, as we focused on subiculum for our analysis of the non-nuclear anti-HA signal, the discrepancies could be caused by differences between the different brain regions, even though this is unlikely. Finally, taking into account the strong background staining in non-knock-in 5xFAD mice, there is a possibility that what has been observed by these studies is only a non-specific background staining related to AD pathology. Amyloid plaques acting as a trap for the antibodies could account for the observed signal surrounding and within the plaques. Indeed, the perfect control would be SUMO1 knock-out mice which were not analysed in any of the studies.

4.2.3. Investigation of SUMO1 conjugation levels upon Alzheimer's disease pathology

Apart from localizing SUMO in mouse models of AD, some authors have used them to examine the levels of SUMO conjugates in comparison to wild type mice using Western blot. In 2011, McMillan and collaborators were the first to explore possible changes in SUMO conjugation using a mouse model of AD – Tg2576. With regard to SUMO1, they did not find any significant differences in the global SUMO1 conjugation levels between 9-month-old transgenic and wild type mice when hippocampus, cortex and cerebellum were examined

(McMillan *et al.*, 2011). Using the same mouse model, Nistico and collaborators showed an increase in SUMO1 conjugation levels in the cortex and the hippocampus of 3- and 6-month-old transgenic mice while 1,5- and 17-month-old mice did not exhibit significant changes in SUMO1 conjugation in these regions (Nistico *et al.*, 2014). Lee *et al.* (2014) also used the same mouse model to show that there are no big changes in the SUMO1 conjugation levels in the hippocampus when mice of ages 1-2-, 7-8- or 13-14 months were examined. Furthermore, Zhao *et al.* (2013) observed an increase in SUMO1 conjugation in different brain regions of 12-month-old APP/PS1 transgenic mice when compared to wild type mice. Finally, a study reported an increase in free SUMO1 levels in the cortex of 18-month-old APPSwedish/PS1ΔE9 transgenic mice (Yun *et al.*, 2013). Reasons for this increase in free SUMO1 could be increased SUMO1 deconjugation or decreased SUMO1 conjugation even though SUMO1 exhibited boosted immunoreactivity, which could mean increased expression levels of SUMO1. In addition to mouse models of AD, the effect of increased Aβ levels on SUMO1 conjugation has been studied in cell cultures. Overexpression of GFP-$A\beta_{1-42}$ resulted in increased levels of free SUMO1 in HBmg cells, while treatment with $A\beta_{1-40}$ applied to the same cells resulted in increased free SUMO1 and SUMO1 conjugation levels (Yun *et al.*, 2013).

The use of quantitative anti-HA Western blot to compare SUMO1 conjugation levels between His_6-HA-SUMO1;5xFAD and His_6-HA-SUMO1 mice did not reveal any significant differences in both hippocampus and cortex at any of the different ages examined. These observations are in contrast to the studies that found changes in SUMO1 conjugation, namely the study by Nistico *et al.* (2014) and Zhao *et al.* (2013). The reason for this discrepancy could be the different properties of the examined mouse models. However, given the discrepancy between the other studies as well, the controversies could arise from unreliable antibodies, insufficient numbers of animals tested, or different ways of analysing Western blot data.

Furthermore, the analysis of the nuclear anti-HA signal intensity of His_6-HA-SUMO1;5xFAD and His_6-HA-SUMO1 mice revealed a significant difference only in the cortical layer V of 8-week-old His_6-HA-SUMO1;5xFAD mice. However, the observations from the two experimental methods should be compared carefully. While the quantitative Western blot focuses on SUMO1 conjugates, the immunostaining analysis cannot distinguish between free and conjugated SUMO1. If free SUMO1 does not relocalize, even a substantial decrease of SUMO1 conjugation would not be detected by analysis of the nuclear anti-HA signal intensity. Furthermore, increases in SUMO1 conjugation accompanied by a decrease in

free SUMO1 but not by an increase in SUMO1 expression would not be detected. This possibility is unlikely due to the lack of a large amount of free SUMO1, described first in COS-7 cells by Saitoh and Hinchey (Saitoh & Hinchey, 2000). Thus, an increase in SUMO1 conjugation would most probably require increased expression of the protein. Furthermore, the technique focuses only on the levels of nuclear SUMO1 conjugates. Increases or decreases in the nuclear signal may just be a result of relocalization of free and/or conjugated SUMO1. Thus, any changes or lack of changes detected by this technique would not directly correlate to changes or lack of changes in SUMO1 conjugation. In spite of these drawbacks, which make studying SUMO1 conjugation levels difficult, the analysis of anti-HA signal intensity has one big advantage – its narrow focus. Examined are the regions in which the AD pathology appears first and therefore is the strongest there. Thus, if the small increase in signal intensity detected in 8-week-old mice is a result of increased SUMO1 conjugation accompanied by increased expression levels of SUMO1, the reason why this is not detected with the Western blot analysis would be a dilution of the effect. However, the small increase could also reflect relocalization of free and/or conjugated SUMO1 into the nucleus, which would also explain the failure to detect this by quantitative Western blot.

In general, the fact that we observed no or only minimal differences between the His_6-HA-SUMO1;5xFAD and His_6-HA-SUMO1 mice with both of the methods used, speaks against a considerable effect of AD pathology on global SUMO1 conjugation. Besides, the small difference that was observed needs to be confirmed by the utilization of a larger number of animals as in most of the cases only 3 animals per genotype were used. The small number of animals used could suggest that the small differences observed could reflect interindividual variability. If the results from the quantification hold true after a larger number of animals is examined, the cortical layer V fluctuations in the ratio between anti-HA signal intensity in His_6-HA-SUMO1;5xFAD and the intensity in His_6-HA-SUMO1 mice could be explained in different ways. One possibility would be that in 8-week-old His_6-HA-SUMO1;5xFAD mice, the AD pathology drives the increase of anti-HA signal intensity. The signal, however, returns back to normal levels and maybe to even lower ones in 16-week-old mice owing to compensatory mechanisms that have started to take place in older mice. Another possibility would be that the initial increase could reflect a compensatory mechanism which continues until a certain point (maybe even until 12 or more weeks of age), at which the mice could not cope with the strengthening of the AD pathology anymore.

4.2.4. Conclusions and outlook

In conclusion, we were not able to find any clear changes in SUMO1 localization and SUMO1 global conjugation levels related to AD-like pathology. This is in contrast to several studies that linked altered SUMO1 conjugation to AD pathology and indicates that SUMO1 conjugation is largely undisturbed in the context of AD pathology. However, since changes in individual proteins may not be detected by examining global SUMO1 conjugation and SUMO1 localization, additional experiments are warranted. Thus, the next step in our investigation, which is currently in progress, includes anti-HA affinity purification of SUMO1 conjugates from brain homogenates of His_6-HA-SUMO1;5xFAD, His_6-HA-SUMO1, 5xFAD and wild type mice and subsequent mass spectrometry analysis, with the aim of identifying differentially SUMOylated substrates under the conditions of AD pathology. The identification of altered substrates would provide many further possibilities for research. The acceptor lysines could be identified and SUMOylation-deficient proteins could be expressed in cell cultures to study the importance of SUMO1-ylation in the AD context.

Furthermore, the SUMO1-ylation of APP and tau has been mainly studied by overexpression of APP or tau and SUMO1 in cell cultures (Dorval & Fraser, 2006; Zhang & Sarge, 2008a; Luo *et al.*, 2014). Thus, it would be interesting to examine their SUMOylation status in the His_6-HA-SUMO1 mouse model and compare with crossbred His_6-HA-SUMO1;5xFAD mice to identify eventual differences in APP and/or tau SUMO1-ylation upon AD pathology.

Another possible future direction that could be explored involves the crossbreeding of the newly generated Strep-Myc-SUMO3 knock-in mouse line with the mouse model of AD – 5xFAD mice in order to explore in a similar way the SUMO3 profile in conditions of AD pathology.

References

Ahmed, M., Davis, J., Aucoin, D., Sato, T., Ahuja, S., Aimoto, S., Elliott, J.I., Van Nostrand, W.E. & Smith, S.O. (2010) Structural conversion of neurotoxic amyloid-beta(1-42) oligomers to fibrils. *Nat Struct Mol Biol*, **17**, 561-567.

Ahn, K., Song, J.H., Kim, D.K., Park, M.H., Jo, S.A. & Koh, Y.H. (2009) Ubc9 gene polymorphisms and late-onset Alzheimer's disease in the Korean population: a genetic association study. *Neurosci Lett*, **465**, 272-275.

Alkuraya, F.S., Saadi, I., Lund, J.J., Turbe-Doan, A., Morton, C.C. & Maas, R.L. (2006) SUMO1 haploinsufficiency leads to cleft lip and palate. *Science*, **313**, 1751.

Alzheimer, A. (1907) Über eine eigenartige Erkrankung der Hirnrinde. *Allgemeine Zeitschrift für Psychiatrie*, **64**, 146-148.

Bales, K.R., Liu, F., Wu, S., Lin, S., Koger, D., DeLong, C., Hansen, J.C., Sullivan, P.M. & Paul, S.M. (2009) Human APOE isoform-dependent effects on brain beta-amyloid levels in PDAPP transgenic mice. *J Neurosci*, **29**, 6771-6779.

Bayona, J.C., Nakayasu, E.S., Laverriere, M., Aguilar, C., Sobreira, T.J., Choi, H., Nesvizhskii, A.I., Almeida, I.C., Cazzulo, J.J. & Alvarez, V.E. (2011) SUMOylation pathway in Trypanosoma cruzi: functional characterization and proteomic analysis of target proteins. *Mol Cell Proteomics*, **10**, M110 007369.

Becker, J., Barysch, S.V., Karaca, S., Dittner, C., Hsiao, H.H., Berriel Diaz, M., Herzig, S., Urlaub, H. & Melchior, F. (2013) Detecting endogenous SUMO targets in mammalian cells and tissues. *Nat Struct Mol Biol*, **20**, 525-531.

Beier, M.T. (2007) Treatment strategies for the behavioral symptoms of Alzheimer's disease: focus on early pharmacologic intervention. *Pharmacotherapy*, **27**, 399-411.

Beltrao, P., Bork, P., Krogan, N.J. & van Noort, V. (2013) Evolution and functional cross-talk of protein post-translational modifications. *Mol Syst Biol*, **9**, 714.

Benson, M.D., Li, Q.J., Kieckhafer, K., Dudek, D., Whorton, M.R., Sunahara, R.K., Iniguez-Lluhi, J.A. & Martens, J.R. (2007) SUMO modification regulates inactivation of the voltage-gated potassium channel Kv1.5. *Proc Natl Acad Sci U S A*, **104**, 1805-1810.

Berdnik, D., Favaloro, V. & Luo, L. (2012) The SUMO protease Verloren regulates dendrite and axon targeting in olfactory projection neurons. *J Neurosci*, **32**, 8331-8340.

Bergink, S. & Jentsch, S. (2009) Principles of ubiquitin and SUMO modifications in DNA repair. *Nature*, **458**, 461-467.

Blomster, H.A., Hietakangas, V., Wu, J., Kouvonen, P., Hautaniemi, S. & Sistonen, L. (2009) Novel proteomics strategy brings insight into the prevalence of SUMO-2 target sites. *Mol Cell Proteomics*, **8**, 1382-1390.

Blomster, H.A., Imanishi, S.Y., Siimes, J., Kastu, J., Morrice, N.A., Eriksson, J.E. & Sistonen, L. (2010) In vivo identification of sumoylation sites by a signature tag and cysteine-targeted affinity purification. *J Biol Chem*, **285**, 19324-19329.

Bohren, K.M., Nadkarni, V., Song, J.H., Gabbay, K.H. & Owerbach, D. (2004) A M55V polymorphism in a novel SUMO gene (SUMO-4) differentially activates heat shock transcription factors and is associated with susceptibility to type I diabetes mellitus. *J Biol Chem*, **279**, 27233-27238.

Borchelt, D.R., Ratovitski, T., van Lare, J., Lee, M.K., Gonzales, V., Jenkins, N.A., Copeland, N.G., Price, D.L. & Sisodia, S.S. (1997) Accelerated amyloid deposition in the brains of transgenic mice coexpressing mutant presenilin 1 and amyloid precursor proteins. *Neuron*, **19**, 939-945.

Braak, H. & Braak, E. (1991) Neuropathological stageing of Alzheimer-related changes. *Acta Neuropathol*, **82**, 239-259.

Braun, L., Cannella, D., Pinheiro, A.M., Kieffer, S., Belrhali, H., Garin, J. & Hakimi, M.A. (2009) The small ubiquitin-like modifier (SUMO)-conjugating system of Toxoplasma gondii. *Int J Parasitol*, **39**, 81-90.

Bruderer, R., Tatham, M.H., Plechanovova, A., Matic, I., Garg, A.K. & Hay, R.T. (2011) Purification and identification of endogenous polySUMO conjugates. *EMBO Rep*, **12**, 142-148.

Callis, J. (2014) The ubiquitination machinery of the ubiquitin system. *Arabidopsis Book*, **12**, e0174.

Castellani, R.J., Nunomura, A., Lee, H.G., Perry, G. & Smith, M.A. (2008) Phosphorylated tau: toxic, protective, or none of the above. *J Alzheimers Dis*, **14**, 377-383.

Castoralova, M., Brezinova, D., Sveda, M., Lipov, J., Ruml, T. & Knejzlik, Z. (2012) SUMO-2/3 conjugates accumulating under heat shock or MG132 treatment result largely from new protein synthesis. *Biochim Biophys Acta*, **1823**, 911-919.

Cavallucci, V., D'Amelio, M. & Cecconi, F. (2012) Abeta toxicity in Alzheimer's disease. *Mol Neurobiol*, **45**, 366-378.

Chalmers, D.T., Dewar, D., Graham, D.I., Brooks, D.N. & McCulloch, J. (1990) Differential alterations of cortical glutamatergic binding sites in senile dementia of the Alzheimer type. *Proc Natl Acad Sci U S A*, **87**, 1352-1356.

Chan, H.Y., Warrick, J.M., Andriola, I., Merry, D. & Bonini, N.M. (2002) Genetic modulation of polyglutamine toxicity by protein conjugation pathways in Drosophila. *Hum Mol Genet*, **11**, 2895-2904.

Chao, H.W., Hong, C.J., Huang, T.N., Lin, Y.L. & Hsueh, Y.P. (2008) SUMOylation of the MAGUK protein CASK regulates dendritic spinogenesis. *J Cell Biol*, **182**, 141-155.

Cho, S.J., Yun, S.M., Jo, C., Lee, D.H., Choi, K.J., Song, J.C., Park, S.I., Kim, Y.J. & Koh, Y.H. (2015a) SUMO1 promotes Abeta production via the modulation of autophagy. *Autophagy*, **11**, 100-112.

Cho, S.J., Yun, S.M., Lee, D.H., Jo, C., Ho Park, M., Han, C. & Ho Koh, Y. (2015b) Plasma SUMO1 Protein is Elevated in Alzheimer's Disease. *J Alzheimers Dis*, **47**, 639-643.

Ciechanover, A., Heller, H., Elias, S., Haas, A.L. & Hershko, A. (1980) ATP-dependent conjugation of reticulocyte proteins with the polypeptide required for protein degradation. *Proc Natl Acad Sci U S A*, **77**, 1365-1368.

Ciechanover, A., Hod, Y. & Hershko, A. (2012) A heat-stable polypeptide component of an ATP-dependent proteolytic system from reticulocytes. 1978. *Biochem Biophys Res Commun*, **425**, 565-570.

Cimarosti, H., Ashikaga, E., Jaafari, N., Dearden, L., Rubin, P., Wilkinson, K.A. & Henley, J.M. (2012) Enhanced SUMOylation and SENP-1 protein levels following oxygen and glucose deprivation in neurones. *J Cereb Blood Flow Metab*, **32**, 17-22.

Cimarosti, H., Lindberg, C., Bomholt, S.F., Ronn, L.C. & Henley, J.M. (2008) Increased protein SUMOylation following focal cerebral ischemia. *Neuropharmacology*, **54**, 280-289.

Comerford, K.M., Leonard, M.O., Karhausen, J., Carey, R., Colgan, S.P. & Taylor, C.T. (2003) Small ubiquitin-related modifier-1 modification mediates resolution of CREB-dependent responses to hypoxia. *Proc Natl Acad Sci U S A*, **100**, 986-991.

Craig, T.J., Anderson, D., Evans, A.J., Girach, F. & Henley, J.M. (2015) SUMOylation of Syntaxin1A regulates presynaptic endocytosis. *Sci Rep*, **5**, 17669.

D'Amelio, M., Cavallucci, V., Middei, S., Marchetti, C., Pacioni, S., Ferri, A., Diamantini, A., De Zio, D., Carrara, P., Battistini, L., Moreno, S., Bacci, A., Ammassari-Teule, M., Marie, H. & Cecconi, F. (2011) Caspase-3 triggers early synaptic dysfunction in a mouse model of Alzheimer's disease. *Nat Neurosci*, **14**, 69-76.

D'Cunha, J., Ramanujam, S., Wagner, R.J., Witt, P.L., Knight, E., Jr. & Borden, E.C. (1996) In vitro and in vivo secretion of human ISG15, an IFN-induced immunomodulatory cytokine. *J Immunol*, **157**, 4100-4108.

Daniel, J. & Liebau, E. (2014) The ufm1 cascade. *Cells*, **3**, 627-638.

Denison, C., Rudner, A.D., Gerber, S.A., Bakalarski, C.E., Moazed, D. & Gygi, S.P. (2005) A proteomic strategy for gaining insights into protein sumoylation in yeast. *Mol Cell Proteomics*, **4**, 246-254.

Dickerson, B.C. & Eichenbaum, H. (2010) The episodic memory system: neurocircuitry and disorders. *Neuropsychopharmacology*, **35**, 86-104.

Dickson, T.C. & Vickers, J.C. (2001) The morphological phenotype of beta-amyloid plaques and associated neuritic changes in Alzheimer's disease. *Neuroscience*, **105**, 99-107.

Dorval, V. & Fraser, P.E. (2006) Small ubiquitin-like modifier (SUMO) modification of natively unfolded proteins tau and alpha-synuclein. *J Biol Chem*, **281**, 9919-9924.

Dorval, V., Mazzella, M.J., Mathews, P.M., Hay, R.T. & Fraser, P.E. (2007) Modulation of Abeta generation by small ubiquitin-like modifiers does not require conjugation to target proteins. *Biochem J*, **404**, 309-316.

Du, H., Guo, L., Yan, S., Sosunov, A.A., McKhann, G.M. & Yan, S.S. (2010) Early deficits in synaptic mitochondria in an Alzheimer's disease mouse model. *Proc Natl Acad Sci U S A*, **107**, 18670-18675.

Dubey, R.C. (2014) *Advanced biotechnology*. S. Chand & Company Pvt. Ltd., New Delhi.

Elder, G.A., Gama Sosa, M.A. & De Gasperi, R. (2010) Transgenic mouse models of Alzheimer's disease. *Mt Sinai J Med*, **77**, 69-81.

Ettlinger, M., Margulis, E.H. & Wong, P.C. (2011) Implicit memory in music and language. *Front Psychol*, **2**, 211.

Evdokimov, E., Sharma, P., Lockett, S.J., Lualdi, M. & Kuehn, M.R. (2008) Loss of SUMO1 in mice affects RanGAP1 localization and formation of PML nuclear bodies, but is not lethal as it can be compensated by SUMO2 or SUMO3. *J Cell Sci*, **121**, 4106-4113.

Fang, H., Du, X., Meng, F.T. & Zhou, J.N. (2011) SUMO negatively regulates BACE expression. *Neuro Endocrinol Lett*, **32**, 313-316.

Fatkin, D., MacRae, C., Sasaki, T., Wolff, M.R., Porcu, M., Frenneaux, M., Atherton, J., Vidaillet, H.J., Jr., Spudich, S., De Girolami, U., Seidman, J.G., Seidman, C., Muntoni, F., Muehle, G., Johnson, W. & McDonough, B. (1999) Missense mutations in the rod domain of the lamin A/C gene as causes of dilated cardiomyopathy and conduction-system disease. *N Engl J Med*, **341**, 1715-1724.

Fei, E., Jia, N., Yan, M., Ying, Z., Sun, Q., Wang, H., Zhang, T., Ma, X., Ding, H., Yao, X., Shi, Y. & Wang, G. (2006) SUMO-1 modification increases human SOD1 stability and aggregation. *Biochem Biophys Res Commun*, **347**, 406-412.

Feliciangeli, S., Bendahhou, S., Sandoz, G., Gounon, P., Reichold, M., Warth, R., Lazdunski, M., Barhanin, J. & Lesage, F. (2007) Does sumoylation control K2P1/TWIK1 background K+ channels? *Cell*, **130**, 563-569.

Feliciangeli, S., Tardy, M.P., Sandoz, G., Chatelain, F.C., Warth, R., Barhanin, J., Bendahhou, S. & Lesage, F. (2010) Potassium channel silencing by constitutive endocytosis and intracellular sequestration. *J Biol Chem*, **285**, 4798-4805.

Feligioni, M., Nishimune, A. & Henley, J.M. (2009) Protein SUMOylation modulates calcium influx and glutamate release from presynaptic terminals. *Eur J Neurosci*, **29**, 1348-1356.

Figueroa-Romero, C., Iniguez-Lluhi, J.A., Stadler, J., Chang, C.R., Arnoult, D., Keller, P.J., Hong, Y., Blackstone, C. & Feldman, E.L. (2009) SUMOylation of the mitochondrial fission protein Drp1 occurs at multiple nonconsensus sites within the B domain and is linked to its activity cycle. *FASEB J*, **23**, 3917-3927.

Flotho, A. & Melchior, F. (2013) Sumoylation: a regulatory protein modification in health and disease. *Annu Rev Biochem*, **82**, 357-385.

Foran, E., Bogush, A., Goffredo, M., Roncaglia, P., Gustincich, S., Pasinelli, P. & Trotti, D. (2011) Motor neuron impairment mediated by a sumoylated fragment of the glial glutamate transporter EAAT2. *Glia*, **59**, 1719-1731.

Games, D., Adams, D., Alessandrini, R., Barbour, R., Berthelette, P., Blackwell, C., Carr, T., Clemens, J., Donaldson, T., Gillespie, F. & et al. (1995) Alzheimer-type neuropathology in transgenic mice overexpressing V717F beta-amyloid precursor protein. *Nature*, **373**, 523-527.

Geiss-Friedlander, R. & Melchior, F. (2007) Concepts in sumoylation: a decade on. *Nat Rev Mol Cell Biol*, **8**, 947-956.

Gendreau, K.L. & Hall, G.F. (2013) Tangles, Toxicity, and Tau Secretion in AD - New Approaches to a Vexing Problem. *Front Neurol*, **4**, 160.

Gill, G. (2004) SUMO and ubiquitin in the nucleus: different functions, similar mechanisms? *Genes Dev*, **18**, 2046-2059.

Giorgino, F., de Robertis, O., Laviola, L., Montrone, C., Perrini, S., McCowen, K.C. & Smith, R.J. (2000) The sentrin-conjugating enzyme mUbc9 interacts with GLUT4 and GLUT1 glucose transporters and regulates transporter levels in skeletal muscle cells. *Proc Natl Acad Sci U S A*, **97**, 1125-1130.

Girach, F., Craig, T.J., Rocca, D.L. & Henley, J.M. (2013) RIM1alpha SUMOylation is required for fast synaptic vesicle exocytosis. *Cell Rep*, **5**, 1294-1301.

Girdwood, D., Bumpass, D., Vaughan, O.A., Thain, A., Anderson, L.A., Snowden, A.W., Garcia-Wilson, E., Perkins, N.D. & Hay, R.T. (2003) P300 transcriptional repression is mediated by SUMO modification. *Mol Cell*, **11**, 1043-1054.

Gocke, C.B., Yu, H. & Kang, J. (2005) Systematic identification and analysis of mammalian small ubiquitin-like modifier substrates. *J Biol Chem*, **280**, 5004-5012.

Golebiowski, F., Matic, I., Tatham, M.H., Cole, C., Yin, Y., Nakamura, A., Cox, J., Barton, G.J., Mann, M. & Hay, R.T. (2009) System-wide changes to SUMO modifications in response to heat shock. *Sci Signal*, **2**, ra24.

Gross, R.G. & Grossman, M. (2008) Update on apraxia. *Curr Neurol Neurosci Rep*, **8**, 490-496.

Grupe, A., Abraham, R., Li, Y., Rowland, C., Hollingworth, P., Morgan, A., Jehu, L., Segurado, R., Stone, D., Schadt, E., Karnoub, M., Nowotny, P., Tacey, K., Catanese, J., Sninsky, J., Brayne, C., Rubinsztein, D., Gill, M., Lawlor, B., Lovestone, S., Holmans, P., O'Donovan, M., Morris, J.C., Thal, L., Goate, A., Owen, M.J. & Williams, J. (2007) Evidence for novel susceptibility genes for late-onset Alzheimer's disease from a genome-wide association study of putative functional variants. *Hum Mol Genet*, **16**, 865-873.

Guo, C. & Henley, J.M. (2014) Wrestling with stress: roles of protein SUMOylation and deSUMOylation in cell stress response. *IUBMB Life*, **66**, 71-77.

Guo, C., Hildick, K.L., Luo, J., Dearden, L., Wilkinson, K.A. & Henley, J.M. (2013) SENP3-mediated deSUMOylation of dynamin-related protein 1 promotes cell death following ischaemia. *EMBO J*, **32**, 1514-1528.

Guo, D., Li, M., Zhang, Y., Yang, P., Eckenrode, S., Hopkins, D., Zheng, W., Purohit, S., Podolsky, R.H., Muir, A., Wang, J., Dong, Z., Brusko, T., Atkinson, M., Pozzilli, P., Zeidler, A., Raffel, L.J., Jacob, C.O., Park, Y., Serrano-Rios, M., Larrad, M.T., Zhang, Z., Garchon, H.J., Bach, J.F., Rotter, J.I., She, J.X. & Wang, C.Y. (2004) A functional variant of SUMO4, a new I kappa B alpha modifier, is associated with type 1 diabetes. *Nat Genet*, **36**, 837-841.

Gwizdek, C., Casse, F. & Martin, S. (2013) Protein sumoylation in brain development, neuronal morphology and spinogenesis. *Neuromolecular Med*, **15**, 677-691.

Haas, A.L., Ahrens, P., Bright, P.M. & Ankel, H. (1987) Interferon induces a 15-kilodalton protein exhibiting marked homology to ubiquitin. *J Biol Chem*, **262**, 11315-11323.

Hannich, J.T., Lewis, A., Kroetz, M.B., Li, S.J., Heide, H., Emili, A. & Hochstrasser, M. (2005) Defining the SUMO-modified proteome by multiple approaches in Saccharomyces cerevisiae. *J Biol Chem*, **280**, 4102-4110.

Harder, Z., Zunino, R. & McBride, H. (2004) Sumo1 conjugates mitochondrial substrates and participates in mitochondrial fission. *Curr Biol*, **14**, 340-345.

Hasegawa, Y., Yoshida, D., Nakamura, Y. & Sakakibara, S. (2014) Spatiotemporal distribution of SUMOylation components during mouse brain development. *J Comp Neurol*, **522**, 3020-3036.

Hay, R.T. (2005) SUMO: a history of modification. *Mol Cell*, **18**, 1-12.

Hayashi, T., Seki, M., Maeda, D., Wang, W., Kawabe, Y., Seki, T., Saitoh, H., Fukagawa, T., Yagi, H. & Enomoto, T. (2002) Ubc9 is essential for viability of higher eukaryotic cells. *Exp Cell Res*, **280**, 212-221.

Henley, J.M., Craig, T.J. & Wilkinson, K.A. (2014) Neuronal SUMOylation: mechanisms, physiology, and roles in neuronal dysfunction. *Physiol Rev*, **94**, 1249-1285.

Herrmann, J., Lerman, L.O. & Lerman, A. (2007) Ubiquitin and ubiquitin-like proteins in protein regulation. *Circ Res*, **100**, 1276-1291.

Herrup, K. (2015) The case for rejecting the amyloid cascade hypothesis. *Nat Neurosci*, **18**, 794-799.

Hippius, H. & Neundorfer, G. (2003) The discovery of Alzheimer's disease. *Dialogues Clin Neurosci*, **5**, 101-108.

Hochstrasser, M. (2009) Origin and function of ubiquitin-like proteins. *Nature*, **458**, 422-429.

Holtzman, D.M., Bales, K.R., Tenkova, T., Fagan, A.M., Parsadanian, M., Sartorius, L.J., Mackey, B., Olney, J., McKeel, D., Wozniak, D. & Paul, S.M. (2000) Apolipoprotein E isoform-dependent amyloid deposition and neuritic degeneration in a mouse model of Alzheimer's disease. *Proc Natl Acad Sci U S A*, **97**, 2892-2897.

Holtzman, D.M., Bales, K.R., Wu, S., Bhat, P., Parsadanian, M., Fagan, A.M., Chang, L.K., Sun, Y. & Paul, S.M. (1999) Expression of human apolipoprotein E reduces amyloid-beta deposition in a mouse model of Alzheimer's disease. *J Clin Invest*, **103**, R15-R21.

Hoppe, J.B., Rattray, M., Tu, H., Salbego, C.G. & Cimarosti, H. (2013) SUMO-1 conjugation blocks beta-amyloid-induced astrocyte reactivity. *Neurosci Lett*, **546**, 51-56.

Hsiao, H.H., Meulmeester, E., Frank, B.T., Melchior, F. & Urlaub, H. (2009) "ChopNSpice," a mass spectrometric approach that allows identification of endogenous small ubiquitin-like modifier-conjugated peptides. *Mol Cell Proteomics*, **8**, 2664-2675.

Hsiao, K., Chapman, P., Nilsen, S., Eckman, C., Harigaya, Y., Younkin, S., Yang, F. & Cole, G. (1996) Correlative memory deficits, Abeta elevation, and amyloid plaques in transgenic mice. *Science*, **274**, 99-102.

Huang, J., Yan, J., Zhang, J., Zhu, S., Wang, Y., Shi, T., Zhu, C., Chen, C., Liu, X., Cheng, J., Mustelin, T., Feng, G.S., Chen, G. & Yu, J. (2012) SUMO1 modification of PTEN regulates tumorigenesis by controlling its association with the plasma membrane. *Nat Commun*, **3**, 911.

Huang, Y. & Mucke, L. (2012) Alzheimer mechanisms and therapeutic strategies. *Cell*, **148**, 1204-1222.

Jaafari, N., Konopacki, F.A., Owen, T.F., Kantamneni, S., Rubin, P., Craig, T.J., Wilkinson, K.A. & Henley, J.M. (2013) SUMOylation is required for glycine-induced increases in AMPA receptor surface expression (ChemLTP) in hippocampal neurons. *PLoS One*, **8**, e52345.

Jakobs, P.M., Hanson, E.L., Crispell, K.A., Toy, W., Keegan, H., Schilling, K., Icenogle, T.B., Litt, M. & Hershberger, R.E. (2001) Novel lamin A/C mutations in two families with dilated cardiomyopathy and conduction system disease. *J Card Fail*, **7**, 249-256.

Johnson, E.S. (2004) Protein modification by SUMO. *Annu Rev Biochem*, **73**, 355-382.

Jones, D.H. & Matus, A.I. (1974) Isolation of synaptic plasma membrane from brain by combined flotation-sedimentation density gradient centrifugation. *Biochim Biophys Acta*, **356**, 276-287.

Kaminsky, R., Denison, C., Bening-Abu-Shach, U., Chisholm, A.D., Gygi, S.P. & Broday, L. (2009) SUMO regulates the assembly and function of a cytoplasmic intermediate filament protein in C. elegans. *Dev Cell*, **17**, 724-735.

Kessler, J.D., Kahle, K.T., Sun, T., Meerbrey, K.L., Schlabach, M.R., Schmitt, E.M., Skinner, S.O., Xu, Q., Li, M.Z., Hartman, Z.C., Rao, M., Yu, P., Dominguez-Vidana, R., Liang, A.C., Solimini, N.L., Bernardi, R.J., Yu, B., Hsu, T., Golding, I., Luo, J., Osborne, C.K., Creighton, C.J., Hilsenbeck, S.G., Schiff, R., Shaw, C.A., Elledge, S.J. & Westbrook, T.F. (2012) A SUMOylation-dependent transcriptional subprogram is required for Myc-driven tumorigenesis. *Science*, **335**, 348-353.

Kho, C., Lee, A., Jeong, D., Oh, J.G., Chaanine, A.H., Kizana, E., Park, W.J. & Hajjar, R.J. (2011) SUMO1-dependent modulation of SERCA2a in heart failure. *Nature*, **477**, 601-605.

Kitazawa, M., Medeiros, R. & Laferla, F.M. (2012) Transgenic mouse models of Alzheimer disease: developing a better model as a tool for therapeutic interventions. *Curr Pharm Des*, **18**, 1131-1147.

Komander, D. (2009) The emerging complexity of protein ubiquitination. *Biochem Soc Trans*, **37**, 937-953.

Komander, D. & Rape, M. (2012) The ubiquitin code. *Annu Rev Biochem*, **81**, 203-229.

Konopacki, F.A., Jaafari, N., Rocca, D.L., Wilkinson, K.A., Chamberlain, S., Rubin, P., Kantamneni, S., Mellor, J.R. & Henley, J.M. (2011) Agonist-induced PKC phosphorylation regulates GluK2 SUMOylation and kainate receptor endocytosis. *Proc Natl Acad Sci U S A*, **108**, 19772-19777.

Krumova, P., Meulmeester, E., Garrido, M., Tirard, M., Hsiao, H.H., Bossis, G., Urlaub, H., Zweckstetter, M., Kugler, S., Melchior, F., Bahr, M. & Weishaupt, J.H. (2011) Sumoylation inhibits alpha-synuclein aggregation and toxicity. *J Cell Biol*, **194**, 49-60.

Krumova, P. & Weishaupt, J.H. (2013) Sumoylation in neurodegenerative diseases. *Cell Mol Life Sci*, **70**, 2123-2138.

Kumar, S., Yoshida, Y. & Noda, M. (1993) Cloning of a cDNA which encodes a novel ubiquitin-like protein. *Biochem Biophys Res Commun*, **195**, 393-399.

Kummer, M.P. & Heneka, M.T. (2014) Truncated and modified amyloid-beta species. *Alzheimers Res Ther*, **6**, 28.

Kunadt, M., Eckermann, K., Stuendl, A., Gong, J., Russo, B., Strauss, K., Rai, S., Kugler, S., Falomir Lockhart, L., Schwalbe, M., Krumova, P., Oliveira, L.M., Bahr, M., Mobius, W., Levin, J., Giese, A., Kruse, N., Mollenhauer, B., Geiss-Friedlander, R., Ludolph, A.C., Freischmidt, A., Feiler, M.S., Danzer, K.M., Zweckstetter, M., Jovin, T.M., Simons, M., Weishaupt, J.H. & Schneider, A. (2015) Extracellular vesicle sorting of alpha-Synuclein is regulated by sumoylation. *Acta Neuropathol*, **129**, 695-713.

Lakso, M., Pichel, J.G., Gorman, J.R., Sauer, B., Okamoto, Y., Lee, E., Alt, F.W. & Westphal, H. (1996) Efficient in vivo manipulation of mouse genomic sequences at the zygote stage. *Proc Natl Acad Sci U S A*, **93**, 5860-5865.

Leach, M.D., Stead, D.A., Argo, E. & Brown, A.J. (2011) Identification of sumoylation targets, combined with inactivation of SMT3, reveals the impact of sumoylation upon growth, morphology, and stress resistance in the pathogen Candida albicans. *Mol Biol Cell*, **22**, 687-702.

Lee, H.G., Zhu, X., Ghanbari, H.A., Ogawa, O., Raina, A.K., O'Neill, M.J., Perry, G. & Smith, M.A. (2002) Differential regulation of glutamate receptors in Alzheimer's disease. *Neurosignals*, **11**, 282-292.

Lee, J.S. & Thorgeirsson, S.S. (2004) Genome-scale profiling of gene expression in hepatocellular carcinoma: classification, survival prediction, and identification of therapeutic targets. *Gastroenterology*, **127**, S51-55.

Lee, L., Dale, E., Staniszewski, A., Zhang, H., Saeed, F., Sakurai, M., Fa, M., Orozco, I., Michelassi, F., Akpan, N., Lehrer, H. & Arancio, O. (2014) Regulation of synaptic plasticity and cognition by SUMO in normal physiology and Alzheimer's disease. *Sci Rep*, **4**, 7190.

Lee, L., Sakurai, M., Matsuzaki, S., Arancio, O. & Fraser, P. (2013) SUMO and Alzheimer's disease. *Neuromolecular Med*, **15**, 720-736.

Lee, Y.J., Miyake, S., Wakita, H., McMullen, D.C., Azuma, Y., Auh, S. & Hallenbeck, J.M. (2007) Protein SUMOylation is massively increased in hibernation torpor and is critical for the

cytoprotection provided by ischemic preconditioning and hypothermia in SHSY5Y cells. *J Cereb Blood Flow Metab*, **27**, 950-962.

Lemere, C.A. & Masliah, E. (2010) Can Alzheimer disease be prevented by amyloid-beta immunotherapy? *Nat Rev Neurol*, **6**, 108-119.

Li, Y., Wang, H., Wang, S., Quon, D., Liu, Y.W. & Cordell, B. (2003) Positive and negative regulation of APP amyloidogenesis by sumoylation. *Proc Natl Acad Sci U S A*, **100**, 259-264.

Lindwall, G. & Cole, R.D. (1984) Phosphorylation affects the ability of tau protein to promote microtubule assembly. *J Biol Chem*, **259**, 5301-5305.

Liu, P., Jenkins, N.A. & Copeland, N.G. (2003) A highly efficient recombineering-based method for generating conditional knockout mutations. *Genome Res*, **13**, 476-484.

Loeb, K.R. & Haas, A.L. (1992) The interferon-inducible 15-kDa ubiquitin homolog conjugates to intracellular proteins. *J Biol Chem*, **267**, 7806-7813.

Loriol, C., Khayachi, A., Poupon, G., Gwizdek, C. & Martin, S. (2013) Activity-dependent regulation of the sumoylation machinery in rat hippocampal neurons. *Biol Cell*, **105**, 30-45.

Loriol, C., Parisot, J., Poupon, G., Gwizdek, C. & Martin, S. (2012) Developmental regulation and spatiotemporal redistribution of the sumoylation machinery in the rat central nervous system. *PLoS One*, **7**, e33757.

Luan, Z., Liu, Y., Stuhlmiller, T.J., Marquez, J. & Garcia-Castro, M.I. (2013) SUMOylation of Pax7 is essential for neural crest and muscle development. *Cell Mol Life Sci*, **70**, 1793-1806.

Luo, H.B., Xia, Y.Y., Shu, X.J., Liu, Z.C., Feng, Y., Liu, X.H., Yu, G., Yin, G., Xiong, Y.S., Zeng, K., Jiang, J., Ye, K., Wang, X.C. & Wang, J.Z. (2014) SUMOylation at K340 inhibits tau degradation through deregulating its phosphorylation and ubiquitination. *Proc Natl Acad Sci U S A*, **111**, 16586-16591.

Manczak, M. & Reddy, P.H. (2012) Abnormal interaction between the mitochondrial fission protein Drp1 and hyperphosphorylated tau in Alzheimer's disease neurons: implications for mitochondrial dysfunction and neuronal damage. *Hum Mol Genet*, **21**, 2538-2547.

Manns, J.R., Hopkins, R.O. & Squire, L.R. (2003) Semantic memory and the human hippocampus. *Neuron*, **38**, 127-133.

Martin, S., Nishimune, A., Mellor, J.R. & Henley, J.M. (2007a) SUMOylation regulates kainate-receptor-mediated synaptic transmission. *Nature*, **447**, 321-325.

Martin, S., Wilkinson, K.A., Nishimune, A. & Henley, J.M. (2007b) Emerging extranuclear roles of protein SUMOylation in neuronal function and dysfunction. *Nat Rev Neurosci*, **8**, 948-959.

Martins, W.C., Tasca, C.I. & Cimarosti, H. (2016) Battling Alzheimer's Disease: Targeting SUMOylation-Mediated Pathways. *Neurochem Res*, **41**, 568-578.

Matic, I., Schimmel, J., Hendriks, I.A., van Santen, M.A., van de Rijke, F., van Dam, H., Gnad, F., Mann, M. & Vertegaal, A.C. (2010) Site-specific identification of SUMO-2 targets in cells reveals an inverted SUMOylation motif and a hydrophobic cluster SUMOylation motif. *Mol Cell*, **39**, 641-652.

Matic, I., van Hagen, M., Schimmel, J., Macek, B., Ogg, S.C., Tatham, M.H., Hay, R.T., Lamond, A.I., Mann, M. & Vertegaal, A.C. (2008) In vivo identification of human small ubiquitin-like modifier polymerization sites by high accuracy mass spectrometry and an in vitro to in vivo strategy. *Mol Cell Proteomics*, **7**, 132-144.

Matunis, M.J., Coutavas, E. & Blobel, G. (1996) A novel ubiquitin-like modification modulates the partitioning of the Ran-GTPase-activating protein RanGAP1 between the cytosol and the nuclear pore complex. *J Cell Biol*, **135**, 1457-1470.

Maurer, K., Volk, S. & Gerbaldo, H. (1997) Auguste D and Alzheimer's disease. *Lancet*, **349**, 1546-1549.

McDoniels-Silvers, A.L., Nimri, C.F., Stoner, G.D., Lubet, R.A. & You, M. (2002) Differential gene expression in human lung adenocarcinomas and squamous cell carcinomas. *Clin Cancer Res*, **8**, 1127-1138.

McFadden, K., Hamilton, R.L., Insalaco, S.J., Lavine, L., Al-Mateen, M., Wang, G. & Wiley, C.A. (2005) Neuronal intranuclear inclusion disease without polyglutamine inclusions in a child. *J Neuropathol Exp Neurol*, **64**, 545-552.

McLean, C.A., Cherny, R.A., Fraser, F.W., Fuller, S.J., Smith, M.J., Beyreuther, K., Bush, A.I. & Masters, C.L. (1999) Soluble pool of Abeta amyloid as a determinant of severity of neurodegeneration in Alzheimer's disease. *Ann Neurol*, **46**, 860-866.

McMillan, L.E., Brown, J.T., Henley, J.M. & Cimarosti, H. (2011) Profiles of SUMO and ubiquitin conjugation in an Alzheimer's disease model. *Neurosci Lett*, **502**, 201-208.

Meluh, P.B. & Koshland, D. (1995) Evidence that the MIF2 gene of Saccharomyces cerevisiae encodes a centromere protein with homology to the mammalian centromere protein CENP-C. *Mol Biol Cell*, **6**, 793-807.

Miller, M.J., Barrett-Wilt, G.A., Hua, Z. & Vierstra, R.D. (2010) Proteomic analyses identify a diverse array of nuclear processes affected by small ubiquitin-like modifier conjugation in Arabidopsis. *Proc Natl Acad Sci U S A*, **107**, 16512-16517.

Minati, L., Edginton, T., Bruzzone, M.G. & Giaccone, G. (2009) Current concepts in Alzheimer's disease: a multidisciplinary review. *Am J Alzheimers Dis Other Demen*, **24**, 95-121.

Mo, Y.Y., Yu, Y., Theodosiou, E., Ee, P.L. & Beck, W.T. (2005) A role for Ubc9 in tumorigenesis. *Oncogene*, **24**, 2677-2683.

Morris, G.P., Clark, I.A. & Vissel, B. (2014) Inconsistencies and controversies surrounding the amyloid hypothesis of Alzheimer's disease. *Acta Neuropathol Commun*, **2**, 135.

Morrissette, D.A., Parachikova, A., Green, K.N. & LaFerla, F.M. (2009) Relevance of transgenic mouse models to human Alzheimer disease. *J Biol Chem*, **284**, 6033-6037.

Moschos, S.J. & Mo, Y.Y. (2006) Role of SUMO/Ubc9 in DNA damage repair and tumorigenesis. *J Mol Histol*, **37**, 309-319.

Moschos, S.J., Smith, A.P., Mandic, M., Athanassiou, C., Watson-Hurst, K., Jukic, D.M., Edington, H.D., Kirkwood, J.M. & Becker, D. (2007) SAGE and antibody array analysis of melanoma-infiltrated lymph nodes: identification of Ubc9 as an important molecule in advanced-stage melanomas. *Oncogene*, **26**, 4216-4225.

Mucke, L. & Selkoe, D.J. (2012) Neurotoxicity of amyloid beta-protein: synaptic and network dysfunction. *Cold Spring Harb Perspect Med*, **2**, a006338.

Mukherjee, S., Thomas, M., Dadgar, N., Lieberman, A.P. & Iniguez-Lluhi, J.A. (2009) Small ubiquitin-like modifier (SUMO) modification of the androgen receptor attenuates polyglutamine-mediated aggregation. *J Biol Chem*, **284**, 21296-21306.

Nacerddine, K., Lehembre, F., Bhaumik, M., Artus, J., Cohen-Tannoudji, M., Babinet, C., Pandolfi, P.P. & Dejean, A. (2005) The SUMO pathway is essential for nuclear integrity and chromosome segregation in mice. *Dev Cell*, **9**, 769-779.

Nie, M., Xie, Y., Loo, J.A. & Courey, A.J. (2009) Genetic and proteomic evidence for roles of Drosophila SUMO in cell cycle control, Ras signaling, and early pattern formation. *PLoS One*, **4**, e5905.

Nishida, T. & Yasuda, H. (2002) PIAS1 and PIASxalpha function as SUMO-E3 ligases toward androgen receptor and repress androgen receptor-dependent transcription. *J Biol Chem*, **277**, 41311-41317.

Nistico, R., Ferraina, C., Marconi, V., Blandini, F., Negri, L., Egebjerg, J. & Feligioni, M. (2014) Age-related changes of protein SUMOylation balance in the AbetaPP Tg2576 mouse model of Alzheimer's disease. *Front Pharmacol*, **5**, 63.

O'Brien, R.J. & Wong, P.C. (2011) Amyloid precursor protein processing and Alzheimer's disease. *Annu Rev Neurosci*, **34**, 185-204.

Oakley, H., Cole, S.L., Logan, S., Maus, E., Shao, P., Craft, J., Guillozet-Bongaarts, A., Ohno, M., Disterhoft, J., Van Eldik, L., Berry, R. & Vassar, R. (2006) Intraneuronal beta-amyloid

aggregates, neurodegeneration, and neuron loss in transgenic mice with five familial Alzheimer's disease mutations: potential factors in amyloid plaque formation. *J Neurosci*, **26**, 10129-10140.

Oddo, S., Caccamo, A., Shepherd, J.D., Murphy, M.P., Golde, T.E., Kayed, R., Metherate, R., Mattson, M.P., Akbari, Y. & LaFerla, F.M. (2003) Triple-transgenic model of Alzheimer's disease with plaques and tangles: intracellular Abeta and synaptic dysfunction. *Neuron*, **39**, 409-421.

Onishi, A., Peng, G.H., Hsu, C., Alexis, U., Chen, S. & Blackshaw, S. (2009) Pias3-dependent SUMOylation directs rod photoreceptor development. *Neuron*, **61**, 234-246.

Onos, K.D., Sukoff Rizzo, S.J., Howell, G.R. & Sasner, M. (2016) Toward more predictive genetic mouse models of Alzheimer's disease. *Brain Res Bull*, **122**, 1-11.

Orias, M., Velazquez, H., Tung, F., Lee, G. & Desir, G.V. (1997) Cloning and localization of a double-pore K channel, KCNK1: exclusive expression in distal nephron segments. *Am J Physiol*, **273**, F663-666.

Owerbach, D., McKay, E.M., Yeh, E.T., Gabbay, K.H. & Bohren, K.M. (2005) A proline-90 residue unique to SUMO-4 prevents maturation and sumoylation. *Biochem Biophys Res Commun*, **337**, 517-520.

Panse, V.G., Hardeland, U., Werner, T., Kuster, B. & Hurt, E. (2004) A proteome-wide approach identifies sumoylated substrate proteins in yeast. *J Biol Chem*, **279**, 41346-41351.

Pedrioli, P.G., Raught, B., Zhang, X.D., Rogers, R., Aitchison, J., Matunis, M. & Aebersold, R. (2006) Automated identification of SUMOylation sites using mass spectrometry and SUMmOn pattern recognition software. *Nat Methods*, **3**, 533-539.

Perl, D.P. (2010) Neuropathology of Alzheimer's disease. *Mt Sinai J Med*, **77**, 32-42.

Pichler, A., Gast, A., Seeler, J.S., Dejean, A. & Melchior, F. (2002) The nucleoporin RanBP2 has SUMO1 E3 ligase activity. *Cell*, **108**, 109-120.

Pichler, A., Knipscheer, P., Oberhofer, E., van Dijk, W.J., Korner, R., Olsen, J.V., Jentsch, S., Melchior, F. & Sixma, T.K. (2005) SUMO modification of the ubiquitin-conjugating enzyme E2-25K. *Nat Struct Mol Biol*, **12**, 264-269.

Pimplikar, S.W. (2009) Reassessing the amyloid cascade hypothesis of Alzheimer's disease. *Int J Biochem Cell Biol*, **41**, 1261-1268.

Plant, L.D., Dementieva, I.S., Kollewe, A., Olikara, S., Marks, J.D. & Goldstein, S.A. (2010) One SUMO is sufficient to silence the dimeric potassium channel K2P1. *Proc Natl Acad Sci U S A*, **107**, 10743-10748.

Poukka, H., Karvonen, U., Janne, O.A. & Palvimo, J.J. (2000) Covalent modification of the androgen receptor by small ubiquitin-like modifier 1 (SUMO-1). *Proc Natl Acad Sci U S A*, **97**, 14145-14150.

Pountney, D.L., Huang, Y., Burns, R.J., Haan, E., Thompson, P.D., Blumbergs, P.C. & Gai, W.P. (2003) SUMO-1 marks the nuclear inclusions in familial neuronal intranuclear inclusion disease. *Exp Neurol*, **184**, 436-446.

Prabakaran, S., Lippens, G., Steen, H. & Gunawardena, J. (2012) Post-translational modification: nature's escape from genetic imprisonment and the basis for dynamic information encoding. *Wiley Interdiscip Rev Syst Biol Med*, **4**, 565-583.

Rajan, S., Plant, L.D., Rabin, M.L., Butler, M.H. & Goldstein, S.A. (2005) Sumoylation silences the plasma membrane leak K+ channel K2P1. *Cell*, **121**, 37-47.

Ren, Q.G., Liao, X.M., Chen, X.Q., Liu, G.P. & Wang, J.Z. (2007) Effects of tau phosphorylation on proteasome activity. *FEBS Lett*, **581**, 1521-1528.

Riley, B.E., Zoghbi, H.Y. & Orr, H.T. (2005) SUMOylation of the polyglutamine repeat protein, ataxin-1, is dependent on a functional nuclear localization signal. *J Biol Chem*, **280**, 21942-21948.

Roger, J.E., Nellissery, J., Kim, D.S. & Swaroop, A. (2010) Sumoylation of bZIP transcription factor NRL modulates target gene expression during photoreceptor differentiation. *J Biol Chem*, **285**, 25637-25644.

Rosas-Acosta, G., Russell, W.K., Deyrieux, A., Russell, D.H. & Wilson, V.G. (2005) A universal strategy for proteomic studies of SUMO and other ubiquitin-like modifiers. *Mol Cell Proteomics*, **4**, 56-72.

Sahin, U., de The, H. & Lallemand-Breitenbach, V. (2014) PML nuclear bodies: assembly and oxidative stress-sensitive sumoylation. *Nucleus*, **5**, 499-507.

Saito, T., Matsuba, Y., Mihira, N., Takano, J., Nilsson, P., Itohara, S., Iwata, N. & Saido, T.C. (2014) Single App knock-in mouse models of Alzheimer's disease. *Nat Neurosci*, **17**, 661-663.

Saitoh, H. & Hinchey, J. (2000) Functional heterogeneity of small ubiquitin-related protein modifiers SUMO-1 versus SUMO-2/3. *J Biol Chem*, **275**, 6252-6258.

Sakono, M. & Zako, T. (2010) Amyloid oligomers: formation and toxicity of Abeta oligomers. *FEBS J*, **277**, 1348-1358.

Sambrook, J. & Russell, D.W. (2001) *Molecular cloning: A laboratory manual*. Cold Spring Harbor Laboratory Press, Cold Spring Harbor, NY.

Saracco, S.A., Miller, M.J., Kurepa, J. & Vierstra, R.D. (2007) Genetic analysis of SUMOylation in Arabidopsis: conjugation of SUMO1 and SUMO2 to nuclear proteins is essential. *Plant Physiol*, **145**, 119-134.

Sarge, K.D. & Park-Sarge, O.K. (2009) Sumoylation and human disease pathogenesis. *Trends Biochem Sci*, **34**, 200-205.

Scheltens, P., Blennow, K., Breteler, M.M., de Strooper, B., Frisoni, G.B., Salloway, S. & Van der Flier, W.M. (2016) Alzheimer's disease. *Lancet*.

Schilling, S., Zeitschel, U., Hoffmann, T., Heiser, U., Francke, M., Kehlen, A., Holzer, M., Hutter-Paier, B., Prokesch, M., Windisch, M., Jagla, W., Schlenzig, D., Lindner, C., Rudolph, T., Reuter, G., Cynis, H., Montag, D., Demuth, H.U. & Rossner, S. (2008) Glutaminyl cyclase inhibition attenuates pyroglutamate Abeta and Alzheimer's disease-like pathology. *Nat Med*, **14**, 1106-1111.

Schmidtke, G., Aichem, A. & Groettrup, M. (2014) FAT10ylation as a signal for proteasomal degradation. *Biochim Biophys Acta*, **1843**, 97-102.

Serpell, L.C. (2000) Alzheimer's amyloid fibrils: structure and assembly. *Biochim Biophys Acta*, **1502**, 16-30.

Serrano-Pozo, A., Frosch, M.P., Masliah, E. & Hyman, B.T. (2011) Neuropathological alterations in Alzheimer disease. *Cold Spring Harb Perspect Med*, **1**, a006189.

Shalizi, A., Gaudilliere, B., Yuan, Z., Stegmuller, J., Shirogane, T., Ge, Q., Tan, Y., Schulman, B., Harper, J.W. & Bonni, A. (2006) A calcium-regulated MEF2 sumoylation switch controls postsynaptic differentiation. *Science*, **311**, 1012-1017.

Shinbo, Y., Niki, T., Taira, T., Ooe, H., Takahashi-Niki, K., Maita, C., Seino, C., Iguchi-Ariga, S.M. & Ariga, H. (2006) Proper SUMO-1 conjugation is essential to DJ-1 to exert its full activities. *Cell Death Differ*, **13**, 96-108.

Spires, T.L. & Hyman, B.T. (2005) Transgenic models of Alzheimer's disease: learning from animals. *NeuroRx*, **2**, 423-437.

Squire, L.R. (1992) Declarative and nondeclarative memory: multiple brain systems supporting learning and memory. *J Cogn Neurosci*, **4**, 232-243.

Steffan, J.S., Agrawal, N., Pallos, J., Rockabrand, E., Trotman, L.C., Slepko, N., Illes, K., Lukacsovich, T., Zhu, Y.Z., Cattaneo, E., Pandolfi, P.P., Thompson, L.M. & Marsh, J.L. (2004) SUMO modification of Huntingtin and Huntington's disease pathology. *Science*, **304**, 100-104.

Subramaniam, S., Sixt, K.M., Barrow, R. & Snyder, S.H. (2009) Rhes, a striatal specific protein, mediates mutant-huntingtin cytotoxicity. *Science*, **324**, 1327-1330.

Takahashi, K., Ishida, M., Komano, H. & Takahashi, H. (2008) SUMO-1 immunoreactivity co-localizes with phospho-Tau in APP transgenic mice but not in mutant Tau transgenic mice. *Neurosci Lett*, **441**, 90-93.

Takahashi-Fujigasaki, J., Arai, K., Funata, N. & Fujigasaki, H. (2006) SUMOylation substrates in neuronal intranuclear inclusion disease. *Neuropathol Appl Neurobiol*, **32**, 92-100.

Tanaka, K., Nishide, J., Okazaki, K., Kato, H., Niwa, O., Nakagawa, T., Matsuda, H., Kawamukai, M. & Murakami, Y. (1999) Characterization of a fission yeast SUMO-1 homologue, pmt3p, required for multiple nuclear events, including the control of telomere length and chromosome segregation. *Mol Cell Biol*, **19**, 8660-8672.

Tang, L.T., Craig, T.J. & Henley, J.M. (2015) SUMOylation of synapsin Ia maintains synaptic vesicle availability and is reduced in an autism mutation. *Nat Commun*, **6**, 7728.

Tatham, M.H., Geoffroy, M.C., Shen, L., Plechanovova, A., Hattersley, N., Jaffray, E.G., Palvimo, J.J. & Hay, R.T. (2008) RNF4 is a poly-SUMO-specific E3 ubiquitin ligase required for arsenic-induced PML degradation. *Nat Cell Biol*, **10**, 538-546.

Tatham, M.H., Jaffray, E., Vaughan, O.A., Desterro, J.M., Botting, C.H., Naismith, J.H. & Hay, R.T. (2001) Polymeric chains of SUMO-2 and SUMO-3 are conjugated to protein substrates by SAE1/SAE2 and Ubc9. *J Biol Chem*, **276**, 35368-35374.

Tatham, M.H., Matic, I., Mann, M. & Hay, R.T. (2011) Comparative proteomic analysis identifies a role for SUMO in protein quality control. *Sci Signal*, **4**, rs4.

Thinakaran, G. & Koo, E.H. (2008) Amyloid precursor protein trafficking, processing, and function. *J Biol Chem*, **283**, 29615-29619.

Tirard, M., Hsiao, H.H., Nikolov, M., Urlaub, H., Melchior, F. & Brose, N. (2012) In vivo localization and identification of SUMOylated proteins in the brain of His6-HA-SUMO1 knock-in mice. *Proc Natl Acad Sci U S A*, **109**, 21122-21127.

Valincius, G., Heinrich, F., Budvytyte, R., Vanderah, D.J., McGillivray, D.J., Sokolov, Y., Hall, J.E. & Losche, M. (2008) Soluble amyloid beta-oligomers affect dielectric membrane properties by bilayer insertion and domain formation: implications for cell toxicity. *Biophys J*, **95**, 4845-4861.

van der Veen, A.G. & Ploegh, H.L. (2012) Ubiquitin-like proteins. *Annu Rev Biochem*, **81**, 323-357.

van Niekerk, E.A., Willis, D.E., Chang, J.H., Reumann, K., Heise, T. & Twiss, J.L. (2007) Sumoylation in axons triggers retrograde transport of the RNA-binding protein La. *Proc Natl Acad Sci U S A*, **104**, 12913-12918.

Vertegaal, A.C. (2010) SUMO chains: polymeric signals. *Biochem Soc Trans*, **38**, 46-49.

Vertegaal, A.C., Andersen, J.S., Ogg, S.C., Hay, R.T., Mann, M. & Lamond, A.I. (2006) Distinct and overlapping sets of SUMO-1 and SUMO-2 target proteins revealed by quantitative proteomics. *Mol Cell Proteomics*, **5**, 2298-2310.

Vertegaal, A.C., Ogg, S.C., Jaffray, E., Rodriguez, M.S., Hay, R.T., Andersen, J.S., Mann, M. & Lamond, A.I. (2004) A proteomic study of SUMO-2 target proteins. *J Biol Chem*, **279**, 33791-33798.

Vierstra, R.D. (2012) The expanding universe of ubiquitin and ubiquitin-like modifiers. *Plant Physiol*, **160**, 2-14.

Wang, H.Y., Lee, D.H., D'Andrea, M.R., Peterson, P.A., Shank, R.P. & Reitz, A.B. (2000) beta-Amyloid(1-42) binds to alpha7 nicotinic acetylcholine receptor with high affinity. Implications for Alzheimer's disease pathology. *J Biol Chem*, **275**, 5626-5632.

Wang, J.Z., Xia, Y.Y., Grundke-Iqbal, I. & Iqbal, K. (2013) Abnormal hyperphosphorylation of tau: sites, regulation, and molecular mechanism of neurofibrillary degeneration. *J Alzheimers Dis*, **33 Suppl 1**, S123-139.

Wang, L. & Banerjee, S. (2004) Differential PIAS3 expression in human malignancy. *Oncol Rep*, **11**, 1319-1324.

Wang, L., Ma, Q., Yang, W., Mackensen, G.B. & Paschen, W. (2012) Moderate hypothermia induces marked increase in levels and nuclear accumulation of SUMO2/3-conjugated proteins in neurons. *J Neurochem*, **123**, 349-359.

Wang, L., Wansleeben, C., Zhao, S., Miao, P., Paschen, W. & Yang, W. (2014) SUMO2 is essential while SUMO3 is dispensable for mouse embryonic development. *EMBO Rep*, **15**, 878-885.

Wang, X., Su, B., Lee, H.G., Li, X., Perry, G., Smith, M.A. & Zhu, X. (2009) Impaired balance of mitochondrial fission and fusion in Alzheimer's disease. *J Neurosci*, **29**, 9090-9103.

Watanabe, M., Takahashi, K., Tomizawa, K., Mizusawa, H. & Takahashi, H. (2008) Developmental regulation of Ubc9 in the rat nervous system. *Acta Biochim Pol*, **55**, 681-686.

Weeraratna, A.T., Kalehua, A., Deleon, I., Bertak, D., Maher, G., Wade, M.S., Lustig, A., Becker, K.G., Wood, W., 3rd, Walker, D.G., Beach, T.G. & Taub, D.D. (2007) Alterations in immunological and neurological gene expression patterns in Alzheimer's disease tissues. *Exp Cell Res*, **313**, 450-461.

Wei, W., Yang, P., Pang, J., Zhang, S., Wang, Y., Wang, M.H., Dong, Z., She, J.X. & Wang, C.Y. (2008) A stress-dependent SUMO4 sumoylation of its substrate proteins. *Biochem Biophys Res Commun*, **375**, 454-459.

Weintraub, S., Wicklund, A.H. & Salmon, D.P. (2012) The neuropsychological profile of Alzheimer disease. *Cold Spring Harb Perspect Med*, **2**, a006171.

Werner, A., Flotho, A. & Melchior, F. (2012) The RanBP2/RanGAP1*SUMO1/Ubc9 complex is a multisubunit SUMO E3 ligase. *Mol Cell*, **46**, 287-298.

Wilkinson, C.R., Dittmar, G.A., Ohi, M.D., Uetz, P., Jones, N. & Finley, D. (2004) Ubiquitin-like protein Hub1 is required for pre-mRNA splicing and localization of an essential splicing factor in fission yeast. *Curr Biol*, **14**, 2283-2288.

Wilkinson, K.A. & Henley, J.M. (2010) Mechanisms, regulation and consequences of protein SUMOylation. *Biochem J*, **428**, 133-145.

Wilkinson, K.A., Nakamura, Y. & Henley, J.M. (2010) Targets and consequences of protein SUMOylation in neurons. *Brain Res Rev*, **64**, 195-212.

Wirths, O. & Bayer, T.A. (2012) Intraneuronal Abeta accumulation and neurodegeneration: lessons from transgenic models. *Life Sci*, **91**, 1148-1152.

Wong, K.H., Todd, R.B., Oakley, B.R., Oakley, C.E., Hynes, M.J. & Davis, M.A. (2008) Sumoylation in Aspergillus nidulans: sumO inactivation, overexpression and live-cell imaging. *Fungal Genet Biol*, **45**, 728-737.

Yamamoto, N., Matsubara, E., Maeda, S., Minagawa, H., Takashima, A., Maruyama, W., Michikawa, M. & Yanagisawa, K. (2007) A ganglioside-induced toxic soluble Abeta assembly. Its enhanced formation from Abeta bearing the Arctic mutation. *J Biol Chem*, **282**, 2646-2655.

Yan, Q., Gong, L., Deng, M., Zhang, L., Sun, S., Liu, J., Ma, H., Yuan, D., Chen, P.C., Hu, X., Liu, J., Qin, J., Xiao, L., Huang, X.Q., Zhang, J. & Li, D.W. (2010) Sumoylation activates the transcriptional activity of Pax-6, an important transcription factor for eye and brain development. *Proc Natl Acad Sci U S A*, **107**, 21034-21039.

Yang, M., Hsu, C.T., Ting, C.Y., Liu, L.F. & Hwang, J. (2006) Assembly of a polymeric chain of SUMO1 on human topoisomerase I in vitro. *J Biol Chem*, **281**, 8264-8274.

Yang, S.H., Jaffray, E., Hay, R.T. & Sharrocks, A.D. (2003) Dynamic interplay of the SUMO and ERK pathways in regulating Elk-1 transcriptional activity. *Mol Cell*, **12**, 63-74.

Yang, W., Ma, Q., Mackensen, G.B. & Paschen, W. (2009) Deep hypothermia markedly activates the small ubiquitin-like modifier conjugation pathway; implications for the fate of cells exposed to transient deep hypothermic cardiopulmonary bypass. *J Cereb Blood Flow Metab*, **29**, 886-890.

Yang, W. & Paschen, W. (2015) SUMO proteomics to decipher the SUMO-modified proteome regulated by various diseases. *Proteomics*, **15**, 1181-1191.

Yang, W., Sheng, H., Thompson, J.W., Zhao, S., Wang, L., Miao, P., Liu, X., Moseley, M.A. & Paschen, W. (2014) Small ubiquitin-like modifier 3-modified proteome regulated by brain ischemia in novel small ubiquitin-like modifier transgenic mice: putative protective proteins/pathways. *Stroke*, **45**, 1115-1122.

Yang, W., Sheng, H., Warner, D.S. & Paschen, W. (2008a) Transient focal cerebral ischemia induces a dramatic activation of small ubiquitin-like modifier conjugation. *J Cereb Blood Flow Metab*, **28**, 892-896.

Yang, W., Sheng, H., Warner, D.S. & Paschen, W. (2008b) Transient global cerebral ischemia induces a massive increase in protein sumoylation. *J Cereb Blood Flow Metab*, **28**, 269-279.

Yang, X. & Bassham, D.C. (2015) New Insight into the Mechanism and Function of Autophagy in Plant Cells. *Int Rev Cell Mol Biol*, **320**, 1-40.

Yun, S.M., Cho, S.J., Song, J.C., Song, S.Y., Jo, S.A., Jo, C., Yoon, K., Tanzi, R.E., Choi, E.J. & Koh, Y.H. (2013) SUMO1 modulates Abeta generation via BACE1 accumulation. *Neurobiol Aging*, **34**, 650-662.

Zhang, D. & Zhang, D.E. (2011) Interferon-stimulated gene 15 and the protein ISGylation system. *J Interferon Cytokine Res*, **31**, 119-130.

Zhang, F.P., Mikkonen, L., Toppari, J., Palvimo, J.J., Thesleff, I. & Janne, O.A. (2008) Sumo-1 function is dispensable in normal mouse development. *Mol Cell Biol*, **28**, 5381-5390.

Zhang, Y.Q. & Sarge, K.D. (2008a) Sumoylation of amyloid precursor protein negatively regulates Abeta aggregate levels. *Biochem Biophys Res Commun*, **374**, 673-678.

Zhang, Y.Q. & Sarge, K.D. (2008b) Sumoylation regulates lamin A function and is lost in lamin A mutants associated with familial cardiomyopathies. *J Cell Biol*, **182**, 35-39.

Zhao, X.Y., Wang, D.D., Shan, Y. & Zhu, C.Q. (2013) [Potential involvement of abnormal increased SUMO-1 in modulation of the formation of Alzheimer's disease senile plaques and neuritic dystrophy in APP/PS1 transgenic mice]. *Sheng Li Xue Bao*, **65**, 253-262.

Acknowledgements

First, I would like to express my gratitude to Prof. Dr. Nils Brose for accepting me as a member of his department and for his excellent guidance and support.

I would like to thank my supervisor Dr. Marilyn Tirard for introducing me to many laboratory techniques and for her constant help and encouragement.

I thank the members of my thesis committee Prof. Dr. Bayer and Dr. Judith Stegmüller for their valuable input. I am also thankful to Prof. Dr. Bayer for providing the 5xFAD mouse model of Alzheimer's disease. Furthermore, I am grateful to Prof. Dr. Christian Griesinger, Prof. Dr. Ralf Heinrich and Prof. Dr. Dr. Ehrenreich for agreeing to be part of my thesis examination board.

I would like to thank Fritz Benseler, Christiane Harenberg, Dayana Schwerdtfeger, Yvonne Thanhäuser and Maik Schlieper from the DNA Core Facility for their valuable help.

I would like to express my sincere gratitude to Klaus Hellmann who provided crucial data with his biochemistry skills. Furthermore, I am very grateful to Dr. Matthieu Hammer who introduced me into confocal microscopy imaging. I am also sincerely thankful to Dr. Cordelia Imig who helped me with recombineering. I thank Xiaomin Zhang for her enormous help with embryonic stem cell work.

I am extremely thankful to Jennifer Day, Dr. James Daniel and Dr. Silvia Ripamonti from the SUMO group for always being ready to help.

I am also grateful to other members in the lab who have helped me during my PhD work – Dr. Kerstin Reim, Sally Wegner, Dr. Noa Lipstein, Dr. Mateusz Ambrozkiewicz, Dr. Tolga Soykan, Dr. Dilja Krüger. Furthermore, I would like to thank everybody else from the Department of Molecular Neurobiology for their support and the friendly atmosphere.

I would also like to express my gratitude to Prof. Dr. Dr. Ehrenreich for her continuous moral support and encouragement.

I thank my friends for being there for me even when times were tough.

I would like to thank my boyfriend for his love and extreme patience. Thank you for putting up with me all that time.

And last but not least, I would like to express my gratitude to my family for believing in me and loving me unconditionally. Without their encouragement, I would have never made it.